

1-1-2008

## Effects of pavement macrotexture on Pm(10) emissions from paved roads

Swarup China  
*University of Nevada, Las Vegas*

Follow this and additional works at: <https://digitalscholarship.unlv.edu/rtds>

---

### Repository Citation

China, Swarup, "Effects of pavement macrotexture on Pm(10) emissions from paved roads" (2008). *UNLV Retrospective Theses & Dissertations*. 2343.

<http://dx.doi.org/10.25669/h9nr-iucg>

This Thesis is protected by copyright and/or related rights. It has been brought to you by Digital Scholarship@UNLV with permission from the rights-holder(s). You are free to use this Thesis in any way that is permitted by the copyright and related rights legislation that applies to your use. For other uses you need to obtain permission from the rights-holder(s) directly, unless additional rights are indicated by a Creative Commons license in the record and/or on the work itself.

This Thesis has been accepted for inclusion in UNLV Retrospective Theses & Dissertations by an authorized administrator of Digital Scholarship@UNLV. For more information, please contact [digitalscholarship@unlv.edu](mailto:digitalscholarship@unlv.edu).

EFFECTS OF PAVEMENT MACROTEXTURE ON PM<sub>10</sub> EMISSIONS FROM  
PAVED ROADS

by

Swarup China

Bachelor of Technology  
Visvesvaraya National Institute of Technology, Nagpur, India  
2006

A thesis submitted in partial fulfillment  
of the requirements for the

**Master of Science Degree in Engineering**  
**Department of Civil and Environmental Engineering**  
**Howard R. Hughes College of Engineering**

**Graduate College**  
**University of Nevada, Las Vegas**  
**August 2008**

UMI Number: 1460463

### INFORMATION TO USERS

The quality of this reproduction is dependent upon the quality of the copy submitted. Broken or indistinct print, colored or poor quality illustrations and photographs, print bleed-through, substandard margins, and improper alignment can adversely affect reproduction.

In the unlikely event that the author did not send a complete manuscript and there are missing pages, these will be noted. Also, if unauthorized copyright material had to be removed, a note will indicate the deletion.

**UMI**<sup>®</sup>

---

UMI Microform 1460463

Copyright 2009 by ProQuest LLC.

All rights reserved. This microform edition is protected against unauthorized copying under Title 17, United States Code.

ProQuest LLC  
789 E. Eisenhower Parkway  
PO Box 1346  
Ann Arbor, MI 48106-1346



**Thesis Approval**  
The Graduate College  
University of Nevada, Las Vegas

July 31, 2008

The Thesis prepared by

Swarup China

Entitled

Effects of Pavement Macrottexture on PM-10 Emissions

from Paved Roads

is approved in partial fulfillment of the requirements for the degree of

Master of Science in Engineering (major: Civil Engineering)

EXAMINATION COMMITTEE MEMBER

Jacimara R. Batista

Examination Committee Member

Examination Committee Member

Ashon K. Sneh

Graduate College Faculty Representative

Examination Committee Chair

Dean of the Graduate College

## ABSTRACT

### **Effects of Pavement Macrotexture on PM<sub>10</sub> Emissions from Paved Roads**

by

Swarup China

Dr. David E. James, Examination Committee Chair  
Associate Vice Provost for Academic Programs, Associate Professor of Civil and  
Environmental Engineering

This study compares two methods for measuring pavement macrotexture and investigates the influence of paved road macrotexture on paved road PM<sub>10</sub> emissions originating both from soil erosion and deposition, and from tire, brake and asphalt wear. Macrotexture was measured using the ASTM Sand patch method and the Digital Surface Roughness Meter (DSRM). PM<sub>10</sub> emissions were estimated using AP-42 sampling and measured with a Mini-PI-SWERL™.

DSRM and sand patch mean texture depths (MTDs) were well-correlated. Silt-normalized ambient PM<sub>10</sub> emissions variations were partially explained by pavement macrotexture. PM<sub>10</sub> emissions experiments using controlled silt loadings showed good correlations with pavement macrotexture. A change in the slope of emitted PM<sub>10</sub> mass vs pavement macrotexture occurred between 0.8 and 0.9 mm MTD.

PM<sub>10</sub> emissions linearly declined with increasing pavement aggregate mode size. Wind erosion theory showed that PM<sub>10</sub> emissions were related to wind stress at a height

of 0.075 mm, threshold friction velocity estimated from soil size distribution mode, and aerodynamic roughness height determined from adjusted pavement aggregate mode size.

## TABLE OF CONTENTS

ABSTRACT .....	.iii
LIST OF TABLES .....	vii
LIST OF FIGURES .....	viii
ACKNOWLEDGEMENT .....	xii
CHAPTER 1 INTRODUCTION.....	1
1.1 Problem Statement.....	1
1.2 Study Objectives.....	4
CHAPTER 2 LITERATURE REVIEW.....	5
2.1 Asphalt Concrete .....	5
2.2 Pavement Surface Texture Measurements.....	7
2.3 PM <sub>10</sub> Measurements from Road Dust.....	15
2.4 PI-SWERL and Mini-PI-SWERL.....	19
2.5 Friction Velocity and Threshold Friction Velocity .....	21
CHAPTER 3 MATERIALS AND METHODS.....	27
3.1 Summary.....	27
3.2 Materials .....	28
3.3 Site Selection Survey.....	30
3.4 Sampling Schedule .....	35
3.5 AP-42 Silt Sampling and Emission Factor Estimation.....	37
3.6 Sand Patch and DSRM Test .....	39
3.7 Mini-PI-SWERL™ Test.....	47
3.8 Sampling Sequence.....	51
CHAPTER 4 AP-42 EMISSION FACTOR RESULTS.....	54
4.1 Silt Loading and Emission Factor Calculations.....	54
4.2 First Quarter, 2008 Results and Comparisons to Prior Measurement .....	55
CHAPTER 5 SAND PATCH AND DSRM RESULTS .....	66
5.1 DSRM Results .....	66
5.2 UNLV Parking Lot Results .....	69
5.3 13 Sampling Sites Results .....	71

CHAPTER 6	PM <sub>10</sub> EMISSION RESULTS.....	80
6.1	Data Reduction and Processing.....	80
6.2	Pavement Texture and PM <sub>10</sub> Emissions.....	86
6.3	Two-way Frequency Distribution and Photographic Analysis.....	107
6.4	Aggregate Size Mode and PM <sub>10</sub> Emissions.....	118
6.5	Application of Wind Erosion Theory to Controlled Studies.....	126
6.6	Thomas & Mack Parking Lot Depletion Study.....	132
CHAPTER 7	CONCLUSIONS AND RECOMMENDATIONS.....	140
7.1	Conclusions.....	140
7.2	Recommendation for Air Quality Control.....	142
7.3	Recommendations for Future Work.....	143
REFERENCES	.....	156
VITA	.....	158



## LIST OF TABLES

Table 1.1	National Ambient Air Quality Standards for Particulate Pollution (US EPA, 2006 a, b).....	2
Table 2.1	Texture Classification.....	7
Table 3.1	Aggregate Size Distribution of Burkholder & Cabrillo Site .....	31
Table 3.2	AP-42 Sampling Sites for Phase V.....	34
Table 3.3	Sampling Schedule for Phase V .....	36
Table 3.4	DSRM Standard outputs (MaGaNa Instruments email correspondence)....	46
Table 4.1	AP-42 Emission Factors for Local Roads First Quarter 2008.....	56
Table 4.2	AP-42 Emission Factors for Collector Roads First Quarter .....	56
Table 4.3	AP-42 Emission Factors for Minor Arterial Roads First Quarter .....	57
Table 4.4	Relationship of AP-42 EF to Prior Measurements .....	58
Table 5.1	Parking lot DSRM and Sand Patch Test Results .....	70
Table 5.2	Sand Patch MTD & DSRM MTD Results for All Data-points.....	72
Table 5.3	Average DSRM and Sand Patch MTD (mm) Results .....	75
Table 5.4	Regression Output for All Data Points .....	77
Table 6.1	Sample Output Data from Mini-PI-SWERL™ (Duneville & Oakey P2S2Controlled Soil).....	82
Table 6.2	Emitted Mass and Shear Calculation for Duneville & Oakey P2S2 Controlled Experiment.....	84
Table 6.3	Mini PI-SWERL™ Emitted Mass at 5000 RPM and Sand Patch MTD .....	99
Table 6.4	Comparing $r^2$ for Different Fits-Soil Mass Emitted vs Sand Patch MTD..	101
Table 6.5	Two-way Frequency Distribution Summary .....	116
Table 6.6	Mean Aggregate Size and Mode Calculation (Maryland & WestminsterP2S1) .....	119
Table 6.7	Average Aggregate size and Mode Correction.....	123
Table 6.8	Statistical Summary for (u0.075)-u*t (controlled experiments).....	129
Table 6.9	Statistical Summary for (u(MTD/10))-u*t (controlled experiments).....	129
Table 6.10	Mass Emitted at 5000 RPM from Smooth Surface .....	133
Table 6.11	Mass Emitted at 5000 RPM from Rough Surface .....	133

## LIST OF FIGURES

Figure 2.1	Microtexture and Macrottexture Illustration based on Henry, 2000 .....	8
Figure 2.2	Simple Waveform Wavelength and Amplitude Fundamentals – constant amplitude and wavelength .....	8
Figure 2.3	Texture Wavelength Influence on Surface Characteristics (based on PIARC, 1987).....	9
Figure 2.4	Outflow Meter (HYDROTIMER Outflow Meter Operator’s Manual) .....	10
Figure 2.5	Computation of Mean Profile Depth (MPD) (based on ASTM E1845, 2001).....	11
Figure 2.6	Segments of Circular Track Profile (based on ASTM E 2157, 2001) .....	14
Figure 2.7	PI-SWERL Schematic Redrawn from Etymezian et al., 2007.....	20
Figure 2.8	Mini-PI-SWERL™ (photo taken by Rodrigues, 2006) .....	21
Figure 2.9	Illustration of Logarithmic velocity profile, (a) Arithmetic (b) Semi logarithmic representation (Source: EPA, 1988).....	22
Figure 2.10	Forces Acting on Particle at Threshold Movement.....	24
Figure 2.11	Gillete Relationship of Threshold Friction Velocity to Size Distribution Mode (Source: EPA Manual, Cowherd et al., 1988).....	25
Figure 3.1	A Close-up Photo of Pavement Surface with a Ruler (Burkholder & Cabrillo) Taken during Fall 2007 Photographic Survey.....	32
Figure 3.2	Aggregate Size Distributions for Burkholder & Cabrillo Pavement Surface .....	32
Figure 3.3	Sand Patch Experiment (Crestdale & Covington Cross).....	33
Figure 3.4	Typical Soil Recovery Layout (Arrows illustrate direction of vacuum wand movement in each subsection).....	38
Figure 3.5	AP-42 Silt Recovery Sampling (Pabco & Tabony) .....	39
Figure 3.6	Experimental Set up for DSRM and Sand Patch.....	40
Figure 3.7	Schematic of sand patch test .....	41
Figure 3.8	Side View of Pavement Surface after Sand Patch Test.....	42
Figure 3.9	Sand Patch Test (Per ASTM E 965, 2001).....	42
Figure 3.10	Schematic of Digital Roughness Meter (Not drawn to scale).....	44
Figure 3.11:	DSRM Setup .....	45
Figure 3.12	Digital Surface Roughness Meter .....	45
Figure 3.13	Schematic of Mini-PI-SWERL™ (Mini-PI-SWERL™ blade photo taken by Rodrigues, 2006) .....	48
Figure 3.14	Mini-PI-SWERL™ .....	48
Figure 3.15	Mini-PI-SWERL™ Experimental Setup.....	49
Figure 3.16	Mini-PI-SWERL™ Sampling (Goldhill & Richmar) .....	49
Figure 3.17	(a) Schematic Plot Layout (existence of tire track) and Experimental Setup of Mini-PI-SWERL™ .....	50
Figure 3.18	Typical Sampling Sequence .....	53

Figure 4.1	AP-42 EF Results of first Quarter 2008 .....	59
Figure 4.2	Armacost & Calmar (Local road) EF with Time .....	60
Figure :4.3	Duneville & Oakey (Local road) EF with Time .....	60
Figure 4.4	Avergold & Coral Sea (Local road) EF with Time .....	61
Figure 4.5	Goldhill & Richmar (Local road) EF with Time.....	61
Figure 4.6	Sapphire Light & Emerald Stone (Local road) EF with Time .....	62
Figure 4.7	Burkholder & Cabrillo (Collector road) EF with Time.....	62
Figure 4.8	Crestdale & Covington Cross (Collector road) EF with Time.....	63
Figure 4.9	Ione & Coral Sea (Collector road) EF with Time .....	63
Figure 4.10	Pabco & Tabony (Collector road) EF with Time.....	64
Figure 4.11	Ann Rd & San Mateo (Minor Arterial) EF with Time.....	64
Figure 4.12	Maryland & Westminster (Minor Arterial) EF with Time.....	65
Figure 4.13	Silver Spring & Spring Hills (Minor Arterial) EF with Time.....	65
Figure 5.1	Ann Rd Plot1 Spot1 (DSRM MTD 1.314 mm) .....	67
Figure 5.2	Ann Rd Plot1 Spot1 ( DSRM Output) .....	67
Figure 5.3	Evergold & Coral Sea Plot1 Spot1 (DSRM MTD 0.45 mm) .....	68
Figure 5.4	Evergold & Coral Sea Plot1 Spot1 (DSRM Output) .....	68
Figure 5.5	Parking lot DSRM and Sand Patch Test Results.....	70
Figure 5.6	Correlation between DSRM and Sand Patch Parking Lot Data.....	71
Figure 5.7	Pavement Texture Measured by Sand Patch (ASTM E965, 2001) at Different Roadway Category .....	76
Figure 5.8	Pavement Texture Measured by DSRM at Different Roadway Category ....	77
Figure 5.9	On Tire and Between Tire Sand Patch Mean Texture Depth.....	78
Figure 5.10	DSRM MTD and Sand Patch MTD with 95% Confidence Limit, n=61 .....	79
Figure 6.1	PM <sub>10</sub> Concentration Raw Data collected every second (Duneville & Oakey P2S2 Soil).....	83
Figure 6.2	Average Emitted Mass vs Shear for Duneville& Oakey P2S2 .....	85
Figure 6.3	Average Emitted Mass vs Shear for Burkholder & Cabrillo P2S1 Soil.....	85
Figure 6.4	Silt Loading vs Sand Patch MTD.....	86
Figure 6.5	Ambient PM <sub>10</sub> Mass Emissions vs silt loading .....	87
Figure 6.6	(a) Linear fit (b) Power fit, (c) Exponential fit, (d) Logarithmic fit (All are Ambient Condition and Summed Actual Emitted Mass) .....	89
Figure 6.7	(a) 2000 RPM Mass, (b) 2000 RPM Mass with Expanded Scale, (c) 3000 RPM Mass, (d) 3000 RPM Mass with Expanded Scale (All are Ambient Condition and Actual Emitted Mass) .....	90
Figure 6.8	(a) 4000 RPM Mass, (b) 4000 RPM Mass with Expanded Scale, (c) 5000 RPM Mass, (d) 5000 RPM Mass with Expanded Scale (Ambient condition).....	91
Figure 6.9	Normalized Sum of all RPM Ambient Mass Emissions vs Sand Patch MTD.....	92
Figure 6.10	(a) 2000 RPM Mass, (b) 2000 RPM Mass, Segmented plot (c) 3000 RPM Mass, (d) 3000 RPM Mass Segmented plot (Normalized Mass by Silt Loading),(Diamonds represent <0.9 mm, and Squares represent >0.9 mm) .....	94
Figure 6.11	(a) 4000 RPM Mass, (b) 4000 RPM Mass with Segmented plot, (c) 5000 RPM Mass, (d) 5000 RPM Mass with Segmented plot	

	(Normalized Mass), (Diamonds represent <0.9 mm, and Squares represent >0.9 mm).....	95
Figure 6.12	2000 RPM Mass, (b) 3000 RPM Mass (c) 4000 RPM Mass, (d) 5000 RPM Mass with Mode (mm) and MTD(mm) (Ambient Condition and Normalized Mass By Silt Loading).....	96
Figure 6.13	(a) 2000 RPM Mass, (b) 3000 RPM Mass (c) 4000 RPM Mass, (d) 5000 RPM Mass vs Mode (mm) (Ambient Condition and Normalized Mass By Silt Loading).....	97
Figure 6.14	5000 rpm power fit log-log plot with 95% Confidence Limit (before back transform).....	102
Figure 6.15	5000 rpm power fit with 95% Confidence Limit (after back transform)...	102
Figure 6.16	(a) 2000 RPM Mass, (b) 2000 RPM Mass with Expanded Scale, (c) 3000 RPM Mass, (d) 3000 RPM Mass with Expanded Scale.....	103
Figure 6.17	(a) 4000 RPM Mass, (b) 4000 RPM Mass with Expanded Scale, (c) 5000 RPM Mass vs Sand Patch MTD.....	104
Figure 6.18	(a) 2000 RPM Mass, (b) 3000 RPM Mass (c) 4000 RPM Mass, (d) 5000 RPM Mass with Exponential Fit.....	105
Figure 6.19	a) 2000 RPM Mass, (b) 3000 RPM Mass (c) 4000 RPM Mass, (d) 5000 RPM Mass with Segmented Linear Fit.....	106
Figure 6.20	Before Mini-PI-SWERL™ Control Experiment at Maryland/ Westminster.....	108
Figure 6.21	Before Mini-PI-SWERL™ Control Experiment (Ann Rd & San Mateo).....	109
Figure 6.22	After Mini-PI-SWERL™ Control Experiment (Ann Rd & San Mateo)....	109
Figure 6.23	DSRM Raw Pixel Data (Ann Rd & San Mateo, P3S1).....	111
Figure 6.24	Pavement Surface Profile (Ann Rd & San Mateo, P3S1, line 3).....	111
Figure 6.25	Pavement Surface Profile (Maryland & Westminster, P3S1, line 1).....	112
Figure 6.26	Peak or Valley vs Width (Ann Rd & San Mateo, P3S1, line 3).....	113
Figure 6.27	Peak or Valley vs Width (Ann Rd & San Mateo, P3S1, line 2).....	113
Figure 6.28	Peak or Valley vs Width (Maryland & Westminster, P1S1, line 1).....	114
Figure 6.29	Peak or Valley vs Width (Maryland & Westminster, P3S1, line 1).....	114
Figure 6.30	Two-way Frequency Distribution of Ann Rd & San Mateo site (P2S1) ...	116
Figure 6.31	Two-way Frequency Distribution of Maryland & Westminster site (P3S1).....	117
Figure 6.32	Aggregate Size Distributions (Maryland & Westminster, P2S1).....	118
Figure 6.33	Mean Aggregate Size vs Sand Patch MTD.....	120
Figure 6.34	Aggregate Size Mode vs Sand Patch MTD.....	121
Figure 6.35	Aggregate Mode Size Correction.....	121
Figure 6.36	Corrected Aggregate Size Mode vs Sand patch MTD.....	122
Figure 6.37	Mode (mm) and (a) 2000 RPM Mass, (b) 3000 RPM Mass (c) 4000 RPM Mass, (d) 5000 RPM Mass) vs MTD(mm).....	124
Figure 6.38	(a) 2000 RPM Mass, (b) 3000 RPM Mass (c) 4000 RPM Mass, (d) 5000 RPM Mass vs Mode (mm).....	125
Figure 6.39	Relationship of Wind speed and Height.....	128
Figure 6.40	2000 RPM (b) 3000 RPM (c) 4000 RPM, (d) 5000 RPM (Soil-Clean) Mass vs $u(0.075\text{mm}-u^*t)$ .....	130

Figure 6.41	2000 RPM (b) 3000 RPM (c) 4000 RPM, (d) 5000 RPM (Soil-Clean) Mass vs $u((MTD/10)-u*t)$ .....	131
Figure 6.42	Mass Emitted at 3000 RPM at Different Run .....	134
Figure 6.43	Mass Emitted at 4000 RPM at Different Run .....	135
Figure 6.44	Mass Emitted at 5000 RPM at Different Run .....	135
Figure 6.45	Mass Emitted at 3000+4000+5000 RPM at Different Run.....	136
Figure 6.46	Mass Removed at First Run at Different Shear Rate .....	137
Figure 6.47	Total Mass Removed for All Run at Different Shear Rate .....	137
Figure 6.48	Cumulative Mass Removed at 3000 RPM Shear Rate.....	138
Figure 6.49	Cumulative Mass Removed at 4000 RPM Shear Rate.....	138
Figure 6.50	Cumulative Mass Removed at 5000 RPM Shear Rate.....	139
Figure 6.51	Cumulative Mass Removed at 3000+4000+5000 RPM Shear Rate .....	139

## ACKNOWLEDGEMENTS

First I would like to thank Dr. David E. James for helping me a lot whenever I needed and for motivating me. I would also like to thank my committee members, Dr. Jaci Batista, Dr. Vic Etyemezian, Dr. Thomas Piechota and Dr. Ashok Singh for servicing on my thesis committee and for reviewing my thesis manuscript.

I would special thanks to Dr. Vic Etyemezian and George Nikolich from Desert Research Institute for providing equipment and materials for this project.

I would like to give my special thanks to the Clark County Department of Air Quality and Environmental Management for their financial support for this project. I am thankful to Mr. Russ Merle and Rodney Langston for their support and helping a lot throughout the field sampling.

I would like thank all of my friends who helped me during the field sampling.

## CHAPTER 1

### INTRODUCTION

#### 1.1 Problem Statement

Airborne particulate matter is a major concern for the human environment as it causes serious health effects such as aggravated asthma, breathing and lung problems, chronic bronchitis and premature death (EPA, 2006a).

Numerous studies have been performed to find the impact of particulate air pollution on daily mortality. Studies have shown a positive association between daily mortality and particulate air pollution. Schwartz et al., 1990 studied air pollution data and deaths in London from 1958-1972 and concluded that there was no threshold value of particulate matter that did not affect health to lowest observed levels of air pollution (Schwartz et al, 1990). Daniels et al., 2000 used a spline model to show that there was a linear relation without indication of threshold for PM<sub>10</sub> and relative risk of death causes both and cardio-respiratory instances. The risk didn't increase until approximately 50 µg/m<sup>3</sup> of PM<sub>10</sub> for other causes.

The Clean Air Act of 1970 and sub segment amendments of 1990 require EPA to set National Ambient Air Quality Standards (NAAQS). The Clean Air Act established two types of National Air Quality Standards for particulate matter, Primary standards and Secondary standards. Primary standard limits are set to protect public health, including

health of “sensitive” populations such as asthmatics, children and the elderly (EPA, 2006b).

Secondary standards set limits to protect public welfare, including protection against visibility, impairment, and damage to animals, vegetation and buildings (EPA, 2006 b).

Primary and secondary standards are shown in Table 1.1.

Table 1.1 National Ambient Air Quality Standards for Particulate Pollution (US EPA, 2006 a, b)

Pollutant	Primary Stds	Averaging Times	Secondary Stds
Particulate Matter (PM <sub>10</sub> )	Revoked (1)	Annual (1) (Arith Mean)	Same as primary
	150 µg/m <sup>3</sup>	24 hr (2)	Same as primary

(1) - *Due to a lack of evidence linking health problems to long-term exposure to coarse particle pollution, the agency revoked the annual PM<sub>10</sub> standard in 2006 (effective December 17, 2006). Originally it was set to 50 µg/ m<sup>3</sup>*

(2) - *Not to be exceeded more than once per year on average over 3 years*

The Las Vegas Valley, located in Clark County, Nevada is designated as a Serious Nonattainment area for airborne particulate matter with an aerodynamic diameter of 10 µm (PM<sub>10</sub>) or less. “Nonattainment” is the designated term by the US Environmental Protection Agency (EPA) where air pollution levels exceed the National Ambient Air Quality Standards (NAAQS) set by the Clean Air Act Amendments (EPA’s 24-hour standard for PM<sub>10</sub> is 150 µg/m<sup>3</sup> ). Nonattainment areas are classified based on the severity of violation. Nonattainment areas for particulate matter have two types of classification, serious and moderate. The Las Vegas Valley is classified as Serious because of the number and intensity of exceedances of the Standard.



PM<sub>10</sub> is defined as airborne particulate matter whose aerodynamic diameter is 10 micrometer or less. Airborne particulate matter can be comprised of different substances. The major sources of PM<sub>10</sub> are pavement wear, mud and dirt carryout from unpaved roads, biological debris, ice compounds, wind erosion and construction activities. Vehicle exhaust and tire wear also contribute to particulate pollution (US EPA 1995).

In addition to contributing to exceedances of particulate matter Air Quality Standards, at extremely high loadings, paved road dust emissions can cause serious vehicle accidents and human injuries due to poor visibility. Windy, dry weather in Las Vegas valley intensifies this problem. Potential sources of paved road dust in southern Nevada include road dust blown from adjacent vacant land surfaces, track-out from construction sites and unpaved roads, sediment carried in stormwater runoff, and brake and tire wear. Additionally fine particles are reentrained by vehicle aerodynamic and tire shear (DAQEM, 2001).

Three major sources of PM<sub>10</sub> emissions were identified in 1998 inventory for the State Implementation Plan (SIP) in the Las Vegas Valley. The major sources of emissions (45%) are non-anthropogenic wind blown dust from vacant land (which includes stable and non stable area). Emissions from construction sites are second largest (37%). Paved road dust emissions are the third largest emission category (13 %) for emission inventory (DAQEM, 2001).

The Clark County Department of Air Quality and Environmental Management (DAQEM) Phase IV study showed that higher mobile-source emissions for a controlled silt loading on the test road than had been observed from ambient mobile source PM<sub>10</sub> emissions on the Las Vegas Valley road network. It was hypothesized that airborne PM<sub>10</sub>

emissions for “freshly” applied soil might have been higher than emissions from ambient equilibrium silt loading because the soil in Phase IV hadn’t sheltered into the spaces between aggregates and was more accessible to tire shear and aerodynamic shear. Pavement macrotexture measurements of the Phase IV Veterans Memorial Blvd site hadn’t been made, so analysis of effects of texture on paved road emissions couldn’t be performed (Langston et al., 2008).

## 1.2 Study Objectives

The main objectives of this study are (a) Compare two different methods; the Digital Surface Roughness Meter (DSRM) and the Sand Patch test (ASTM E 965, volumetric technique) for measurement of pavement surface macrotexture and determine if a correlation between two methods can be established, (b) evaluate the effects of pavement surface macrotexture on  $PM_{10}$  emissions from paved roads. This part of the study compares the mass emissions of particulate matter ( $PM_{10}$ ) as a function of pavement texture at different shear forces (c) conduct quarterly AP42 sampling and estimation of paved road dust  $PM_{10}$  emission factors measurements and compare 2008 estimated emission factors to historical data collected in 2001-2006

## CHAPTER 2

### LITERATURE REVIEW

#### 2.1 Asphalt Concrete

Asphalt concrete consists of a hot bituminous material mixed with aggregates and then allowed to cool to solidify and bind the aggregates together and form a pavement surface. Bitumens that have been used in paving include: native asphalt, rock asphalt, tars and petroleum asphalt (Atkins, 1997). The main asphalt paving material is asphalt concrete which is also known by many different names: hot mixed asphalt, bituminous mix, bituminous concrete etc. Asphalt concrete is a high quality pavement surface composed of asphalt cement and aggregates, hot mixed in an asphalt plant and then hot laid. Sometimes binding between aggregates is loose as asphalt cement seeps into air voids in the aggregate particles and therefore asphalt cement is not available to coat and bind the aggregates together (Atkins, 1997).

Pavement surface profile and texture measurements play an important role in pavement design. Pavement surface texture determines ride quality (smoothness, roughness) and durability of pavement (deformation, aggregate segregation and roughness) (FHWA, 2005). Pavement surface texture provides friction which reduces wet weather accidents. Texture also affects tire noise.

Aggregate size distribution and texture analyses have been carried out to evaluate their effects on skid resistance. Macrottexture is one of the important pavement

characteristic which is responsible for skid resistance in both dry and wet weather. The macro texture generated from inter-granular roughness and particle size distribution of mixture. Macro texture produces tire deformation and horizontal reaction force. Skid resistance is generated from interactions between the pavement surface and the tire (Cafiso et al., 2007).

Because concrete asphalt pavement surfaces have many of the statistical properties of random signals, Cafiso et al., 2007 evaluated a power spectrum density technique to analyze pavement macrotexture and microtexture. Pavement aggregate parameters and adherence of aggregate sample had significant correlation (Cafiso et al., 2007).

Road dust is a major source of  $PM_{10}$ . Tervahattu (2006) cited several studies showing that many winter cities of Scandinavia, North America and Japan suffer from serious environmental problems cause by particulate matter generated from paved road dust (Amemiya et al., 1984, Fukuzaki et al., 1986 and Kantamaneni et al., 1996). Anti-skid aggregate on the pavement surfaces was found to increase the  $PM_{10}$  emissions regardless of the tire type but some amount of  $PM_{10}$  was also generated due to the sand paper effect. The “sand paper effect” is the asphalt concrete wear caused by abrasion of the antiskid aggregate grains between tires and asphalt concrete. Tervahattu (2006) used studded tires and friction tires to evaluate the impacts on pavement surfaces and  $PM_{10}$  emissions. The study concluded that studded tires have greater impact on  $PM_{10}$  generation than friction tires, but friction tires produced more organic particles from tire wear.

Tervahattu (2006) also found that granite rock is better to use than mafic volcanic rock as a traction control material, the aggregate as granite produces less particulate matter than mafic volcanic rock (Tervahattu et al., 2006).

## 2.2 Pavement Surface Texture Measurements

During the late 1940s and early 1950s, the relationship of pavement surface texture characteristics to roadway safety was first studied when increases in traffic volumes and vehicle speed resulted in wet-weather crashes (ACI, 1988). Different techniques have been developed for measuring pavement surface macrotexture. The main applications of surface macrotexture are to evaluate the frictional properties of the pavement surface and to detect hot mix asphalt (HMA) non uniform construction segregation (Flintsch, et al., 2003).

Pavement texture has been categorized into three major categories based on wavelength (Table 1). These are (1) microtexture, consisting of wavelengths of 1  $\mu\text{m}$  to 0.5 mm (0.0004 in to 0.02 in), (2) macrotexture, with wavelengths of 0.5mm to 50mm (0.02in to 2 in) and (3) megatexture, with wavelengths of 50 mm to 500 mm (Henry, 2000). Pavement texture influences most tire-road interactions such as wet friction, noise, splash and spray, rolling resistance, and tire wear. Skid resistance depends on macrotexture and microtexture. Pavement macrotexture contributes to adhesion and skid resistance (Henry, 2000). The large aggregate particles in the asphalt mixture are responsible for pavement macrotexture. Figure 2.1 illustrates the macrotexture and microtexture concept (Henry, 2000). The concept of wavelength is shown in Figure 2.2.

Table 2.1 Texture Classification

Texture Classification	Relative Wavelengths
Microtexture	$\lambda < 0.5 \text{ mm}$
Macrotexture	$0.5 \text{ mm} < \lambda < 50 \text{ mm}$
Megatexture	$50 \text{ mm} < \lambda < 500 \text{ mm}$
Roughness/Smoothness	$0.5 \text{ m} < \lambda < 50 \text{ m}$

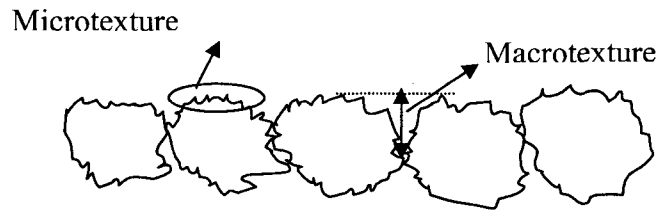


Figure 2.1 Microtexture and Macrottexture Illustration based on Henry, 2000

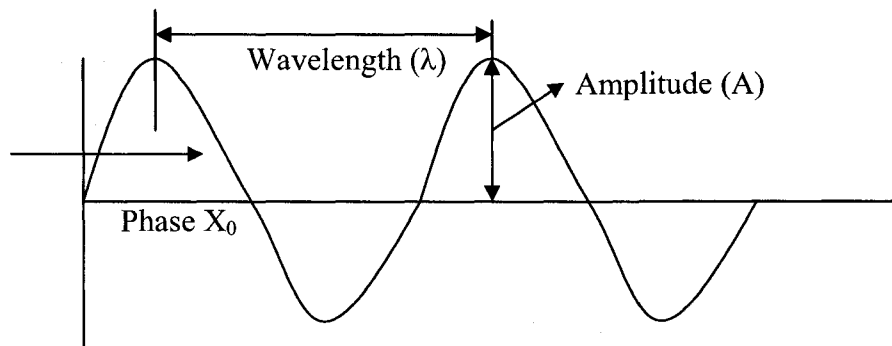


Figure 2.2 Simple Waveform Wavelength and Amplitude Fundamentals – constant amplitude and wavelength

At the 18<sup>th</sup> World Road Congress, the committee on Surface Characteristics of the World Road association (PIARC) proposed the following ranges of wavelength influence for each category (shown in Figure 2.3 PIARC, 1987).

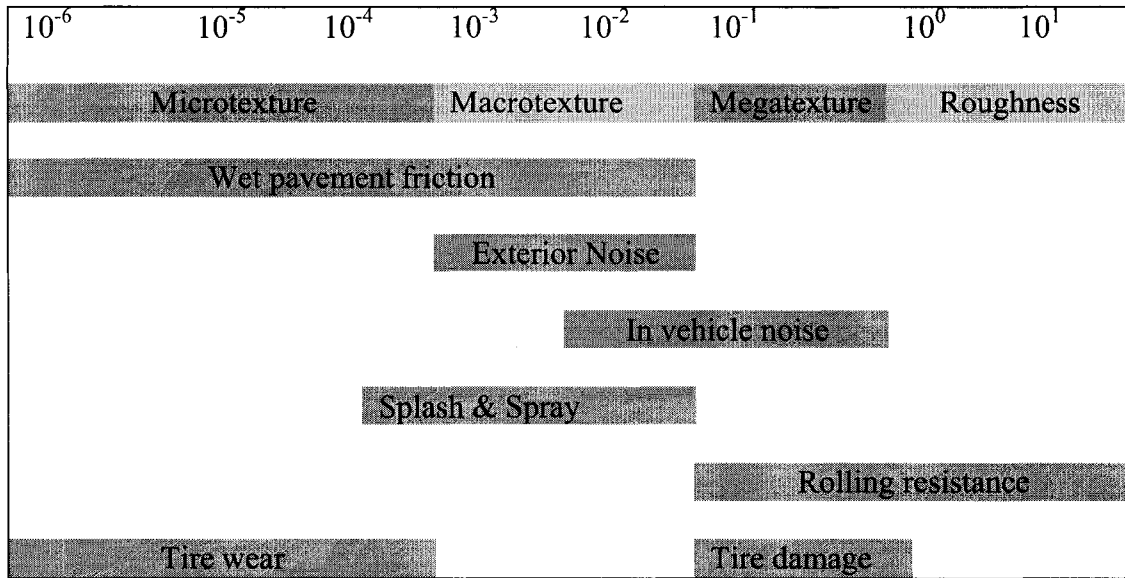


Figure 2.3 Texture Wavelength Influence on Surface Characteristics (based on PIARC, 1987)

Different methods have been used to measure pavement surface texture. The first and classic measurement of macrottexture is the sand patch method (ASTM E 965) (ASTM, 2001). This method is a volumetric technique, where a known volume of glass spheres is used to create a “pancake” on the road surface. The Mean Texture Depth (MTD) is calculated by dividing the known volume of glass spheres by the pancake area.

The Outflow meter (Figure 2.4) can measure the outflow time (OFT), a texture-related statistic that is highly correlated with both the MTD and the mean profile depth (MPD) on non-porous pavements (Henry, 2000). The outflow meter consists of a transparent vertical cylinder and a valve. The cylinder rests on the pavement with a rubber pad. The valve is closed when the cylinder is filled with water. The valve is opened and the time is measured for the water level to fall by a fixed amount. This measured amount of time is the OFT. The correlation between OFT and the MTD was

studied by the FHWA for non-porous surfaces at the NASA Wallops Flight Facility, and was found to be

$$(1/OFT) = 0.58 * (MTD) - 0.15 \quad (r^2 = 0.99) \quad (2.1)$$

Here OFT is reported in seconds and MTD is reported in mm (Henry, 2000).

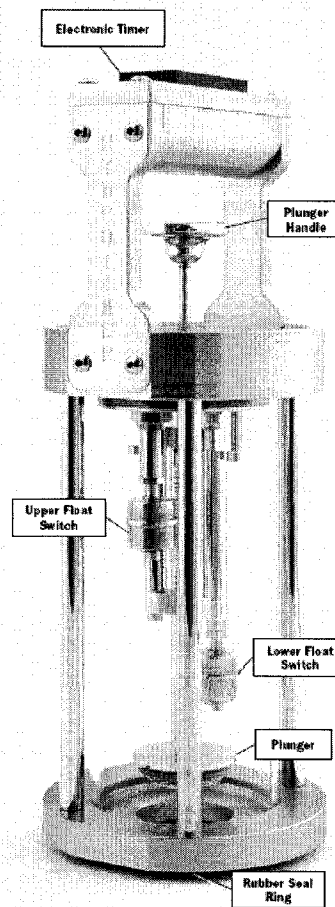


Figure 2.4 Outflow Meter (HYDROTIMER Outflow Meter Operator's Manual)

Laser technology can be used to measure macrotexture at traffic speed. The mean profile depth (MPD) is measure by laser technology. The Mean Profile Depth is a



statistic computed by analyzing 102 mm (4 in) segments of the collected profile data (Henry, 2000, ASTM E 1845).

Surfan Engineering & Software Inc and Federal Highway Administration (FHWA) developed a laser based technology, ROad Surface ANalyzer-Vehicle mounted (ROSAN<sub>V</sub>) (FHWA 1997). ROSAN<sub>V</sub> consists of lightweight, bumper mounted portable laser system and a portable computer. This technique is advanced and can provide large numbers of surface texture measurements without hampering traffic. Current ROSAN<sub>V</sub> technology can measure MPD with a high level of resolution (0.03 mm) along a linear path. It was developed to measure pavement texture at highway speed along a linear path (FHWA, 2002).

ASTM Standard E1845 describes how to calculate Mean Profile Depth (MPD) from surface profile measurements. Figure 2.5 graphically depicts the fundamentals of mean profile depth (MPD), (ASTM E 1845, 2001).

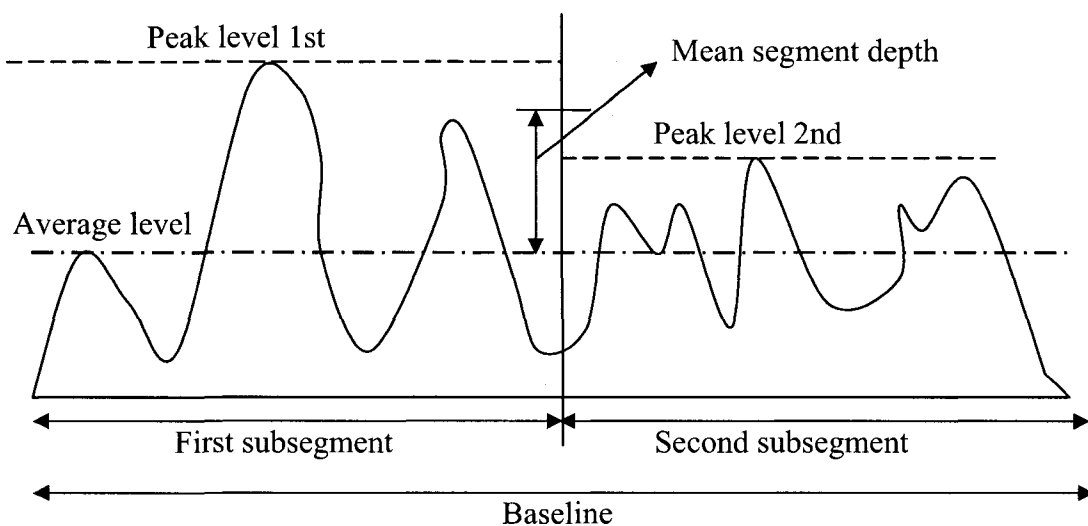


Figure 2.5 Computation of Mean Profile Depth (MPD) (based on ASTM E1845, 2001)

The ASTM E1845 procedure for computing Mean Profile Depth is calculated as follows:

(1) The measured profile is divided into segments of  $100 \pm 2$  mm for analysis in subsequent steps

(2) Individual profile depths are measured and recorded.

(3) A linear regression of each segments profile values is performed and the regression line is subtracted from profile values of the segment to suppress the slope of the segment and give a zero mean value for the segment.

(4) According to ASTM E1845, 2001, each segment is divided into two subsegments, each 50 mm long. The peak level is found above the average level of each subsegment (Figure 2.5)

(5) The peak level of the first subsegment and peak level of second subsegment are averaged to find the mean segment depth (Equation 2.2).

$$\text{Mean segment depth} = \frac{\text{Peak level (1}^{\text{st}}) + \text{Peak level (2}^{\text{nd}})}{2} \quad (2.2)$$

The average value of mean segment depths for all segments of the measured profile will give the MPD value. The MPD may be transformed to an estimated texture depth (ETD) by following transformation equation (ASTM E1845, 2001).

$$ETD = 0.22 + 0.8 * MPD \quad (2.3)$$

A laser based device, the Circular Texture Meter (CT Meter, Nippo Sangyo, Co, Ltd., Japan) was introduced in 1998 to measure Mean Profile Depth. The CT meter test procedure is presented in ASTM E2157. Figure 2.6 shows segmentation of the surface profile performed by the CT meter. The CT Meter uses a laser to measure the profile of a

circle 284 mm (11.2 in) in diameter or 892 mm (35 in) in circumference. The profile is divided into eight segments of 111.5 mm (4.4 in). The MPD is computed from an average of the eight segment depths (Hanson and Prowell, 2004).

Hanson and Prowell, 2004 conducted CT meter (ASTM E2157, 2001) and sand patch tests (ASTM E 965, 2001) in five locations in each of 45 sections of the 2000 National Center of Asphalt Technology (NCAT) test track. The test track consisted of a wide range of surfaces, like (1) coarse and fine graded superpave mixes, (2) Open graded friction coarse, (3) stone mastic asphalt etc. The CT meter was found to produce comparable result with sand patch test. The study concluded that offset was not significant between sand patch results and the CT meter when open-graded mixtures were excluded. The slope of the best fit line was statistically significant (Hanson and Prowell, 2004). Abe et al., 2002 suggested the following relationship for sand patch MTD and CT meter MPD.

$$MTD = 1.03 \times MPD + 0.15 \quad (2.4)$$

Flintsch et al., 2003 found an excellent correlation ( $r^2=0.94$ ) between the CT meter and sand patch measurements in measurements at Virginia Smart Road. They also found a good correlation ( $r^2=0.88$ ) between MPD (determined using laser profiler) and ASTM E 965, 2001 sand patch test. Sand patch and CT meter tests were conducted on 22 runway and taxiway test sections from the National Aeronautics & Space Administration Wallops Flight facility and 7 surfaces from Virginia's smart road. Sand patch test results and CT meter results showed a remarkable agreement. The MGPS system (owned by FHWA) and CT meter also showed good agreement (McGhee.K. and Flintsch, 2003).

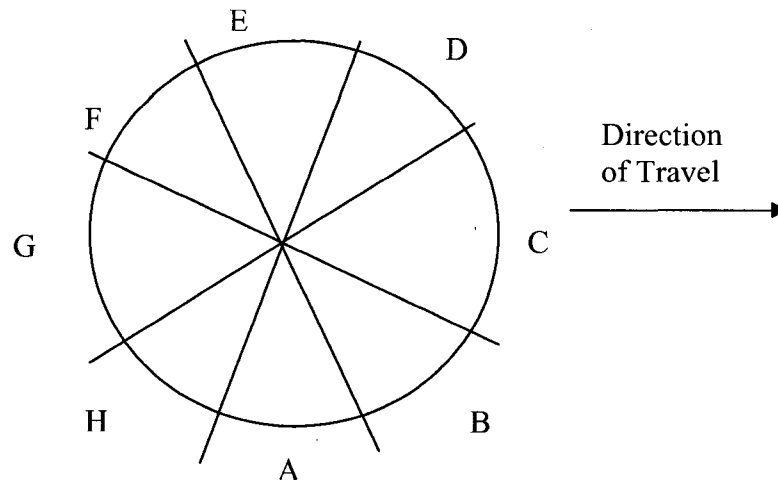


Figure 2.6 Segments of Circular Track Profile (based on ASTM E 2157, 2001)

The Digital Surface Roughness Meter (DSRM) was developed by MaGaNa Instruments, (Rolla, Mo.) for macrotexture measurements. Virginia Transportation Research Council (VTRC) researchers conducted surface measurements of a series of concrete and asphalt surfaces with the DSRM, sand patch and CT meter. They found the DSRM as a better device to use for quick measurements. Results indicated a good correlation among DSRM, sand patch and CT meter. The Study concluded that the DSRM measuring technique was more efficient than the sand patch test (Mokarem, 2006).

Gendy and Shalaby proposed a laboratory technique to measure macrotexture using a four-source photometric stereo system. The system consists of still digital camera (5.1 megapixel with 12 X optical zoom and macro function) and four light sources mounted in a retractable frame to allow angle and height adjustment of light source. An image processing algorithm was developed to compute surface orientation and image intensities. They found good correlation between manual reading using a depth dial gauge and estimated MPDs from photometric stereo method (Gendy and Shalaby, 2007).

### 2.3 PM<sub>10</sub> Measurements from Road Dust

Fine particulate matter emitted from paved roads is primarily generated from loose material on the road surface (CDT, 2000). Particulate matter can be removed by different controls, but loose materials are replenished by other sources, such as wind erosion from surrounding areas, application of ice control compounds and soil carry out from construction activities. The traditional control methodology assumes that paved road silt loading reaches an equilibrium value in the absence of additional silt sources. The equilibrium occurs when the rate at which material suspended and removed from the road surface matches rates of silt deposition. The equilibrium silt depends on different factors. Those are average vehicle speed, the average daily traffic (ADT), number of lanes and average daily traffic per lane, fraction of heavy vehicles traveling, rain or snow fall and presence or absence of curbs and parking lanes (US EPA, 1995).

Roads are classified according to average daily traffic (ADT). The US Department of Transportation classifies roads as Local roads (ADT < 5000), Collector roads (5000<ADT<15000) and Minor arterial roads (15000<ADT<35000), and Major arterial roads (ADT>35000) (Light, 1998).

Particulate matter (PM<sub>10</sub>) emission from paved roads has been studied using an EPA approved AP-42 methodology (EPA, 1993). AP-42 sampling and silt analysis methods are explained in AP-42 appendices C.1 and C.2 (EPA, 1995). Mass emission measurements were calculated using tower-mounted filters located upwind and downwind of a road with a known amount of silt (EPA, 1993). The basic method for upwind-downwind method involves measurement of airborne particulate concentration both upwind and downwind of the pollutant source. Downwind measurement should be

conducted 5 meters from the source and background equipment should be placed 15 m upwind from source. Sampling consists of six to eight PM<sub>10</sub> samplers equipped with volumetric flow control. In addition to PM<sub>10</sub> concentration measurements several other measurements were taken such as, wind speed, traffic counts, travel speed etc. Silt samples were collected by vacuuming dust from paved road surfaces. A series of stepwise regression analyses were conducted with different predictive equations. The following equation was presented in March 1993 for emission factor estimations. (EPA, 1997)

$$E = k(sL)^{0.65} \times (W)^{1.5} \quad (2.5)$$

E = particulate emission factor,

sL= road surface silt loading

W= Mean vehicle weights in Tons

k== particle size multiplier for particle size range and units of interest

Equation 2.5 was modified to account for vehicle exhaust, brake wear; and tire wear (EPA, 2006c).

The following equation is for paved road dust PM<sub>10</sub> emission factor calculation

$$E = k(sL)^{0.65} \times (W)^{1.5} - C \quad (2.6)$$

Where,

E = particulate emission factor

k = particle size multiplier for particle size range and units of interest (The value of K is 7.3 for gm/VMT and 4.6 for gm/VKT)

sL= road surface silt loading (material smaller than 75 μm in gm/m<sup>2</sup>)

The range for road surface silt loading (sL) used for this equation is 0.02-400 g/m<sup>2</sup>

W= average weight (tons) of the vehicles traveling the road

C = correction factor for Emission Factor for vehicle fleet exhaust, brake wear and tire wear (The value of C is 0.2119 for gm/VMT and 0.1317 for gm/VKT)

The MOBILE 6.2 emission model has been used separately to estimate emissions from vehicle exhaust, tire wear and brake wear. PM<sub>10</sub> emission factors calculated from MOBILE 6.2 for vehicle exhaust, tire wear, and brake wear are subtracted from the total to represent the emission factor from road surface dust.

The Desert Research Institute's (DRI) Testing RE-Entrained Kinetic Emissions from Roads (TRAKER) is a mobile technology for PM<sub>10</sub> measurements. TRAKER samples particulate matter in front and behind a vehicle's tire. TRAKER measures the differential concentration of dust suspended by vehicle tire and pavement surface interaction. TRAKER consists of real time aerosol sensors for particulate matter concentration measurement and a Global Positioning System (GPS) for tracking locations of measurements (Kuhns et al., 2001).

Etyemezian et al., 2003a conducted a simultaneous measurement of PM<sub>10</sub> dust emissions behind the TRAKER's tires and PM<sub>10</sub> flux measurement by tower using upwind-downwind methods. Results indicated that the emission factor for road dust was proportional to the cube root of the TRAKER signal. The study concluded that the TRAKER signal increased as the cube of the speed for given road dust loading (Etyemezian et al., 2003a).

The TRAKER was used to investigate the seasonal changes in emissions potential from paved roads and unpaved roads and effect of street sweepers in the Treasure Valley in Southwest Idaho (Kuhns et al., 2003). Kuhns et al., 2003 found no upward or

downward trends in PM<sub>10</sub> emissions potential during summertime and winter sampling for paved roads. The results also showed that no measurable PM<sub>10</sub> emissions potential reduction after street sweeping with mechanical sweeper and vacuum sweeper (Kuhns et al., 2003).

Etyemezian et al., 2003b found that the season, location and setting of a road have significant effect on PM<sub>10</sub> emission potential. Their study concluded that emission potential was higher for a low travel speed road than a high travel speed road. Etyemezian et al., 2005 studied the repeatability and precision of TRAKER with repeated measurements around Las Vegas, NV area over the same roadway. They found that the coefficient of variation varies from 10 % to 70 % and the coefficient of variation decreased with increased speed (Etyemezian et al., 2005).

A vehicle equipped with trailer-mounted real time PM sensors has been used to measure PM concentrations in front of the vehicle and in the vehicle's wake (Fitz and Bufalino, 2002; Fitz, 2005). The system, called SCAMPER (System of Continuous Aerosol Monitoring of Particulate Emissions from Roadways), is a mobile technology for particulate matter emission measurements using particulate matter concentration in front of vehicle and behind the vehicle, in its turbulent wake, using real time PM sensors. It consists of a sampling inlet attached to the vehicle, Global Positioning System (GPS), light scattering optical PM<sub>10</sub> sensors for PM<sub>10</sub> concentration measurements (TSI DustTraks) and a PC to collect data from GPS and PM 10 measuring devices (Fitz, 2005).

An isokinetic sampling probe collects particulate samples from a moving vehicle at a speed of 0 mph to 60 mph. The front probe is located 1.5 m above the ground surface and



0.5 m in front of the front bumper of the test vehicle (Fitz et al., 2005). The emission factor is calculated as the product of the frontal area of the vehicle, and the difference in time-averaged concentration between the front of vehicle and its wake, giving units of mass per distance (Fitz et al., 2005). Fitz et al., 2005 conducted a study in Las Vegas and found that the peak  $PM_{10}$  emission rates were within a factor of two for two days of sampling and that the level of reproducibility was better than silt sampling (Fitz et al., 2005).

#### 2.4 PI-SWERL and Mini-PI-SWERL

The Portable In situ Wind Erosion Lab (PI-SWERL) was developed by the Desert Research Institute for dust emission measurement. This device consists of an annular ring, 51 cm outer diameter, and 39 cm inner diameter which rotates 6 cm above from test surface (Figure 2.7). A fan ventilates the chamber at a constant rate. Irwin sensors were used to measure PI-SWERL shear stress at different RPMs. An Irwin sensor is an omnidirectional friction meter which measures vertical pressure gradient near surface (Irwin, 1981). For calibration the PI-SWERL, was placed on a smooth plywood surface containing the Irwin sensors.

Etyemezian et al., 2007 found that the average flow inside the PI-SWERL is at steady state and the flow is symmetrical about the ring's axis of rotation. They concluded that PI-SWERL measured dust emissions from soil surfaces of varying wind erodibility (Etyemezian et al., 2007). Sweeny et al., 2008 compared PI-SWERL dust emissions with dust emission measurements from a straight-line wind tunnel at 32 different fields setting

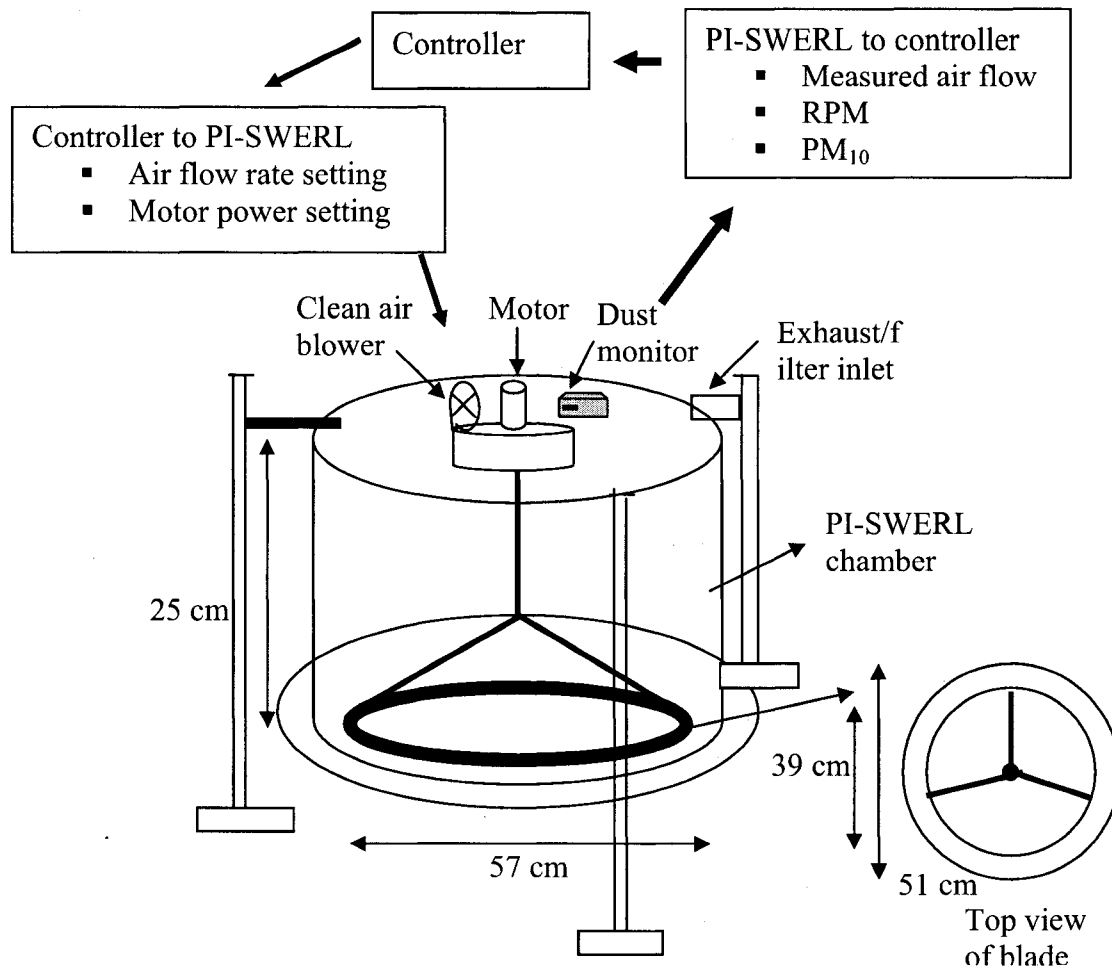


Figure 2.7 PI-SWERL Schematic Redrawn from Etymezian et al., 2007

and test condition in the Mojave Desert of Southern California. The experimental data showed a good agreement between two instruments, but deviations were found for densely packed gravel surfaces (Sweeney et al., 2008).

DRI also developed the Mini-PI-SWERL™ which is a smaller version of the PI-SWERL (Figure 2.8). The internal diameter of the chamber is 30 cm and internal height is 20 cm. The annular blade rotates 5.2 centimeters from ground surface.

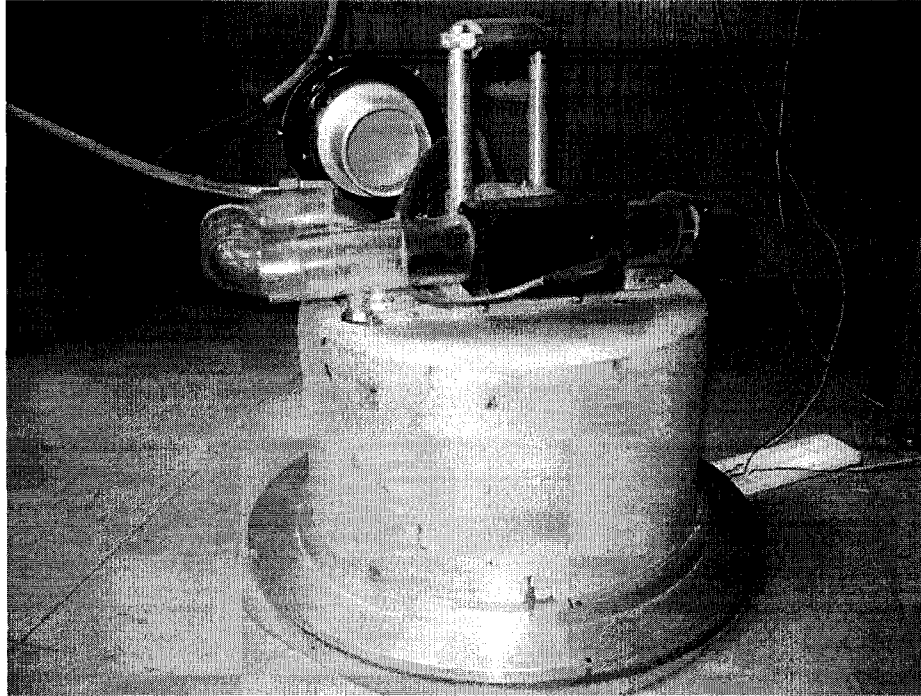


Figure 2.8 Mini-PI-SWERL™ (photo taken by Rodrigues, 2006)

The Mini-PI-SWERL was used by Rodrigues, 2006. She measured emissions factors with the Mini-PI-SWERL and compared them to AP-42 emissions factors at 30 sites. Rodrigues, 2006 found that shear produced by Mini-PI-SWERL™ ranged from 0.06 to 0.73 N/m<sup>2</sup> which is higher than the estimated aerodynamic shear produced by a vehicle undercarriage (Rodrigues, 2006).

## 2.5 Friction Velocity and Threshold Friction Velocity

Air flow rates near the ground surface are slowed because of friction from surface roughness. A logarithmic velocity profile has been found to describe the near-surface wind speed profile (EPA, 1988). The mathematical form of the velocity profile is stated as follows:

$$u(z) = (u^* / k) * \ln(z / z_0) \text{ Where } z > z_0 \quad (2.7)$$

$u$  = Wind speed, cm/s

$u^*$  = Friction velocity, cm/s

$z$  = Height above test surface, cm

$z_0$  = Roughness height, cm

$k$  = Von Karman's constant (0.4)

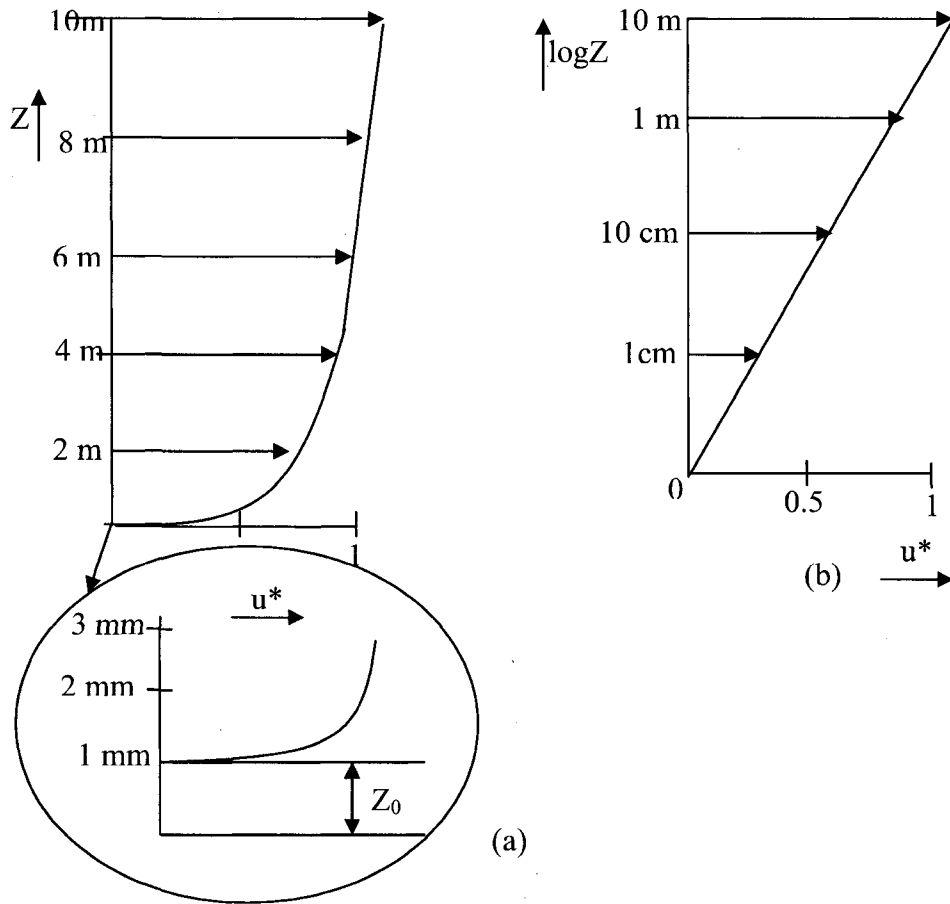


Figure 2.9 Illustration of Logarithmic velocity profile, (a) Arithmetic (b) Semi logarithmic representation (Source: EPA, 1988)

Friction velocity is a near-surface wind shear stress which is responsible for wind erosion from erodible surfaces. Friction velocity ( $u^*$ ,  $\text{ms}^{-1}$ ) is equal to square root of the surface shear stress ( $\tau$ ,  $\text{N m}^{-2}$ ) divided by the density of air ( $\rho$ ,  $\text{kg m}^{-3}$ ).

$$u^* = \frac{\tau}{\rho} \quad (2.8)$$

Friction velocity ( $u^*$ ) can be calculated from an experimentally-determined logarithmic velocity profile. The following equation provided by the EPA manual (US EPA, 1988) for calculating friction velocity:

$$u^* = A * u_{10} \quad (2.9)$$

Where A is a function of roughness height ( $Z_0$ ) and  $U_{10}$  is the wind speed measured at height of 10 meters. The expression for A is

$$A = k / \ln(10 / Z_0), \text{ Where } k=0.4 \quad (2.10)$$

Roughness height is calculated from the z intercept of the velocity profile. Aerodynamic roughness height can be related to physical roughness height by

$z_0 = \varepsilon / 30$  Where  $\varepsilon$  is mode size of non erodible particles (Chepil, 1952, Gillette, 1980).

Wind erosion starts when the friction velocity exceeds a particular friction velocity which is called the threshold friction velocity. Threshold wind speed produces a critical shear force on soil surface to initiate particle transport particle (Bagnold, 1941 as cited in EPA 1988). Therefore, the threshold friction velocity (TFV, or  $u^*t$ ) is defined as the critical velocity for initiation of soil particle movement. TFV depends on different parameters such as soil texture, surface crust, size and number of roughness elements, vegetation distribution and soil moisture. On a clean asphalt surface,  $u^*t$  can be defined as a function of only aggregate particle size. A simple expression was developed for  $u^*t$

considering balance between driving forces (aerodynamic drag and lift) and the retarding forces (cohesion and gravity). Garland, 1983, as cited in EPA, 1988, found that the critical shear force is proportional to the square of the threshold friction velocity.

Several theories have been developed that use threshold friction velocity for soils with uniform and spherical aggregates spread loosely over dry and bare surfaces. Bagnold (1941), as cited in US EPA 1988, found that threshold friction velocity varied as the square root of the diameter of particle size,  $u^* \propto \sqrt{d}$ , considering the balance between aerodynamic drag and gravity force (Bagnold, 1941, cited in EPA, 1988) (Figure 2.10). This expression is valid for particle sizes larger than 100  $\mu\text{m}$ .

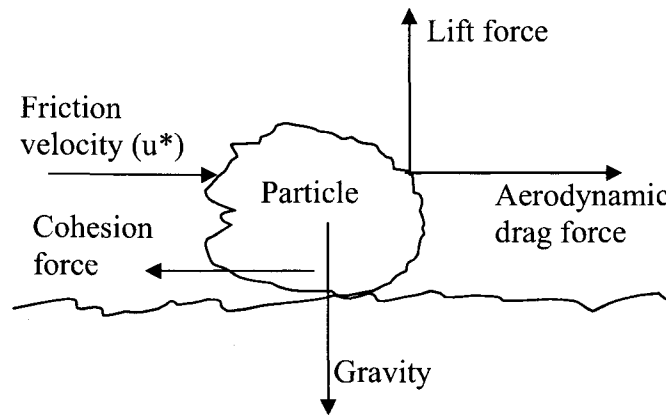


Figure 2.10 Forces Acting on Particle at Threshold Movement

The following expression was recommended for  $u^*$  calculation on the basis of wind tunnel measurements by Greeley and Iverson, 1985

$$u^*_{t} = \sqrt{A_N(\sigma_p g d + \gamma / \rho d)} \quad (2.11)$$

Where  $A_N$  is around 0.0123,  $\gamma$  is around  $3 \cdot 10^{-4} \text{ kg s}^{-2}$ ,  $\sigma_p$  is the particle to air density ratio,  $g$  is acceleration due to gravity and  $d$  is particle size (meters) (Shao and Lu, 2006).

The EPA manual, (EPA, 1988) described the procedure for estimating threshold friction velocity for an uncrusted surface with a dry aggregate soil structure. The mode size of the dry aggregate is rapidly determined by a hand sieving test of surface soil, developed by Chepil, 1952 as cited in EPA, 1988. EPA, 1988 uses a relationship developed by Gillette, 1980 to determine threshold friction velocity from the mode of the aggregate size distribution. The relationship is shown in Figure 2.11. The slope of Gillette's line shows that threshold friction velocity varies with mode size raised to the power 0.4.

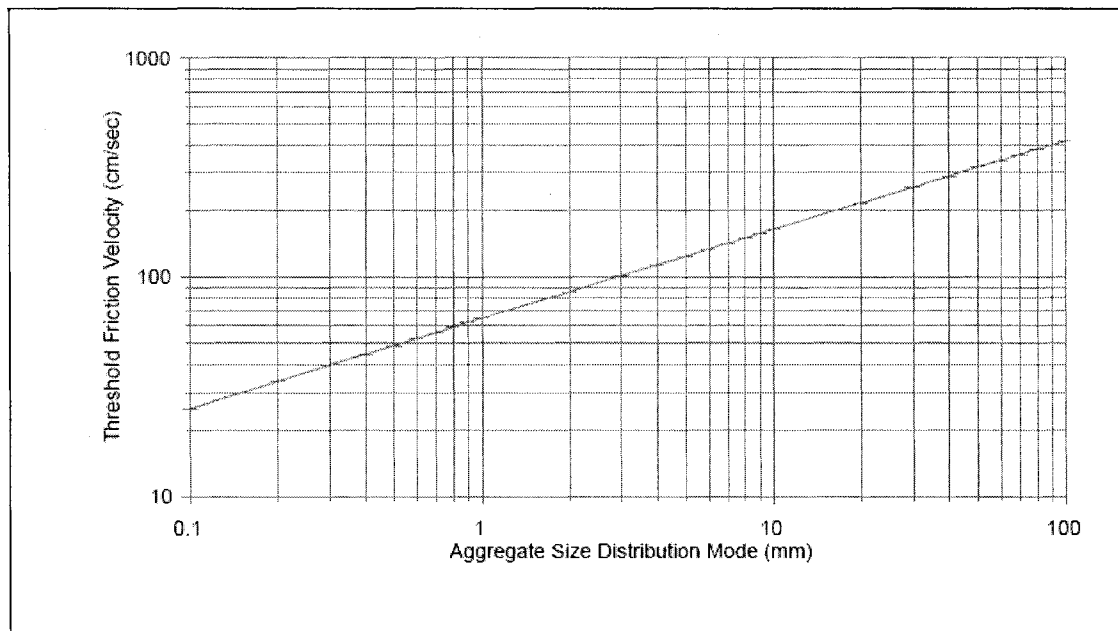


Figure 2.11 Gillete Relationship of Threshold Friction Velocity to Size Distribution Mode (Source: EPA Manual, Cowherd et al., 1988)

EPA characterizes the erodible material site either a “limited reservoir” or “unlimited reservoir” for selecting correct wind erosion equation. Unlimited reservoirs are defined as bare surfaces of finely divided material. A limited reservoir is defined to consist of large aggregates and non erodible surface protrusions (EPA, 1988). The expression for erosion potential (P) for a dry and exposed surface (for limited erosion potential) is (Eq.6-3, EPA 1988)

$$P = 58(U^* - U^*_t)^2 + 25(U^* - U^*_t) \quad (2.12)$$

$$P = 0 \text{ for } U^* \leq U^*_t$$

Where,

$U^*$  = Friction velocity (m/s)

$U^*_t$  = Threshold friction velocity (m/s)



## CHAPTER 3

### MATERIAL AND METHODS

#### 3.1 Summary

Road soil samples were recovered and analyzed according to the US Environmental Protection Agency (EPA). AP-42, standard method for estimating particulate matter (PM<sub>10</sub>) emission factors from paved road dust by brushing and vacuuming the road surface (US EPA 1993). The recovered samples were sieved to determine the silt fraction of the soil. The sampled soil was sieved according to EPA's AP 42 method, section 13.2.1, Appendix C.2 (US EPA 1993). The sieve stacks consist of 3/8 inch, 4, 10, 20, 40, 100, 140 and 200 mesh sizes. Silt fractions were reported as mass passing by the 200 mesh (75 micron). The PM<sub>10</sub> emission factor was calculated from an equation provided by EPA. Silt samples were collected from 13 sites.

Pavement textures were measured at all 13 AP-42 sampling sites. Two techniques were applied for pavement texture measurement. The first technique was the sand patch method which is a volumetric technique of pavement macrotexture depth measurement described in the ASTM standard E965 (ASTM, 2001). The sand patch method determines the average depth of pavement surface macrotexture. The second technique was Digital Surface Roughness Meter (DSRM) which is a laser based method for macrotexture measurement.

The Mini-PI-SWERL sampling was conducted by using the Desert Research Institute's Mini-PI-SWERL™ to estimate mass emission rate and cumulative mass emitted from pavement surfaces. Mini-PI-SWERL™ samplings were completed in all 13 sites which have varieties of pavement surfaces (texture variation) to find out the relationship between pavement surface texture and emission rate. Additional Mini-PI-SWERL™ experiments were conducted in the Thomas & Mack parking lot to estimate depletion rate of particulate matter from rough and smooth surfaces.

### 3.2 Materials

The following materials were used during, the AP-42 sampling

1. Two Hoover Wind Tunnel plus® canister vacuum cleaners (model S 3639), with motors rated at 12 amperes and rated at 3750 watts.
2. Two portable 120 volt Coleman generators
3. Hoover vacuum cleaner bags( type S Allergen Canister)
4. Pelouze SP5 postal scale and Sunbeam Freightmaster® 150 scale ( has readability of  $\pm 1$  gram , calibrated with Rite-O-Weigh® brass weights meeting ASTM class 6 adjustment tolerance)
5. Hoover hard floor tool
6. Masking tape (1 inch) for laying out the sampling area
7. Vacuum cleaner exhaust filter
8. Push broom
9. Power cord
10. Extension cord

11. Wrap rolls for wrapping the vacuum cleaner bag
12. Sample layout Strings ( 10×10, 10×11.5, 10×12, 10×13.5, 10×15 ft)
13. Four standard bricks to set corners of sample plots
14. Brown envelop for storing vacuum cleaner bags
15. Tape measure 25 ft

The following materials were used for the sand patch experiment

1. Glass spheres having 90% roundness in accordance with ASTM test method D1155 and with a minimum of 90% by weight passing a ASTM 60 sieve (250  $\mu\text{m}$ ) and retained on a ASTM 80 sieve (180  $\mu\text{m}$ ) (McMaster-Carr Supply Co, CA)
2. 25 ml plastic graduated cylinder
3. A ice hockey puck as a spreader tool (162 gram, and 7.5 mm diameter)
4. Wind screen to protect the material sample from wind and turbulence created by traffic (19 ft × 31 ft)
5. Soft bristle hand-held brush to clean pavement surface
6. Portable digital strain-gauge based laboratory balance (readable to  $\pm 0.1$  gram) (Acculab, PP-201)

The following materials were used for DSRM measurement

1. Digital Surface Roughness Meter (MaGaNu Instruments, Rolla, MO)
2. DSRM battery
3. Video Capture Essential PCMCIA card
4. Video receiver
5. Receiver battery

6. Dell laptop with PCMCIA slot (running Windows XP)
7. DSRM Calibration plate, provided by MaGaNa Instruments

The following materials were used during the Mini-PI-SWERL™ experiment

1. Mini-PI-SWERL™ , developed by the Desert Research Institute (loaned from DRI, Las Vegas)
2. Mini-PI-SWERL™ control box (DRI)
3. Gateway laptop (Solo 9550 model) running Windows XP
4. TSI DustTrak™ (model no 8520) Aerosol Monitor (serial no 21622)
5. Two 12 volt car batteries
6. Power cable for the control box
7. Two connectors for connecting two 12 volt batteries in series
8. Connection cable for Mini-PI-SWERL™ and control box
9. Two 9-pin serial ports cables to connect the laptop to the Control box and control box with DustTrak
10. White water soluble paint to mark Mini-PI-SWERL™ footprint

### 3.3 Site Selection Survey

Sampling sites were selected from previous Clark County AP-42 sites (phase I to phase IV, all quarters). There was a total of 27 sampling sites from Phase I to Phase III and one site (Veterans Memorial Blvd, Boulder City) from phase IV studies. Clark County and UNLV arranged a field survey on August 29, 2007 and September 4, 2007 to survey and evaluate the sampling sites for Phase V study. Photographic surveys were made of 24 AP-42 sampling sites from the Phase II and III studies. Close-up photos of

pavement surfaces with a ruler were taken using Canon Power shot (PS1 model, 3.2 mega pixel) camera. Figure 3.1 shows the close up photo of Burkholder & Cabrillo pavement surface.

Average sizes of the aggregate and aggregate classification were estimated from the close up photos by counting the number and size of aggregates along the ruler. Table 3.1 shows the aggregate size distribution of Burkholder & Cabrillo site.

Figure 3.2 shows an example of aggregate size distribution of asphalt concrete pavement surface (Burkholder & Cabrillo site).

Table 3.1 Aggregate Size Distribution of Burkholder & Cabrillo Site

<u>Category</u>	<u>Count(f)</u>	<u>Percent</u>	
<1mm	0	0.000	
1-2mm	0	0.000	
2-3mm	1	0.022	
3-4mm	5	0.250	
4-5mm	4	0.200	
5-6mm	5	0.250	
6-7mm	3	0.150	
7-8mm	1	0.050	
8-9mm	1	0.050	
9-10mm	0	0.000	
Total	20	0.972	

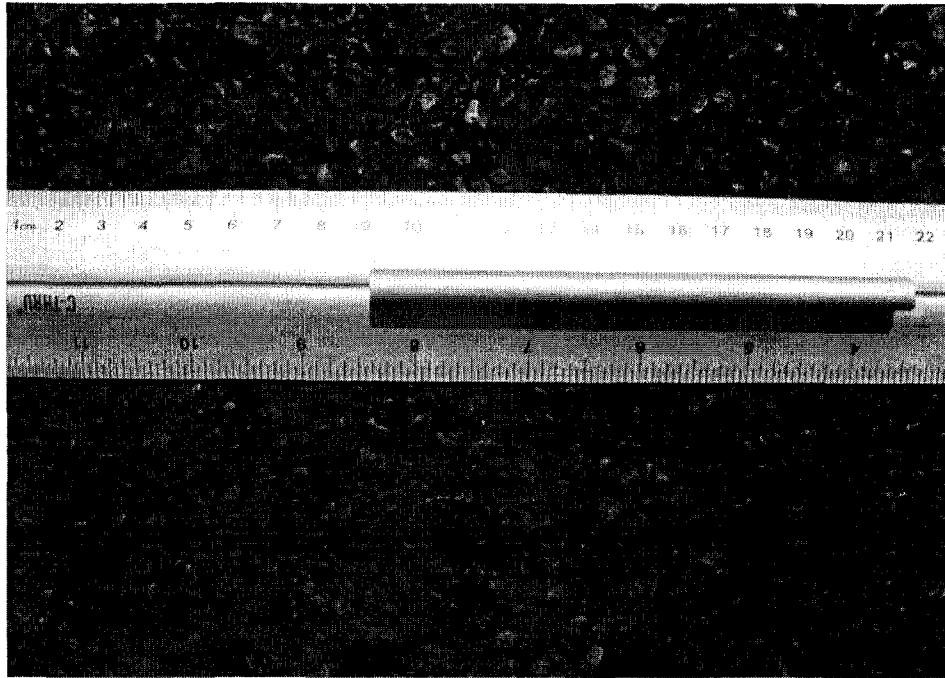


Figure 3.1 A Close-up Photo of Pavement Surface with a Ruler (Burkholder & Cabrillo)  
Taken during Fall 2007 Photographic Survey

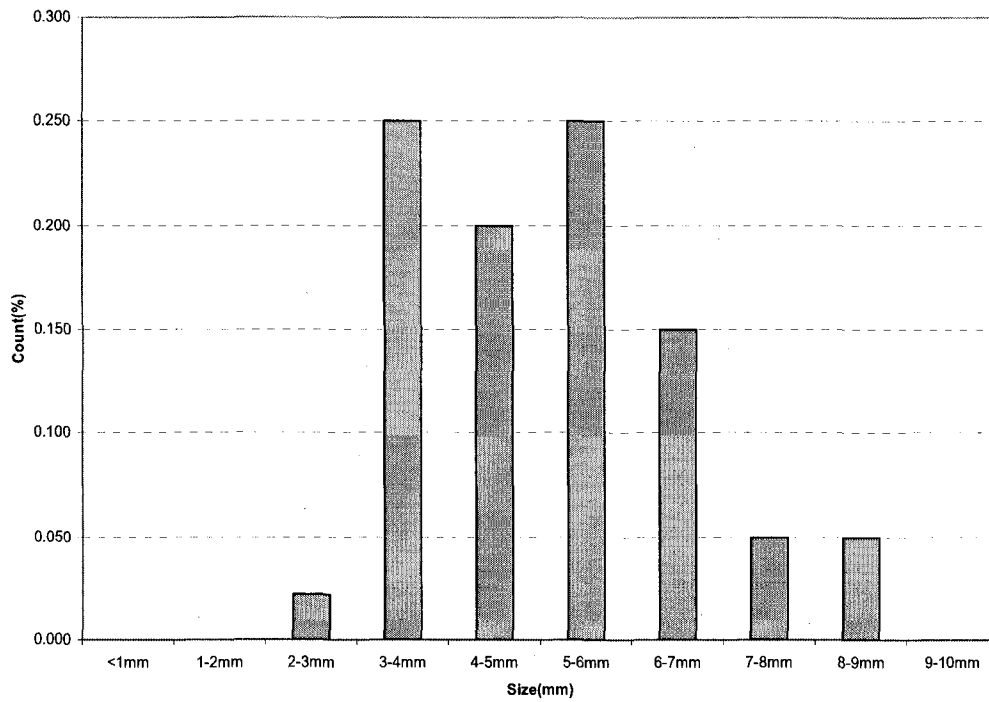


Figure 3.2 Aggregate Size Distributions for Burkholder & Cabrillo Pavement Surface

Preliminary sand patch experiments were conducted at the Ione, Duneville and Crestdale sites to evaluate the pavement surface texture. As a part of the site selection process, these evaluations were made because of observed variations in macrotexture across a road travel lane due to pavement wear.

Figure 3.3 is the aerial photo of sand patch measurements experiment in Crestdale & Covington Cross site.



Figure 3.3 Sand Patch Experiment (Crestdale & Covington Cross)

Preliminary size classification and pavement condition analyses were completed from the photographic survey. UNLV and Clark County developed a list of 13 sites for the Phase V study after evaluating pavement aggregate size distribution, and pavement surface conditions (sealed or not sealed). Table 3.2 shows all 24 evaluated sites road dust sampling.

Table 3.2 AP-42 Sampling Sites for Phase V

Site Name	Roadway Type	Aggregate Classification	Sealed	Mean (mm)	Sampled
Ann	Minor Arterial	Medium-coarse	No	4.18	Yes
Armocost	Local	Medium	?	3.59	Yes
Bonanza	Collector	Fine	Yes	0.97	No
Burkholder†	Collector	Coarse	No	5.05	Yes
Crestdale †	Collector	Fine	Yes	1.66	Yes
Duneville	Local	Medium	No	3.31	Yes
Durango	Minor Arterial	Very coarse	No	6.65	No
El Capitan	Collector	Fine-medium	Semi-sealed	2.88	No
Evergold	Local	Fine	Yes	1.97	Yes
Gowan	Collector	Coarse	Semi sealed	4.97	No
Hacienda	Collector	Medium-coarse	No	4.76	No
Ione	Collector	Fine	Sealed	1.86	Yes
Losee	Minor Arterial	Coarse	Yes	5.03	No
Maryland & Pyle	Minor Arterial	Very coarse	Possibly sealed	6.44	No
Maryland/Westminster	Minor Arterial	Medium-coarse	No	4.89	Yes
Pabco road	Collector	Medium	No	3.80	No
Pecos	Collector	Fine-medium	?	2.13	No
Quailbush		Fine-medium	Yes	2.74	No
Richmar	Local	Fine	?	1.97	Yes
Sapphire Light	Local	Fine	Yes	1.81	Yes
Silver Spring	Minor Arterial	Fine-medium	Yes	2.20	Yes
Valle Verde	Minor Arterial	Fine-medium	Semi sealed	2.33	No
Veterans Memorial Blvd	Collector	Fine-medium	Yes	2.01	Yes
Washburn	Collector	Coarse	Yes	5.17	No

† Crestdale & Covington Cross and Burkholder & Cabrillo sites labeled as 1 & 2 as they were sampled twice, because of equipment failure for other experiment.



### 3.4 Sampling Schedule

UNLV and Clark County sampled for texture and PM<sub>10</sub> emissions on March 18th, March 24th and March 31st week, 2008. The schedules were set up to minimize travel time between sites. The barricade scheduling was prepared by Mr. Russ Merle from DAQEM. The request was sent to the Trench Plate for scheduling of road barricading.

Table 3.3 shows the sampling schedule for phase V road dust sampling. Generally two sites were sampled everyday, one in the morning and the one in the afternoon. Two local roads (Evergold & Coral Sea and Armacost & Calmar) were selected for the first day to develop coordinated crew procedures as these two sites are spacious with low traffic.

The Maryland & Westminster site was postponed due to barricading problem from March 20<sup>th</sup>, 2008 to March 26<sup>th</sup>, 2008. Two other “cushion days” were used as there were equipment problems with the Mini-PI-SWERL™ and DSRM on March 21<sup>st</sup> and March 24<sup>th</sup> (Burkholder & Cabrillo and Crestdale & Covington site). These sites were visited again on March 26<sup>th</sup> and April 22<sup>nd</sup> respectively (Table 3.3).

Table 3.3 Sampling Schedule for Phase V

Sampling Date	Site	Classification	Jurisdiction	Plot Size	Plot Sampled for AP-42
3/18/2008	Evergold & Coral Sea	Local	Henderson	12×10	3
3/18/2008	Armacost & Calmar	Local	Henderson	11.5×10	3
3/19/2008	Goldhill & Richmar	Local	Henderson	11×10	6
3/19/2008	Ione & Coral Sea	Collector	Henderson	12×10	3
3/20/2008	Silver Spring & Spring Hill	Minor Arterial	Henderson	15×10	3
3/21/2008	Pabco & Tabony	Collector	Henderson	11×10	4
3/21/2008	Burkholder & Cabrillo 1	Collector	Henderson	11×10	3
3/26/2008	Maryland & Westminster	Minor Arterial	Las Vegas	11×10	3
3/26/2008	Burkholder & Cabrillo 2	Collector	Henderson	11×10	4
3/27/2008	Duneville & Oakey	Local	Las Vegas	11×10	3
3/27/2008	Crestdale & Covington Cross 1	Collector	Henderson	12×10	3
3/28/2008	Sapphire Light & Emerald Stone	Local	North Las Vegas	12×10	3
3/28/2008	Ann & San Mateo	Minor Arterial	North Las Vegas	12×10	3
3/31/2008	Veretans Memorial Blvd	Collector	Boulder City	13.5×10	13
4/22/2008	Crestdale & Covington Cross 2	Collector	Henderson	12×10	5

### 3.5 AP-42 Silt Sampling and Emission Factor Estimation

Silt recovery was conducted at all 13 sites according to the EPA AP-42 method. Normally silt recoveries were performed on only one day however the AP-42 silt recovery was performed twice at Burkholder & Cabrillo and Crestdale & Covington Cross due to equipment failure on the first sampling day. Silt was recovered from three AP-42 locations, south end, north end and near tower at the Veterans Memorial Blvd site. Three plots were usually sampled per site but sometimes more than three plots were vacuumed to recover a minimum mass of 100 grams of road soil.

Four bricks and bi-colored string-squares were used to layout the rectangular plots for AP-42 sampling. The sizes of the plots were adjusted to maintain the width of the barricading area and traffic conditions. The various plot sizes in feet are shown in Table 3.3. Masking tape was used to mark the rectangular plot. Tape was removed after soil recovery. Two sets of strings with gravel filled can attached at ends were used to subdivide the rectangular plot during vacuum soil recovery.

Vacuum cleaner tare bags were pre weighed in the lab and the tare mass was labeled on the top of the bag. The Vacuum cleaner bag was installed in the vacuum cleaner. The vacuum cleaner was connected to the generator with an extension cord. Two sets of vacuum passes were completed parallel to the travel direction and two passes across the travel direction. Stepping on the AP-42 plots was avoided until after all four silt recovery passes had been completed. The vacuum cleaner bag was weighed after vacuuming one plot and again installed into the vacuum cleaner. One bag was used per site. After completing all the plots in one site the vacuum cleaner bag was sealed with a polythene

film. The sealed bag was kept in a 10" × 14" envelope and labeled with date, ID no and bag no.

Envelopes were sent to Ninyo and Moore, contracted with Clark County for sieving. The sieving was performed according to the AP-42 method described in appendix C2, US EPA 1993 b. Recommended U.S. standards sieve sizes are 3/8 in. No.4, No.40, No.100, No.200, and pan. Usual shaking time was 20 minutes. Ninyo and Moore completed 'blind sampling' as they didn't know the sampling locations. Figure 3.4 illustrate a typical plot layout for AP-42 sampling and Mini-PI-SWERL™ measurements.

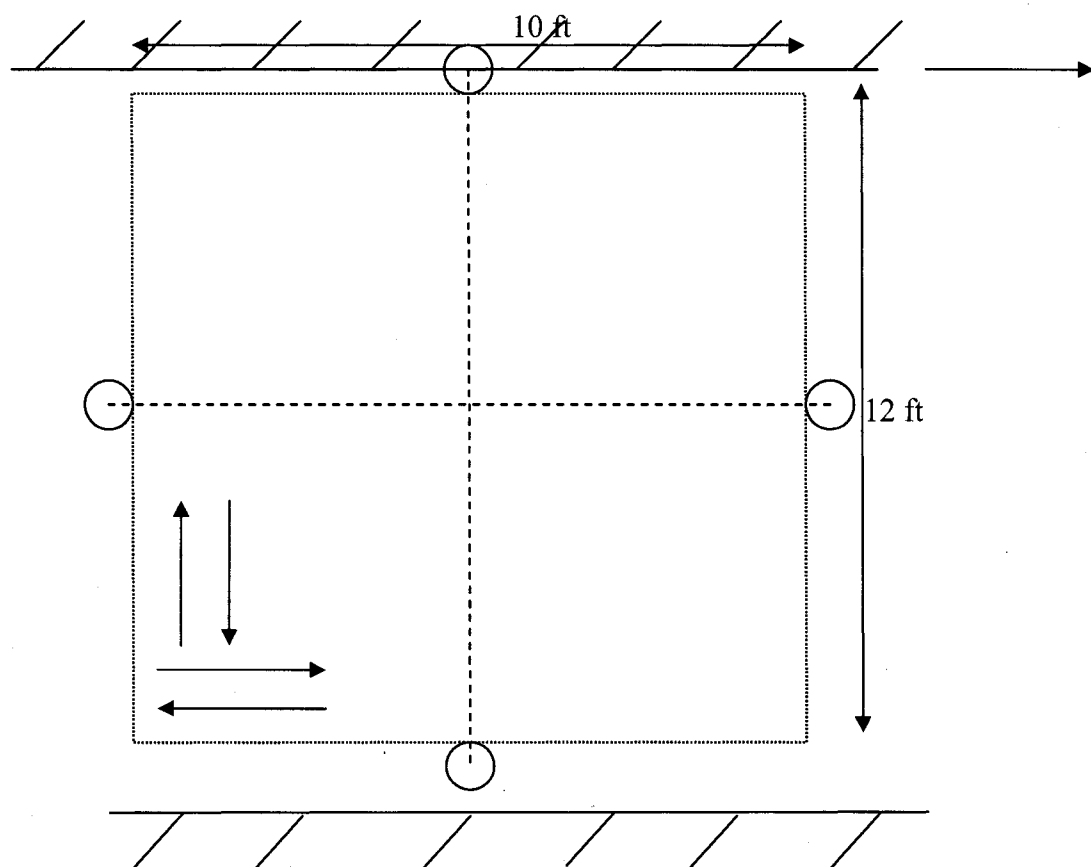


Figure 3.4 Typical Soil Recovery Layout (Arrows illustrate direction of vacuum wand movement in each subsection)

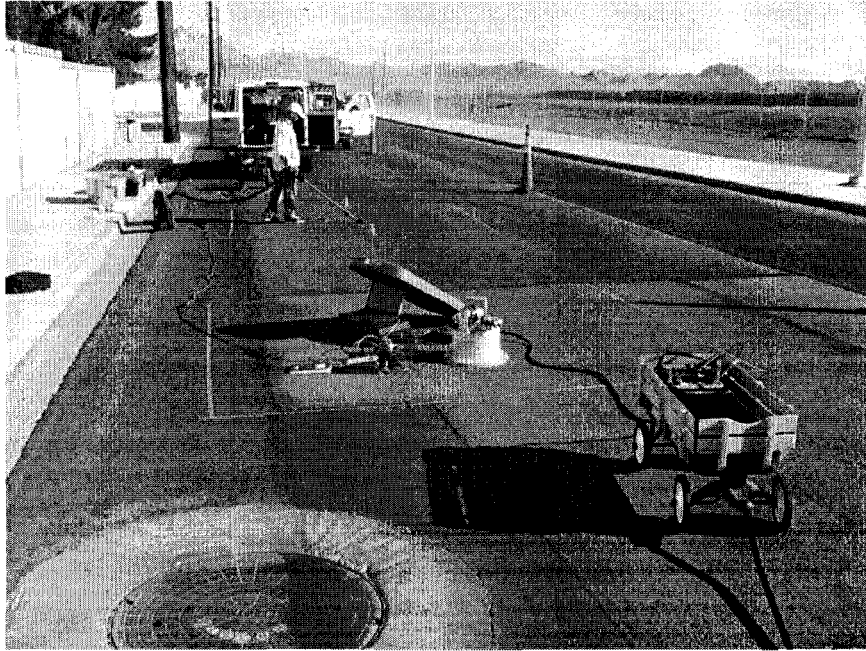


Figure 3.5 AP-42 Silt Recovery Sampling (Pabco & Tabony)

### 3.6 Sand Patch and DSRM Test

The sand patch and DSRM experiments were conducted on every Mini-PI-SWERL™ footprint to estimate the average mean texture depth of that area. Figure 3.6 illustrate a typical site layout for sand patch and DSRM. The Mini-PI-SWERL™ test area is 0.0707 m<sup>2</sup>. The sand patch test was completed in the middle of Mini-PI-SWERL™ footprint after all other measurements had been made. Normally four sets of DSRM measurements were taken within the circumference of a circle. Sometimes the DSRM output provided the out-of-range values. If this happened, the data were discarded and additional measurements were taken in either the center of the Mini-PI-SWERL™ footprint circle or elsewhere within the circumference of the Mini-PI-SWERL™ footprint.

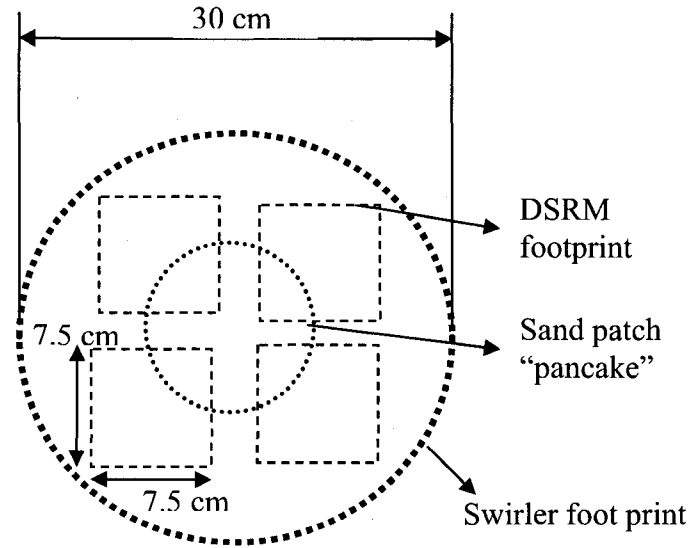


Figure 3.6 Experimental Set up for DSRM and Sand Patch

### 3.6.1 Sand Patch Method

The tested areas had already been cleaned by AP-42 method. The soft bristle brush was used to remove the left over material; from the controlled Mini-PI-SWERL™ experiments. The known volume of cylinder was filled by glass spheres and mass of the glass spheres was determined by the field balance. The mass was adjusted to within  $\pm 0.1$  gram of 37.8 grams. The measured volume of glass spheres was poured on the cleaned pavement surface within the area protected by wind screen. The glass spheres were spread on the pavement by moving the ice hockey puck in a circular motion in order to make a flat “pancake” of glass spheres on the asphalt surface. The sphere pile was spread out outward until the hockey puck couldn’t push them any further out. The diameter of the sand patch pancake was measured six times, and the average diameter was calculated.

The internal volume of the sample cylinder is

$$V = \pi \times (d^2) / 4 \times h \quad (3.1)$$

Where:

V= Known volume of the pancake (25000 mm<sup>3</sup>)

d= Average diameter of pancake (mm)

h = Pancake height (mm), which is interpreted as the mean texture depth (MTD)

Equation 3-1 can be rearranged to

$$MTD = 4 \times V / \pi \times d^2 \quad (3.2)$$

MTD = Mean texture depth of pavement macrotexture

Figure 3.7 explains the sand patch test and Figure 3.8 shows that valleys of pavement surface filled with glass beads.

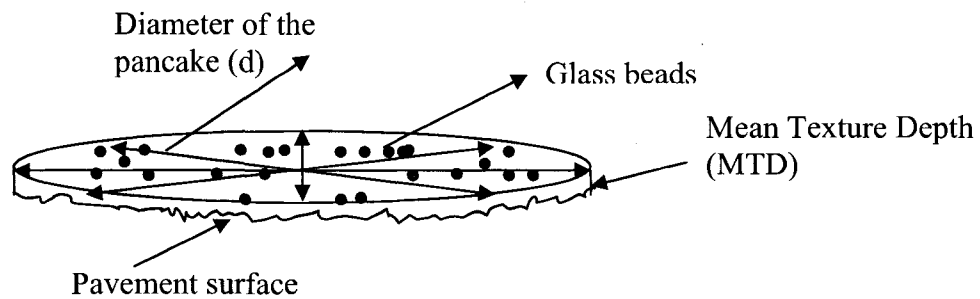


Figure 3.7 Schematic of sand patch test

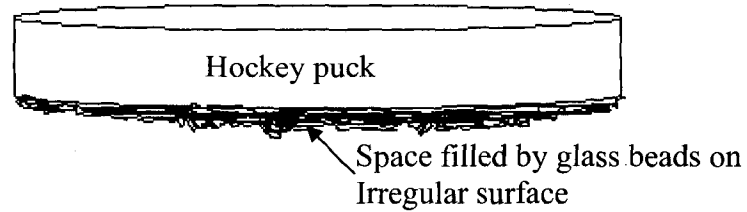


Figure 3.8 Side View of Pavement Surface after Sand Patch Test

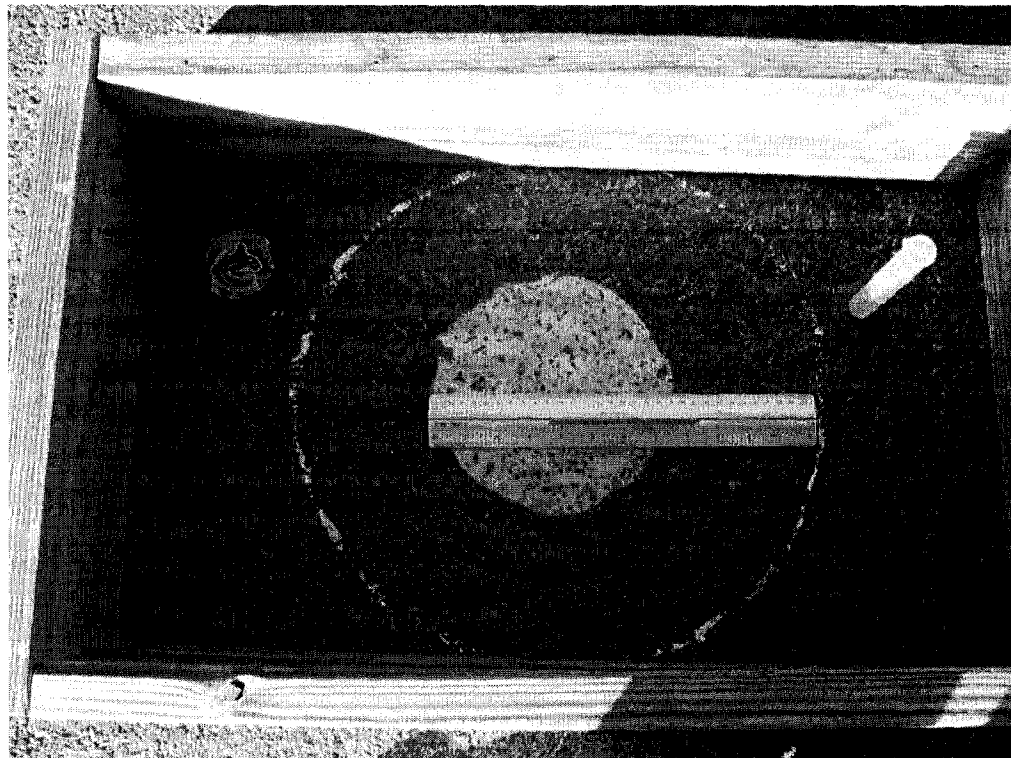


Figure 3.9 Sand Patch Test (Per ASTM E 965, 2001)

### 3.6.2 Digital Surface Roughness Meter Method

An electronic photograph was recorded of the displacement of five laser lines across a 7.5 cm \* 7.5 cm pavement surface. Each laser line produces 630 data points within each pixel representing 0.08 mm on the surface. A video transmitter transfers the image from DSRM to laptop through a Bluetooth connection. The electronic photos analyzed with



the ConcRuf software for displacement of the laser lines. Geometric principles are used to calculate the surface roughness which caused the observed displacement.

The calibration was used to adjust the amplitude and the angle measurements so that all the DSRM units read the same. The DSRM was calibrated with the standard calibration plate provided by MaGaNa Instruments. The basic ConcRuf software program was used to calibrate the DSRM. The amplitude scalar value was set after amplitude calibration. The amplitude and angle were both calibrated.

Before field measurements, the angle of the laser was checked and adjusted accordingly so that top edge of each laser line lies between the guidelines on the edge of the image, shown in Figure 3.10. The angle of the laser was fixed by adjusting the set screws on the laser end of DSRM with supplied screw driver (DSRM Manual).

The Digital Surface Roughness Meter (DSRM) was set inside the circumference of the Mini-PI-SWERL™ footprint. DSRM measurements were taken in four locations occurring on the same pavement surface where sand patch measurement were taken

The basic ConcRuf software program was provided with DSRM which calculates several surface characteristics. They are listed in the Table 3.4 with their definitions. The most important parameter is the average peak to valley roughness (R) value. The R value represents the average of all individually measured peak to valley heights. The R value is fundamentally similar to the MPD calculated by the CT meter. ASTM standard E 2157 recommended that the relationship for the estimated MTD computed from the CT meter's MTD is

$$MTD = 0.947 \times MPD + 0.069 \quad (3.3)$$

when MTD and MPD are expressed in millimeters.

Values shown in Table 3.4 are the output file (transferred from text file) calculated in ConcRuf software. The raw profile (pixel data) data saved in a .CSV file and the photos of the analyzed surface are saved in a .BMP file.

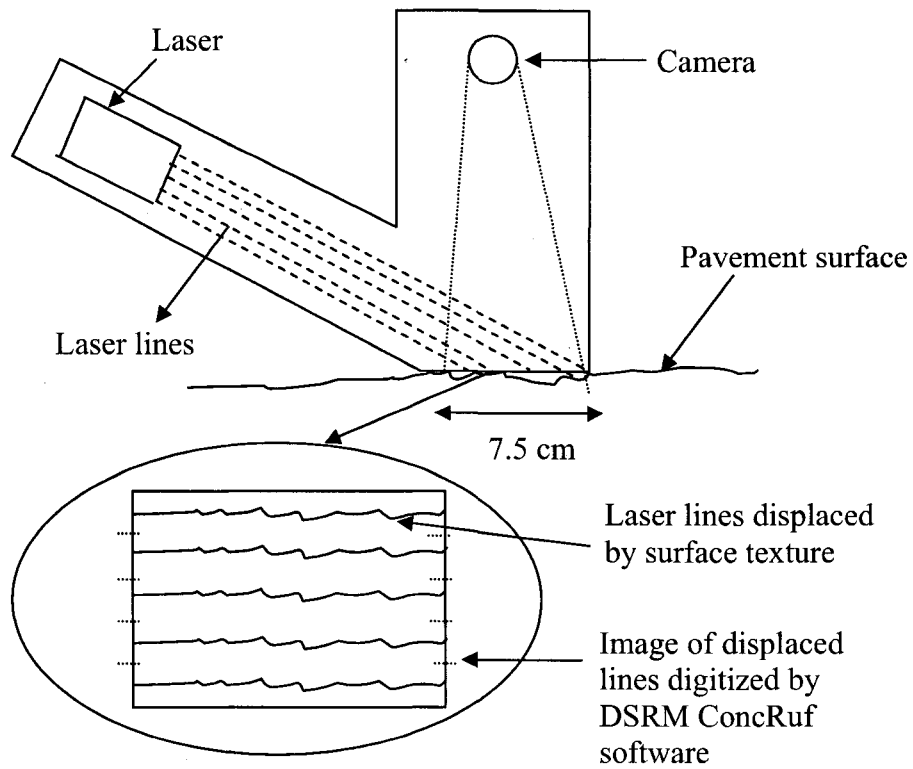


Figure 3.10 Schematic of Digital Roughness Meter (Not drawn to scale)

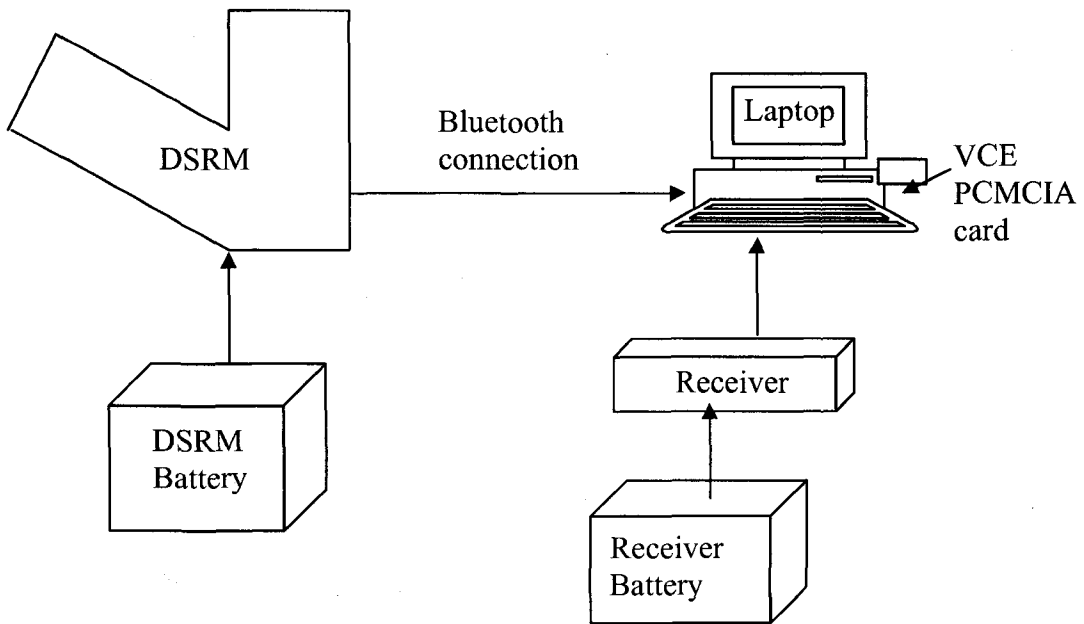


Figure 3.11: DSRM Setup

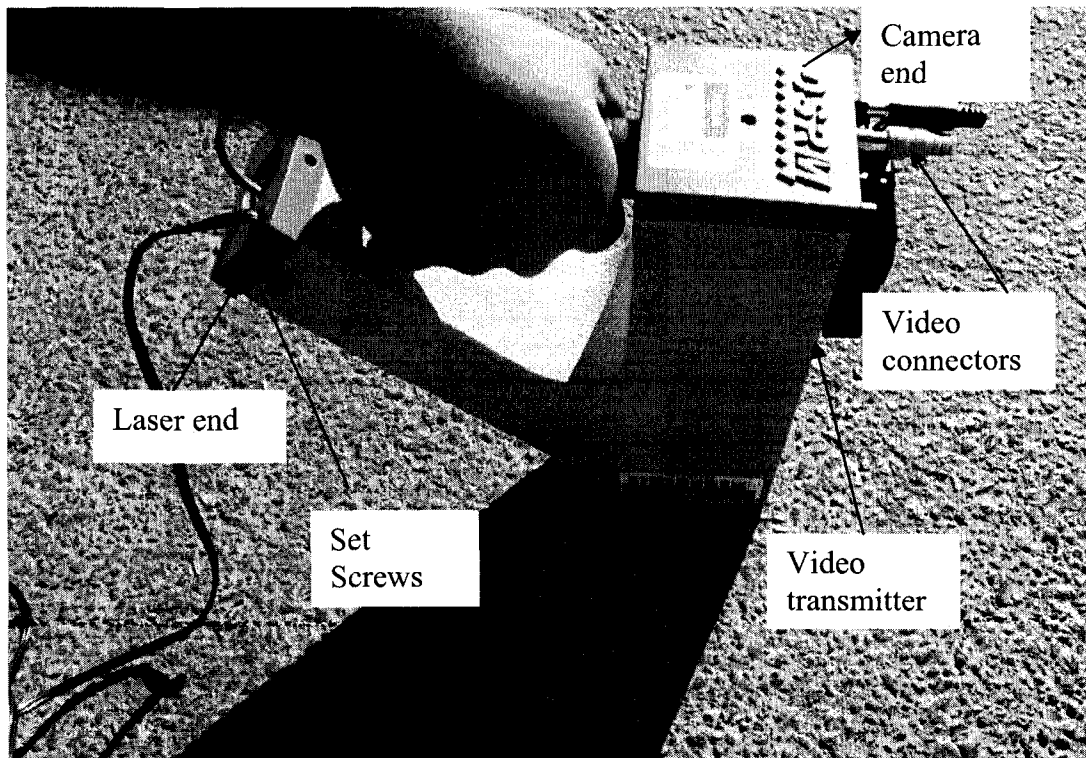


Figure 3.12 Digital Surface Roughness Meter

Table 3.4 DSRM Standard outputs (MaGaNa Instruments email correspondence)

Output	CLA	RMS	Rmax	MSV	Rz	Re	Rp	R
Meaning	Centerline average(mm)	Root mean square(mm)	Maximum peak to valley roughness height, mm	Mean square value, (mm) <sup>2</sup>	10 point height (mm)	Leveling depth (mm)	roughness profile index	Average peak-to-valley roughness, (mm)
Definition	Average of absolute values of heights above centerline	Square root of average of (squares of heights above centerline)	Vertical distance between highest peak and lowest valley	Average of squares of heights above centerline	10-point height, measures average vertical distance between five highest peaks and 5 lowest valleys	Vertical distance from highest peak to centerline profile	Ratio of true length of a fracture surface to its projected length in the fracture plane	Average of all individually measured peak to valley heights

### 3.7 Mini-PI-SWERL™ Test

The Mini-PI-SWERL™ (Portable In-Situ Wind Erosion Lab) is a device to measure PM<sub>10</sub> emissions from pavement or soil surfaces, developed by Desert Research Institute (DRI). The Mini-PI-SWERL™ consists of one control box, 2 batteries (12 Volt each), laptop running Microsoft® Windows 2000 or Windows XP and a cylindrical enclosure with a fan and flat annular blade. The blade rotates at a distance of 5.2 cm from the ground surface. The internal diameter of the Mini-PI-SWERL™ is 30 cm and the internal height is 20 cm. The bottom portion of the cylinder is open and a foam material was attached to the circumference of the open end to seal the instrument to the road surface.

A TSI DustTrak (model 8520, serial no 21622) was used to record the PM<sub>10</sub> concentration. The Mini-PI-SWERL™ central and instrument setup is similar to that of the PI-SWERL. The annular flat blade rotates at a speed that is controlled by a DC motor, which is controlled by a computer according to a provided cycle length through the control box (Sweeney et al, 2008).

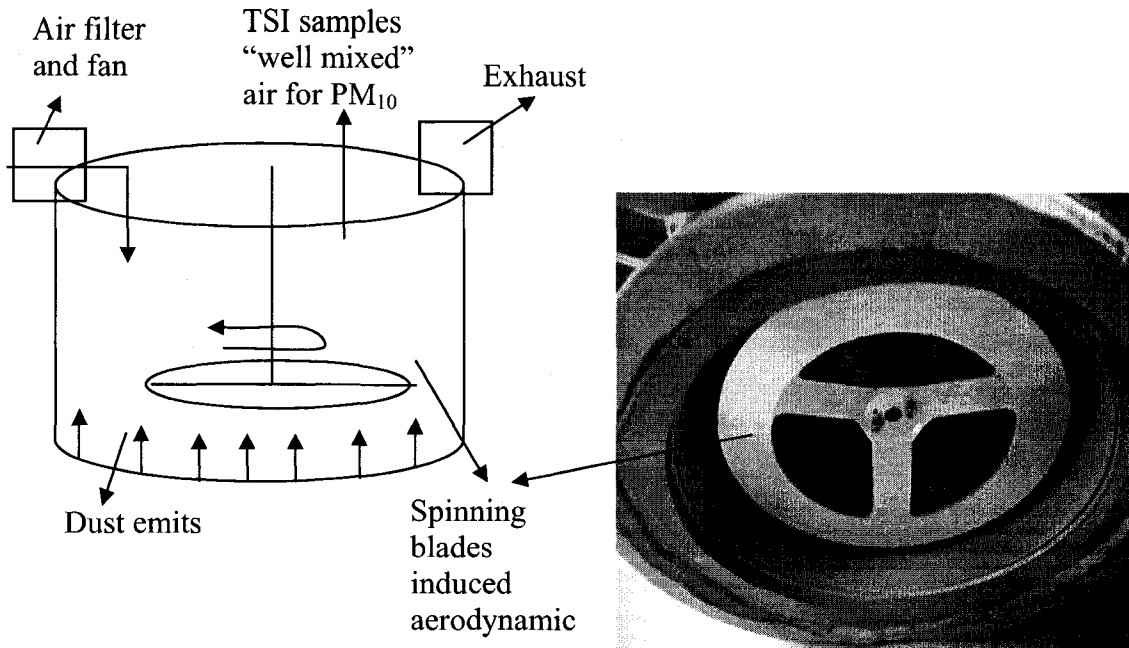


Figure 3.13 Schematic of Mini-PI-SWERL™ (Mini-PI-SWERL™ blade photo taken by Rodrigues, 2006)

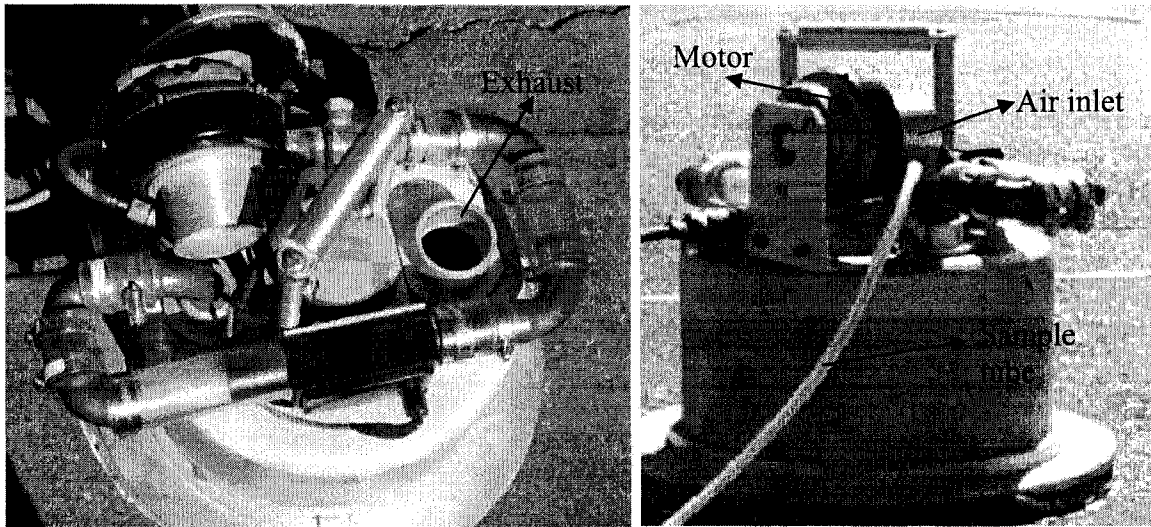


Figure 3.14 Mini-PI-SWERL™

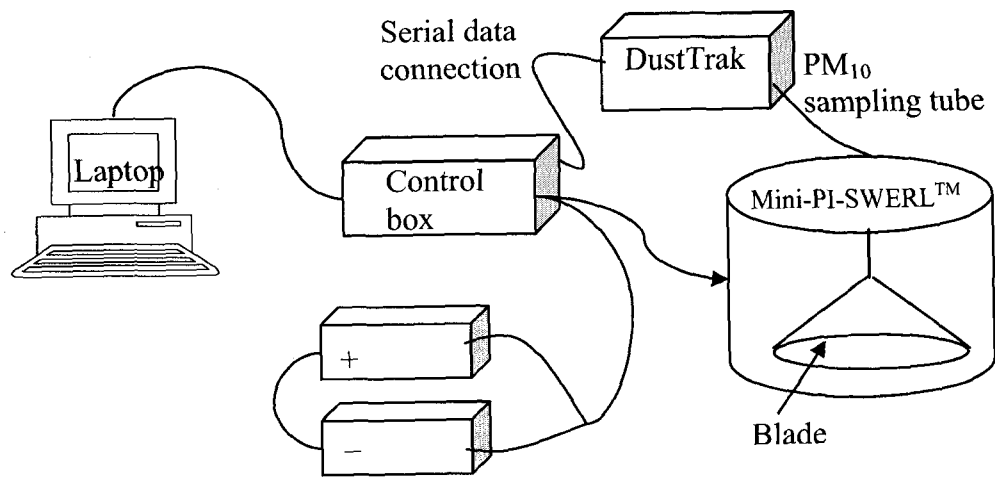


Figure 3.15 Mini-PI-SWERL™ Experimental Setup

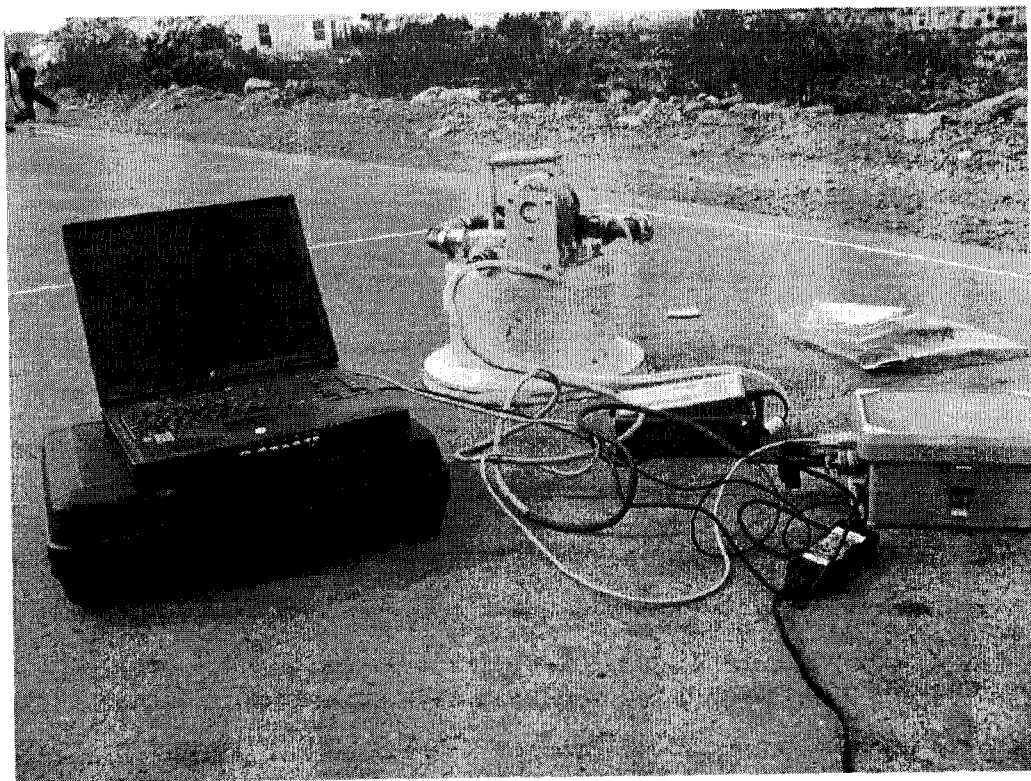


Figure 3.16 Mini-PI-SWERL™ Sampling (Goldhill & Richmar)

Thirteen sites were sampled in the Las Vegas Valley and in Boulder city. Each site had three experimental plots and each plot had either two or one spots depending on the tire track. If a visual assessment of the each site determined that tire track was prominent then two spots were selected per plot for the experiment, if a tire track was not prominent then only one spot per plot was measured. Five sites were selected for two spots per plot among 13 sites due to visually prominent tire track. The Mini-PI-SWERL<sup>TM</sup> was performed with 1000 RPM steps, going from 0 to 5000 RPM.

Figure 3.17 (a) and (b) show the layout of Mini-PI-SWERL<sup>TM</sup> experiment at one site where two spots were selected per plot as tire track is prominent. The rectangles are the AP-42 sampling plots. The Mini-PI-SWERL<sup>TM</sup> spot on the off tire track was selected randomly and any defects (pavement gauges) was avoided.

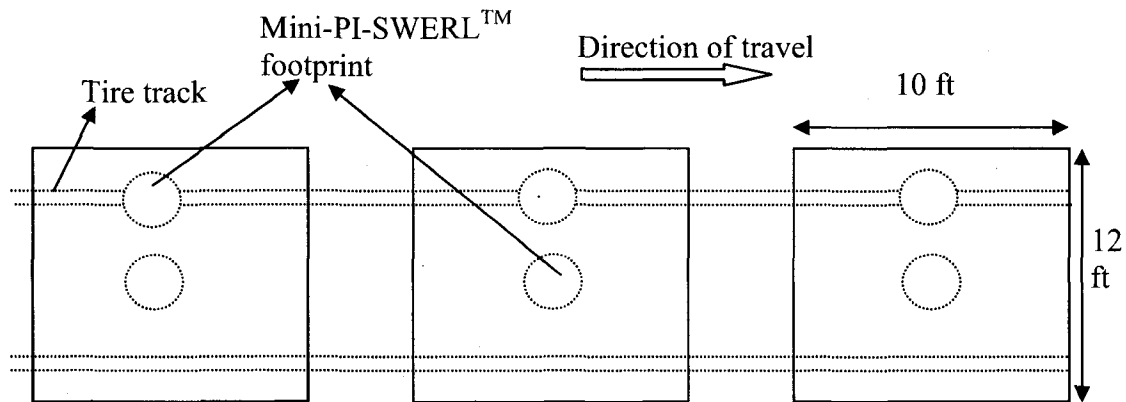


Figure 3.17 (a) Schematic Plot Layout (existence of tire track) and Experimental Setup of Mini-PI-SWERL<sup>(TM)</sup>



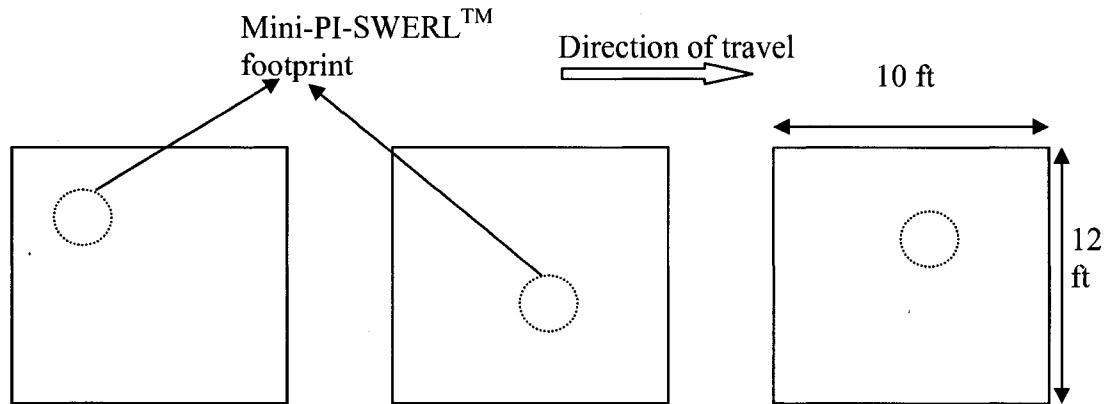
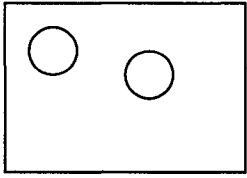


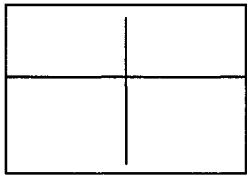
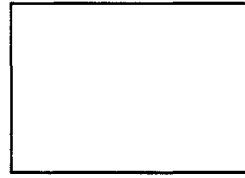
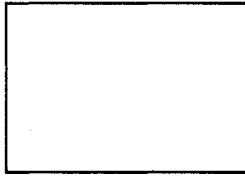
Figure 3.17 (b) Schematic Plot Layout (no tire track) and Experimental Setup of Mini-PI-SWERL™

### 3.8 Sampling Sequence

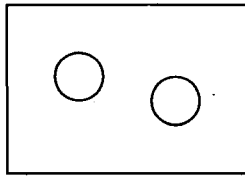
Mini-PI-SWERL™ experiments were conducted for three conditions: ambient, cleaned and controlled experiment i.e. applied soil conditions. Figure 3.18 shows a typical sampling sequence for one site. The first sets of ambient runs were completed before the road surface was vacuumed. Then the AP-42 plot was vacuumed with a Hoover vacuum cleaner. The second sets of Mini-PI-SWERL™ experiments were conducted on the cleaned surface. Finally the controlled experiments were conducted on the cleaned surfaces using a constant application of soil (1.0 gram  $\pm$  0.1 gram) with known silt loading (2 gm/m<sup>2</sup>). One gram of soil was measured by a scale (readability  $\pm$  0.1 gram) and poured on the Mini-PI-SWERL™ footprint area. Then the soil was spread across the entire Mini-PI-SWERL™ footprint with a soft bristle brush so that the pavement texture was not disturbed.



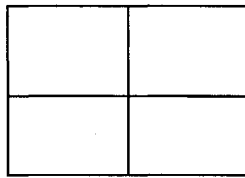
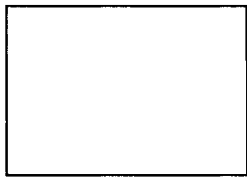
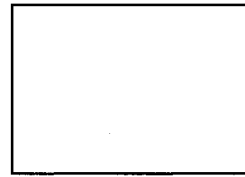
Mini-PI-SWERL™  
ambient



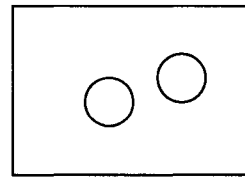
AP-42



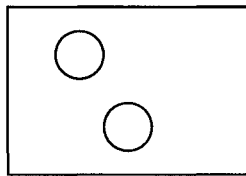
Mini-PI-SWERL™  
ambient



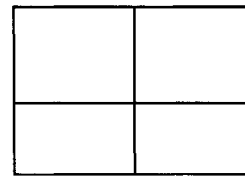
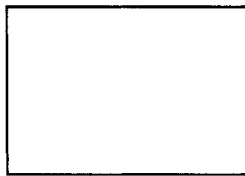
AP-42



Mini-PI-SWERL™  
ambient



Mini-PI-SWERL™ clean,  
then soil



AP-42

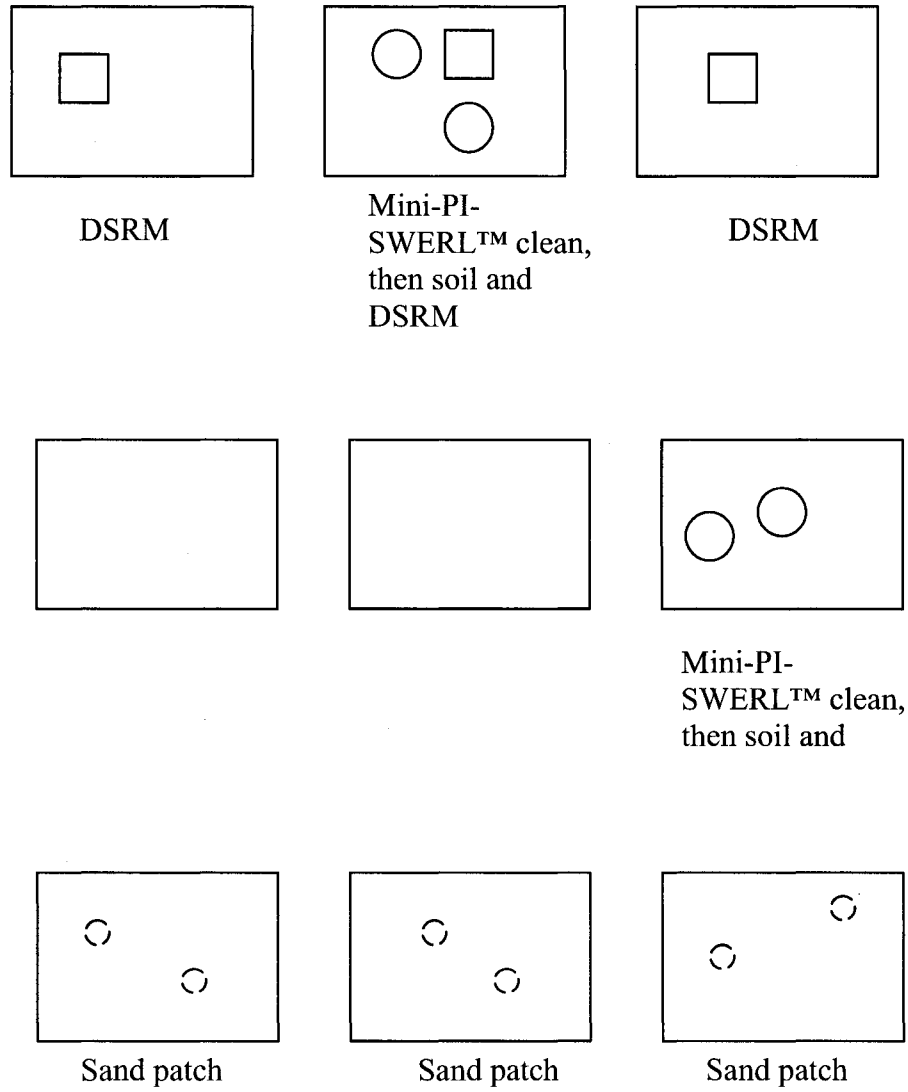


Figure 3.18 Typical Sampling Sequence

## CHAPTER 4

### AP-42 EMISSION FACTOR RESULTS

#### 4.1 Silt Loading and Emission Factor Calculations

Ninyo and Moore soil mass was used for silt mass and silt loading calculation. Silt mass were calculated from silt fraction and net soil mass. Silt loading is the silt mass per unit area. The Root mean square (RMS) uncertainty analysis method (Holman, 2001) was used for calculation of silt loading uncertainty. The uncertainty in silt loadings was calculated using the experimental uncertainty in silt mass and estimated uncertainty in plot area.

The relative individual uncertainty was calculated by dividing their individual uncertainty by silt loading. The emission factors for each site were calculated using Equation 4.1 provided by US EPA.

$$E = k(sL/2)^{0.65} * (W/3)^{1.5} - C \quad (4.1)$$

Where,

E = particulate emission factor

k = particle size multiplier for particle size range and units of interest (The value of K is 7.3 for gm/VMT and 4.6 for gm/VKT)

sL= road surface silt loading (material smaller than 75  $\mu\text{m}$  in  $\text{gm}/\text{m}^2$ )

The range for road surface silt loading (sL) using for this equation is 0.02-400 g/m<sup>2</sup>

W= average weight (tons) of the vehicles traveling the road

C = correction factor for Emission Factor for vehicle fleet exhaust, brake wear and tire wear (The value of C is 0.2119 for gm/VMT and 0.1317 for gm/VKT)

AP-42 emission factors were calculated in gram/VMT. A weight of 3 tons, 7.3 gram/VMT as particle size multiplier and 0.2119 gm/VMT as correction factor are used for emission factor calculation.

#### 4.1.1 Sample Calculation for Emission Factor

For example using silt loading (sL) of 0.619 g/m<sup>2</sup> and vehicle weight of 3 tons.

$$K = 7.3 \text{ gm/ VMT}$$

$$C=0.2119$$

$$E = 7.3 * (0.619/2)^{0.65} * (3/3)^{1.5} - 0.2119$$

$$E = 3.19 \text{ gm/ VMT}$$

#### 4.2 First Quarter, 2008 Results and Comparisons to Prior Measurement

Uncertainty in emission factors were calculated using uncertainty in silt loading. Plot to plot emission factor uncertainty was calculated for each site by computing the deviation of calculated emissions factors on each plot. The emission factors and uncertainties are listed in Table 4.1, 4.2 and 4.3 for local, collector and minor arterial respectively. The highest plot to plot uncertainty (1.01) was found at the Maryland and Westminster site.

Table 4.1 AP-42 Emission Factors for Local Roads First Quarter 2008

Site Name	Silt Fraction (%)	Sampled Area (m <sup>2</sup> )	Silt loading, (g/m <sup>2</sup> )	EF (g/VMT)	Plot-Plot Uncertainty	Relative Individual Uncertainty
Armacost	0.249	32.05	1.168	4.910	0.178	0.2%
Duneville	0.179	30.66	0.712	3.490	0.158	0.3%
Evergold	0.397	33.44	2.152	7.420	0.225	0.1%
Goldhill	0.468	61.31	0.657	3.298	0.138	0.2%
Sapphire Light	0.452	33.44	0.619	3.180	0.096	0.4%

Table 4.2 AP-42 Emission Factors for Collector Roads First Quarter

Site Name	Silt Fraction (%)	Sampled Area, m <sup>2</sup>	Silt Loading (g/m <sup>2</sup> )	EF (g/VMT)	Plot-Plot Uncertainty	Relative Individual Uncertainty
Burkholder1	0.192	30.66	0.841	3.900	0.207	0.3%
Burkholder2	0.319	40.88	0.640	3.170	0.268	0.3%
Crestdale1	0.346	33.44	0.466	2.610	0.092	0.5%
Crestdale2	0.336	55.74	0.560	2.970	0.056	0.2%
Ione	0.244	33.44	0.754	3.650	0.081	0.3%
Pabco	0.175	40.88	0.400	2.330	0.061	0.4%
Veretans Memorial Blvd(near tower)	0.084	50.17	0.160	1.200	0.034	0.8%
Veretans Memorial Blvd(North end)	0.133	62.71	0.202	1.430	0.019	0.5%
Veretans Memorial Blvd(South end)	0.191	50.17	0.404	2.360	0.075	0.3%

Table 4.3 AP-42 Emission Factors for Minor Arterial Roads First Quarter

Site Name	Silt Fraction (%)	Sampled Area (m <sup>2</sup> )	Silt Loading (g/m <sup>2</sup> )	EF (g/VMT)	Plot-Plot Uncertainty	Relative Individual Uncertainty
Ann Rd	0.088	33.44	0.505	2.770	0.066	0.4%
Maryland Silver Spring	0.053	30.66	1.097	4.730	1.010	0.2%
	0.275	41.8	1.074	4.660	0.054	0.2%

The relationship of first quarter 2008 AP-42 emission factors to the most recent AP-42 emission factors are listed in Table 4.4. The emission factors increased for all sites except for the Sapphire Light & Emerald Stone site, where the emission factor decreased about 70 % from prior measurements. The Goldhill and Richmar site showed the highest increase of about 4.6 times the prior measurement.

Figure 4.1 shows the emission factor for first quarter 2008. The 1 Y- error bars indicate the plot to plot uncertainty. 11 out of 12 sampled sites showed higher emission factors than their most recent sampling.

Figures 4.2 to 4.13 show the previous AP-42 emission factor comparison for all 12 sites. Figure 4.1 and Tables 4.1, 4.2 and 4.3 shows that Veterans Memorial Blvd, a collector road in Boulder city was the cleanest sampled road. Within Las Vegas Valley, the highest emission factor and silt loading was found at Evergold and Coral Sea. Pabco & Tabny, an improved collector (2.33/g/VMT) and Ann Rd & San Mateo, an improved minor arterial (2.77 g/VMT), had the lowest silt loadings and emissions factors.

Table 4.4 Relationship of AP-42 EF to Prior Measurements

Site Name	Roadway Type	1Q-08 AP-42 EF (g/VMT)	AP-42 EF Prior Measurement (g/VMT)	Prior Measurement	Relationship to Prior Measurement
Armacost & Calmar	Local	4.91	2.08	3Q-05	2.4
Duneville & Oakey	Local	3.49	2.14	3Q-05	1.6
Evergold & Coral Sea	Local	7.42	5.7	3Q-05	1.3
Goldhill & Richmar	Local	3.30	0.72	3Q-05	4.6
Sapphire Light & Emerald Stone	Local	3.18	11.09	1Q-06	0.3
Burkholder & Cabrillo	Collector	3.17	2.34	3Q-05	1.4
Crestdale & Covington	Collector	2.97	0.25	3Q-05	11.9
Ione & Coral Sea	Collector	3.65	3.04	1Q-06	1.2
Pabco & Tabony	Collector Minor	2.33	1.58	3Q-05	1.5
Ann Rd & San Mateo	Arterial Minor	2.77	2.20	3Q-05	1.3
Maryland & Westminster	Arterial	4.73	1.10	3Q-05	4.3
Silver Spring & Spring Hill	Minor Arterial	4.66	1.99	3Q-05	2.3



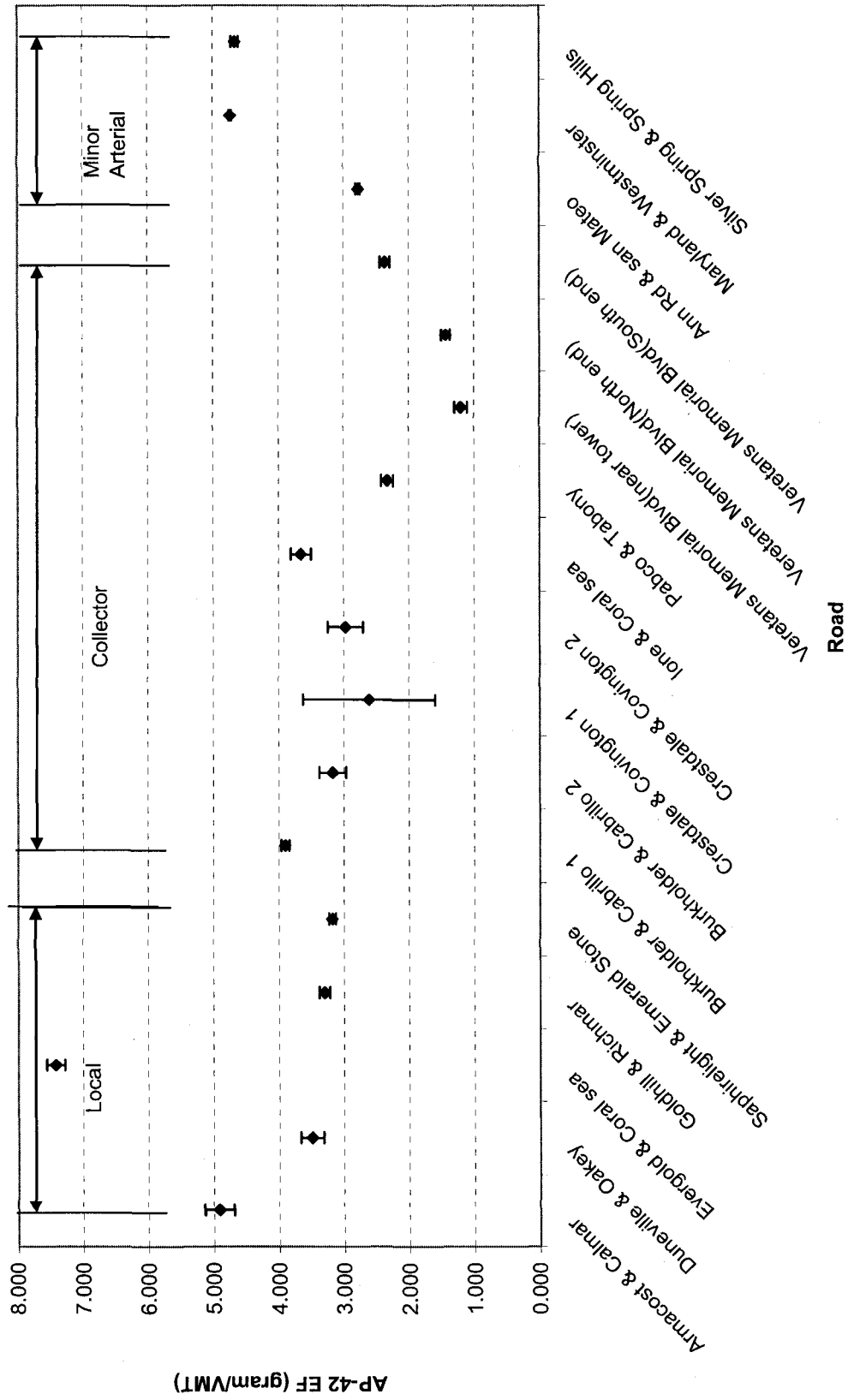


Figure 4.1 AP-42 EF Results of first Quarter 2008

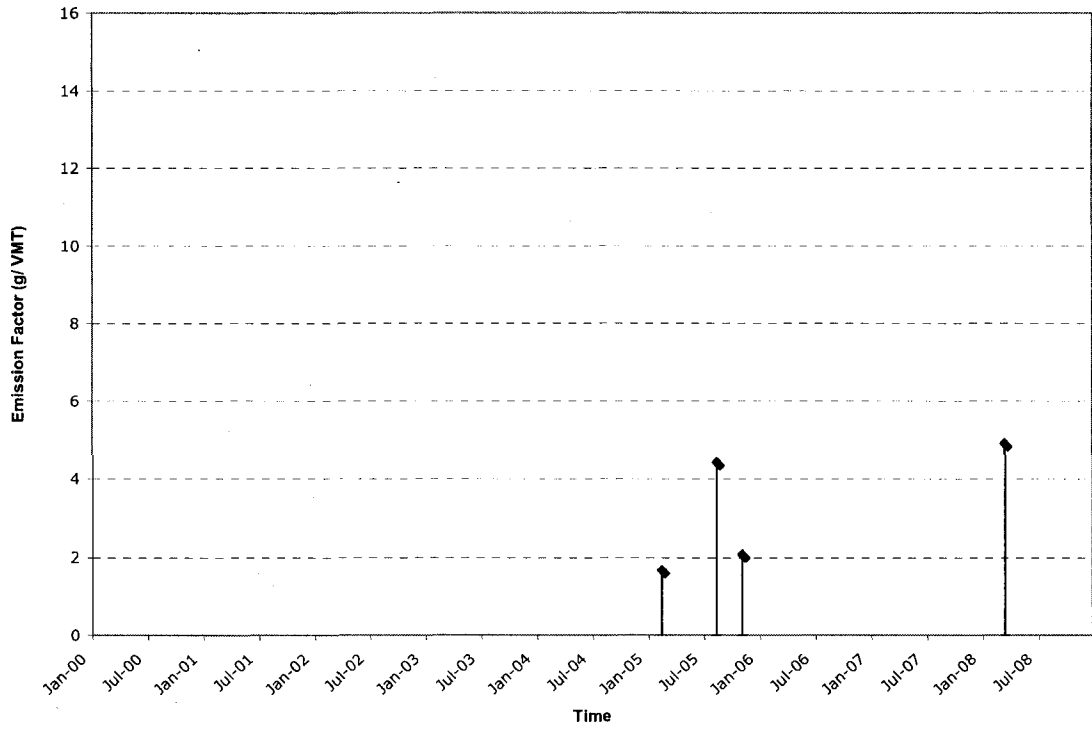


Figure 4.2 Armacost & Calmar (Local road) EF with Time

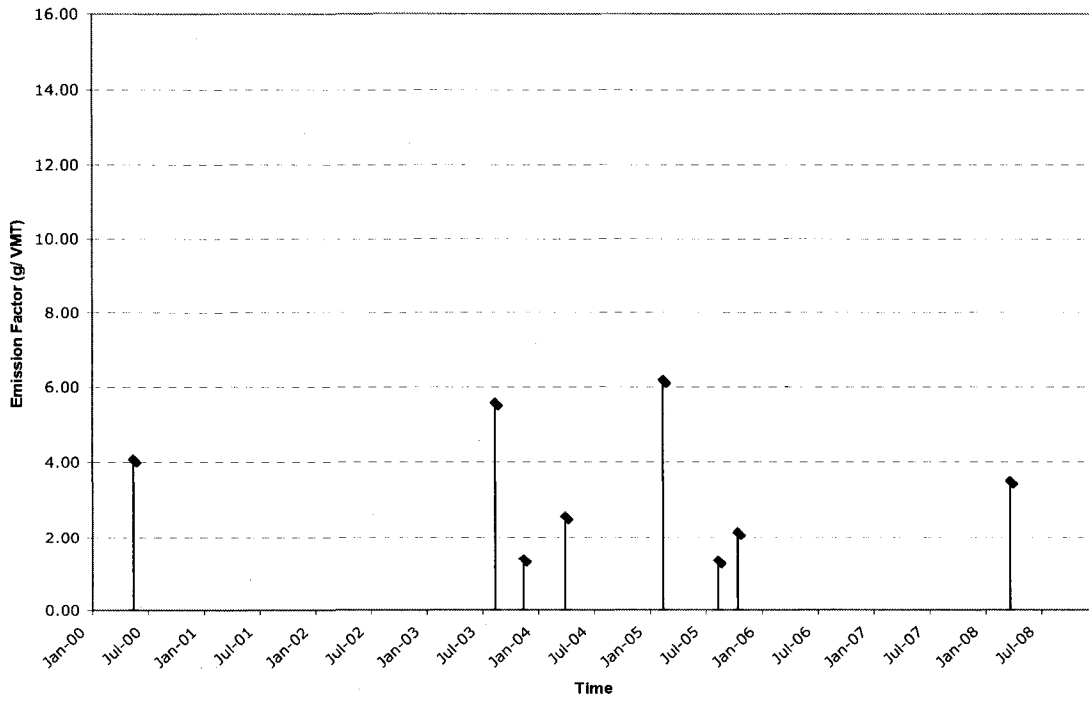


Figure :4.3 Duneville & Oakey (Local road) EF with Time

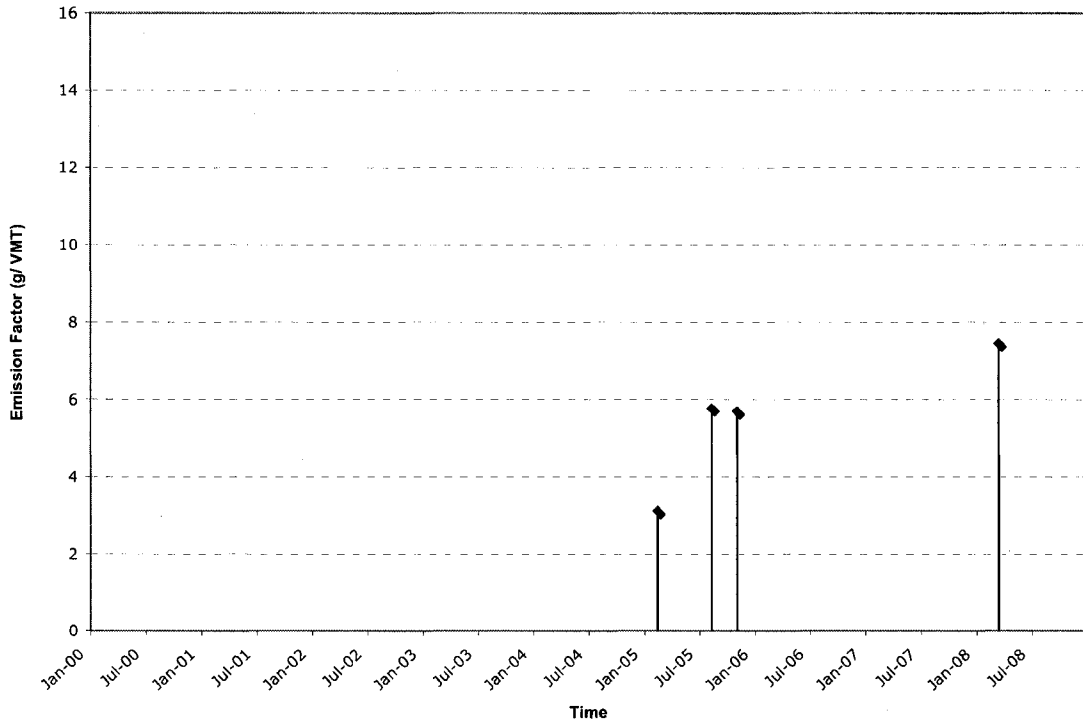


Figure 4.4 Evergold & Coral Sea (Local road) EF with Time

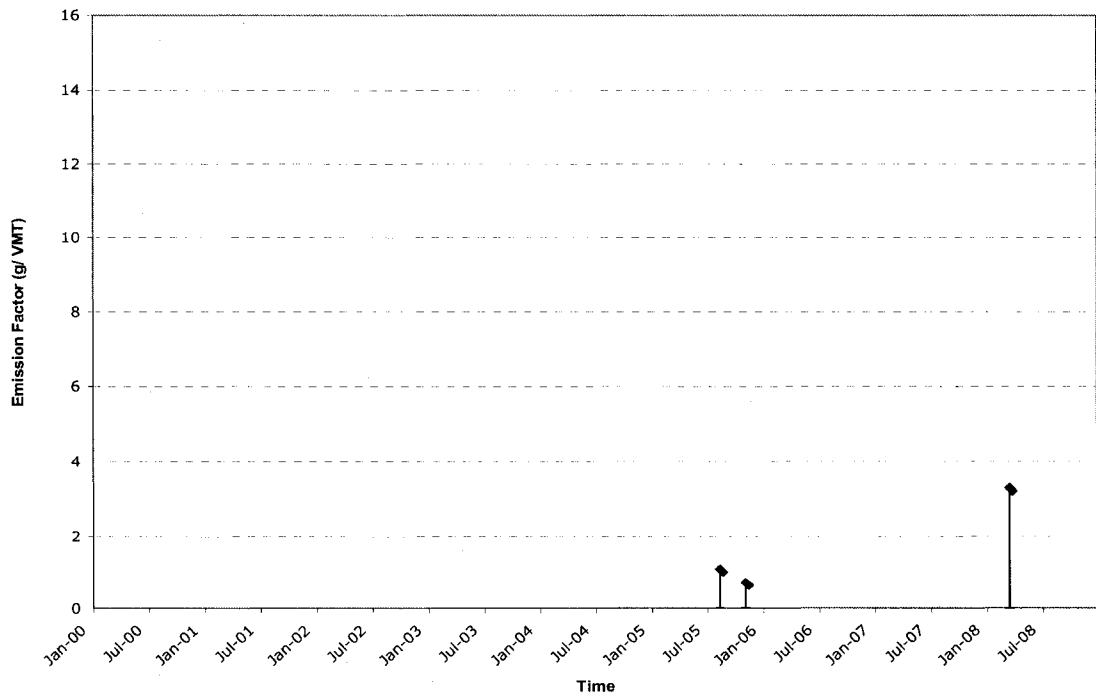


Figure 4.5 Goldhill & Richmar (Local road) EF with Time

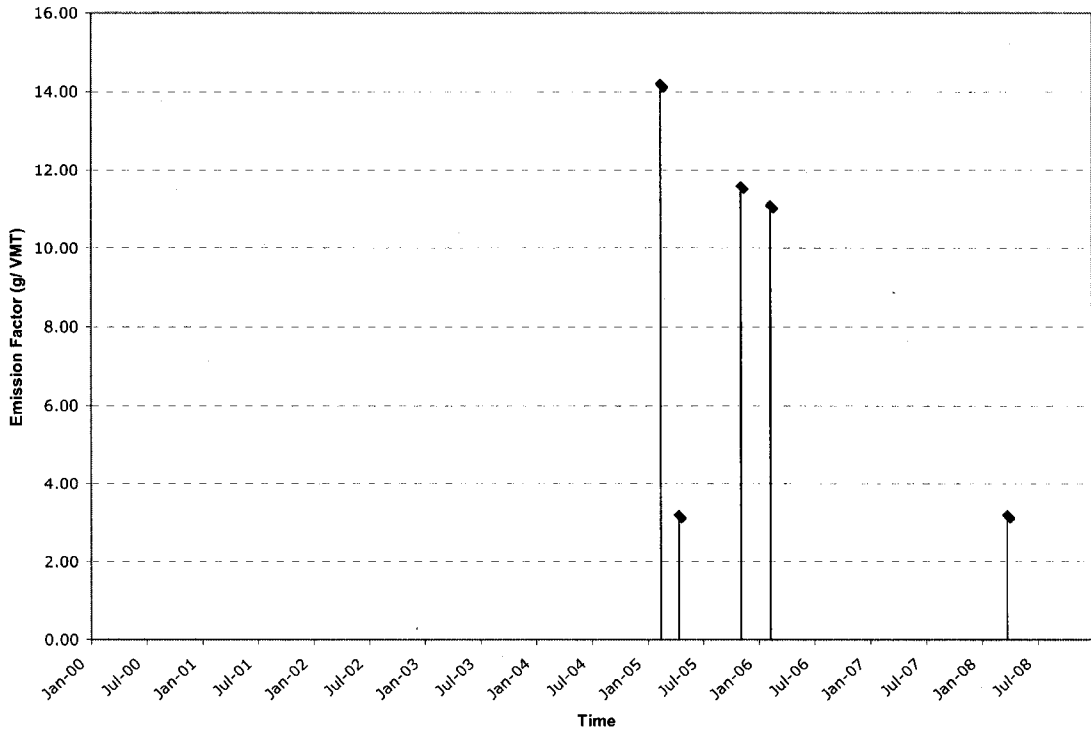


Figure 4.6 Sapphire Light & Emerald Stone (Local road) EF with Time

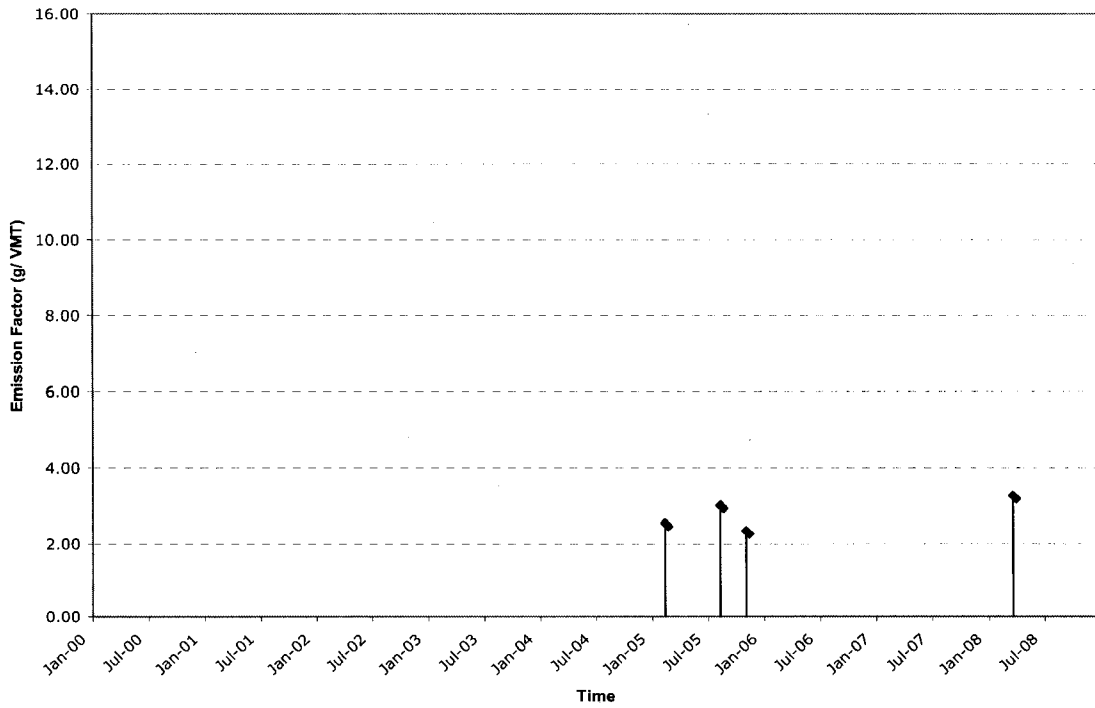


Figure 4.7 Burkholder & Cabrillo (Collector road) EF with Time

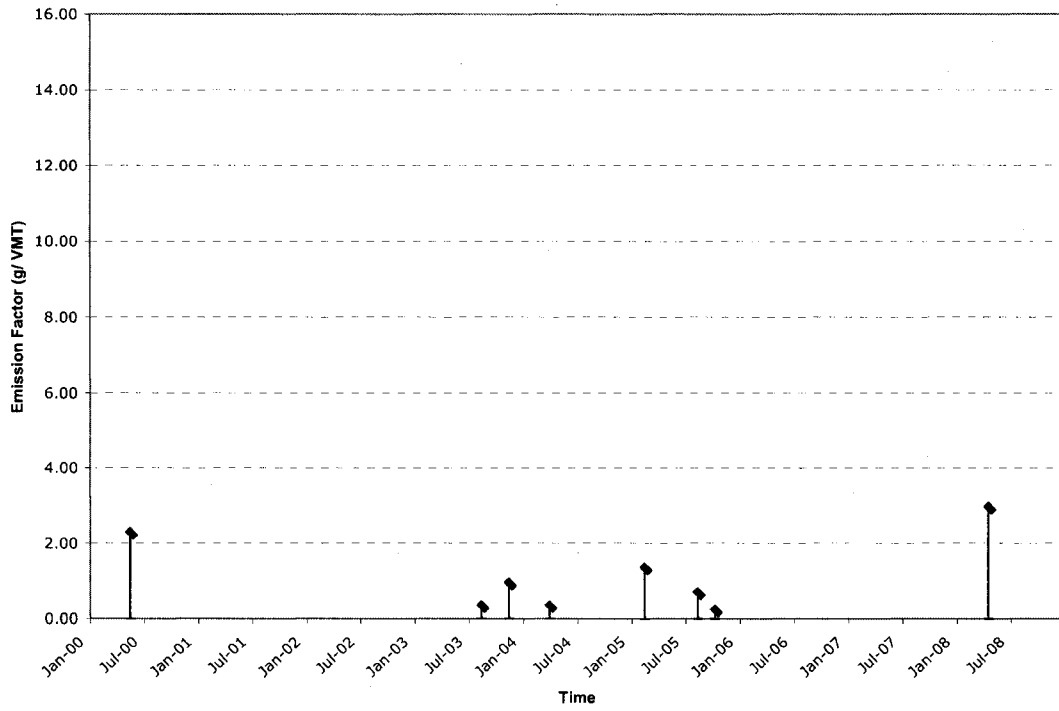


Figure 4.8 Crestdale & Covington Cross (Collector road) EF with Time

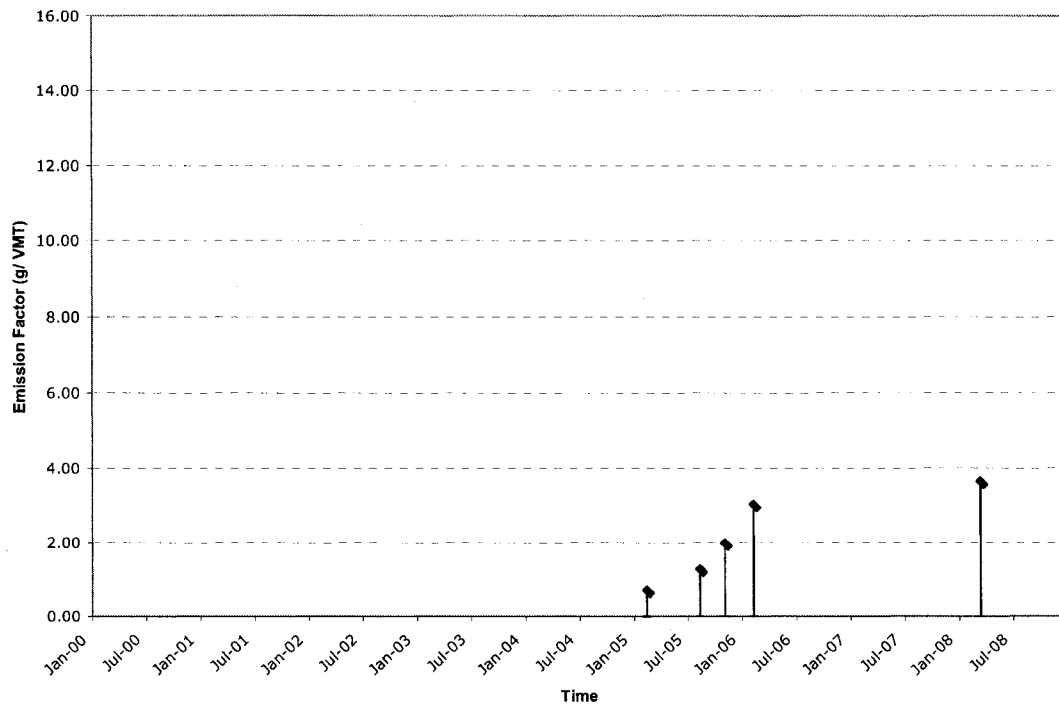


Figure 4.9 Ione & Coral Sea (Collector road) EF with Time

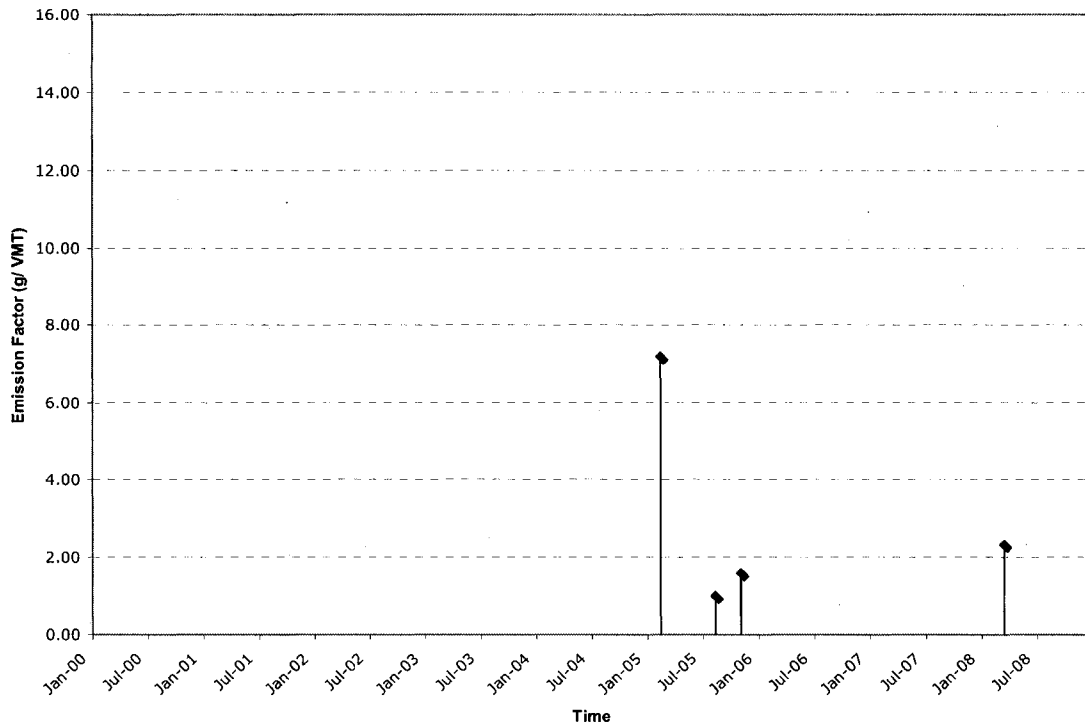


Figure 4.10 Pabco & Tabony (Collector road) EF with Time

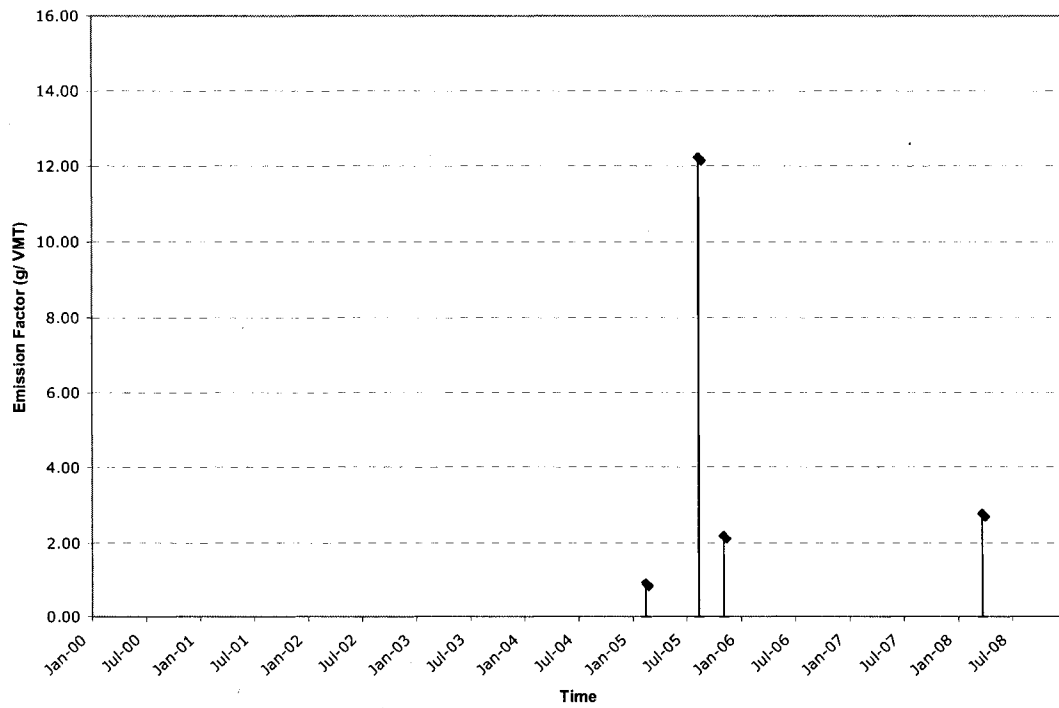


Figure 4.11 Ann Rd & San Mateo (Minor Arterial) EF with Time

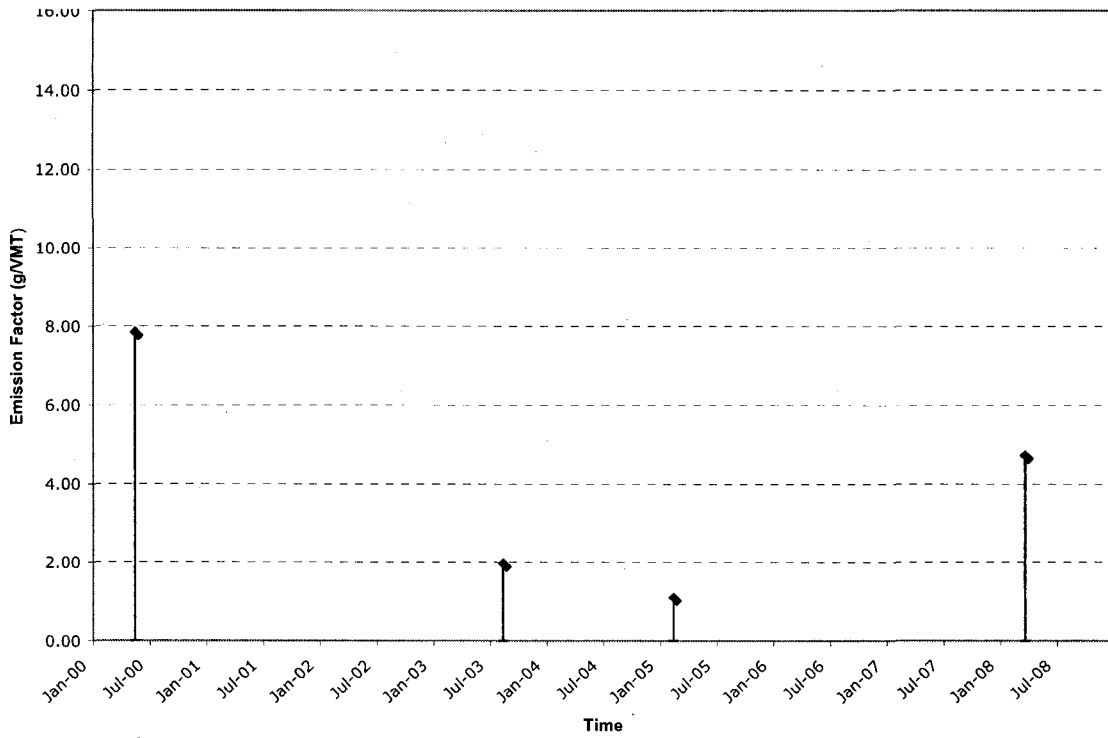


Figure 4.12 Maryland & Westminster (Minor Arterial) EF with Time

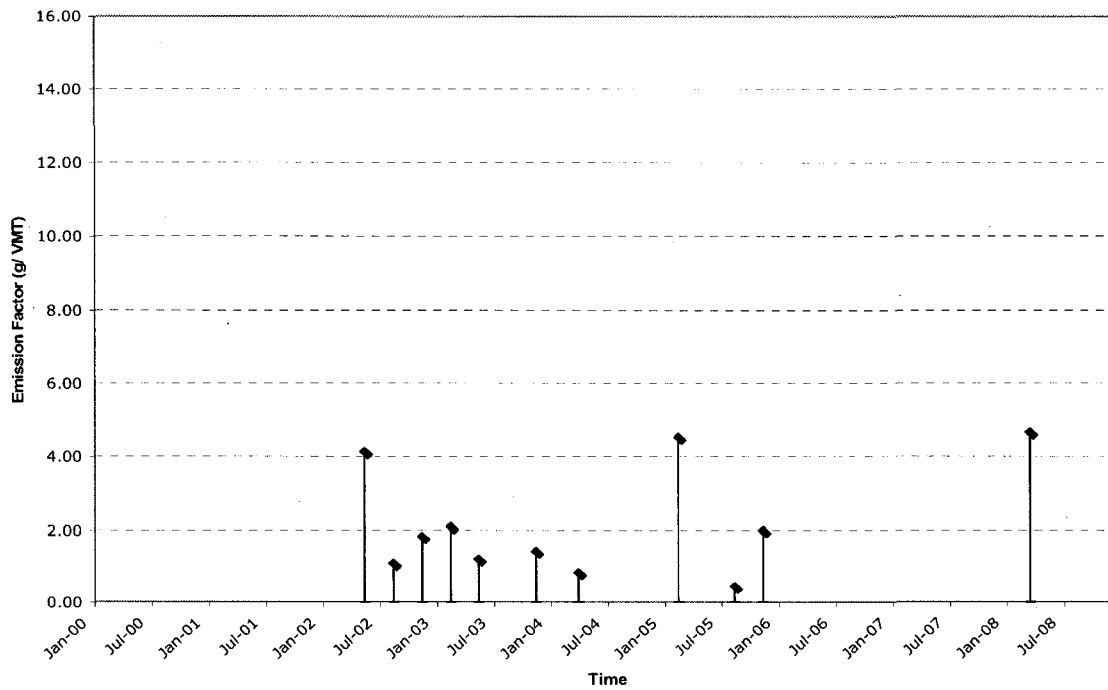


Figure 4.13 Silver Spring & Spring Hills (Minor Arterial) EF with Time

## CHAPTER 5

### SAND PATCH AND DSRM RESULTS

#### 5.1 DSRM Results

The DSRM standard output provides average peak to valley roughness (R) value which is similar to mean profile depth (Mokarem, 2006). Equation 3.3 was used to transform mean profile depth to mean texture depth. Figure 5.1 shows a close-up picture of the pavement surface at the Ann Rd & San Mateo site (Plot1 Spot1). The photo was taken using an Olympus Evolt E-510 35 mm 1:3:5 macro lens. The height of the lens from the pavement surface was 9.5 cm and the focal length was 34 mm.

Figure 5.2 shows the DSRM output of approximately the same spot. The DSRM MTD of Ann Road (Plot1 Spot1) is 1.314 mm. Ann Road represents open aggregate and aggregates that are not sealed. The average size of the aggregate was computed directly from the picture. The average aggregate size of Ann Rd & San Mateo site (P1S1) is 4.18 mm. The DSRM laser lines are not straight which indicates the pavement surface is rough.

Figure 5.3 is the close up photo of Evergold & Coral Sea site (Plot1 Spot1). The photo was taken with the Olympus Evolt E-510 14-42 mm 1:3.5-5.6 zoom lens and with a field view of 75 mm across by 56 mm. The height of the lens from the pavement surface was 9.5 cm and the focal length was 32 mm. Figure 5.4 shows the output of DSRM at approximately same spot.





Figure 5.1 Ann Rd Plot1 Spot1 (DSRM MTD 1.314 mm)

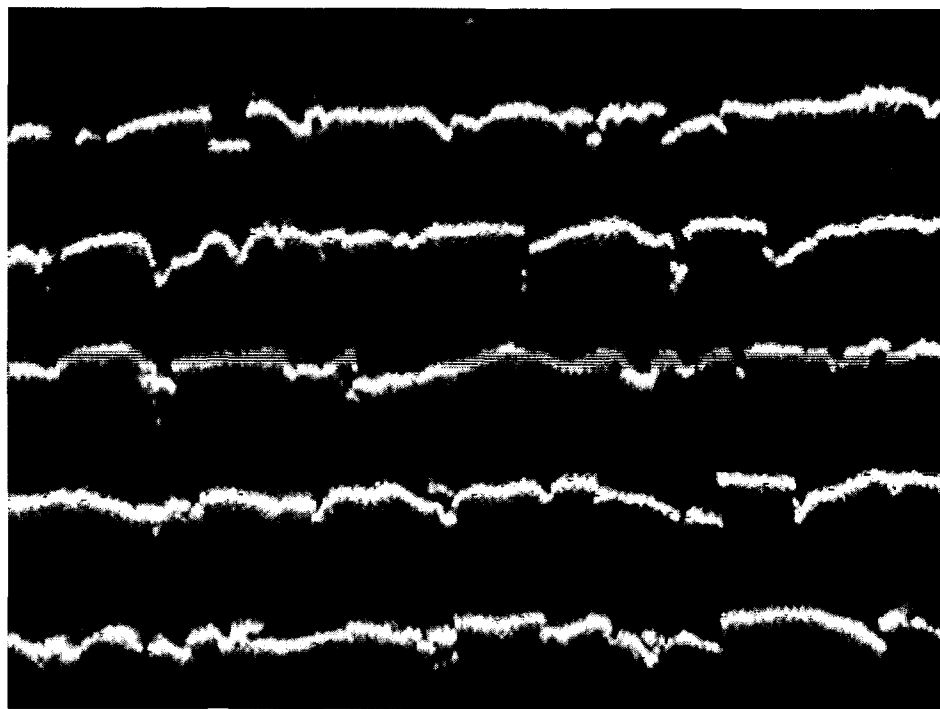


Figure 5.2 Ann Rd Plot1 Spot1 ( DSRM Output)

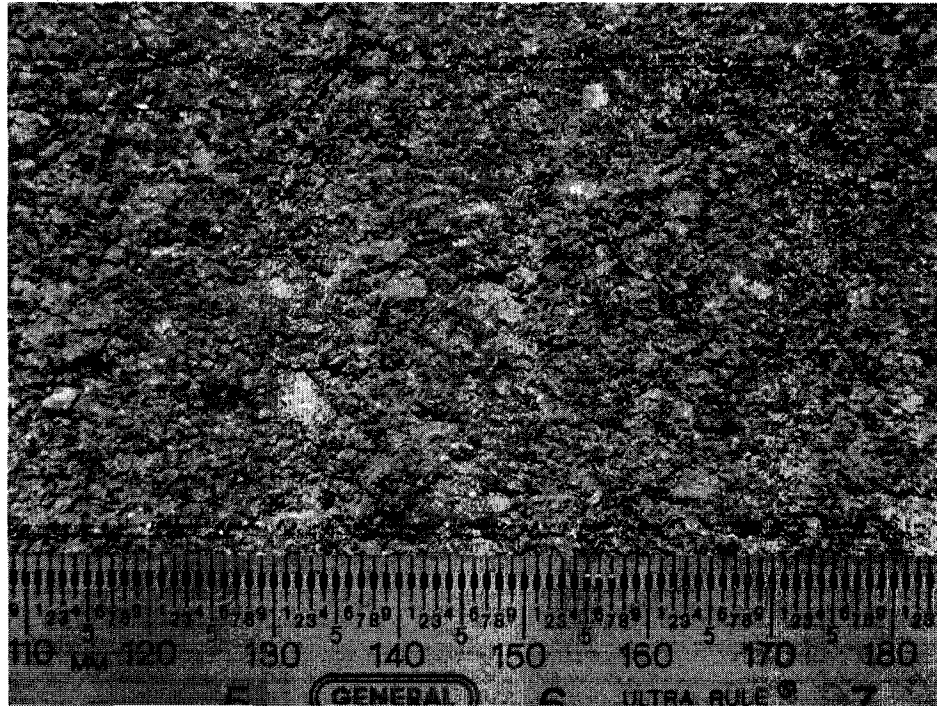


Figure 5.3 Evergold & Coral Sea Plot1 Spot1 (DSRM MTD 0.45 mm)

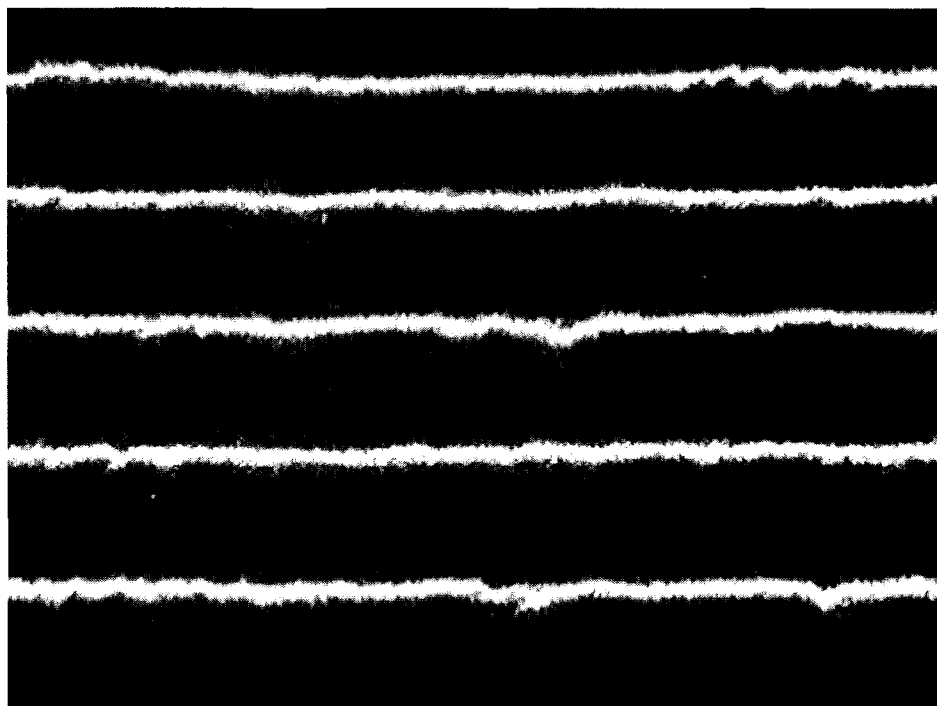


Figure 5.4 Evergold & Coral Sea Plot1 Spot1 (DSRM Output)

The DSRM MTD of Evergold & Coral Sea (Plot1Spot1) is 0.45 mm. Evergold & Coral Sea represents a fine aggregate with average aggregate size of 1.97 mm and the pavement surface is sealed. The laser lines are straighter, resulting in a lower R value, compared to Ann Road, as the Evergold & Coral Sea pavement surface is smoother than Ann road.

## 5.2 UNLV Parking Lot Results

Several preliminary measurements were taken in the UNLV asphalt parking lot and the Thomas & Mack parking lot. For every sand patch location, four DSRM measurements were taken. Two smooth surfaces and two rough surfaces were selected from the UNLV parking lot and one smooth surface and one rough surface were selected from the Thomas and Mack parking lot. Table 5.1 represents the MTD results and Figure 5.5 represents the data graphically.

UNLV-smooth and UNLV-rough surface showed good agreement on DSRM and sand patch measurements. The Thomas and Mack smooth surface sand patch result was much lower than the DSRM value, and the rough surface sand patch results was much higher than the DSRM value.

Table 5.1 Parking lot DSRM and Sand Patch Test Results

Set Number	Set Name	Sand Patch MTD	DSRM MTD(calculated)	DSRM-"R" value (MPD)
1	UNLV-Smooth1	0.577	0.574	0.533
2	UNLV-Smooth2	0.498	0.445	0.595
3	UNLV-Rough1	0.750	0.777	0.747
4	UNLV-Rough2	0.758	0.786	0.757
5	T& Mack-smooth	0.480	0.625	0.587
6	T& Mack-rough	1.201	1.073	1.060

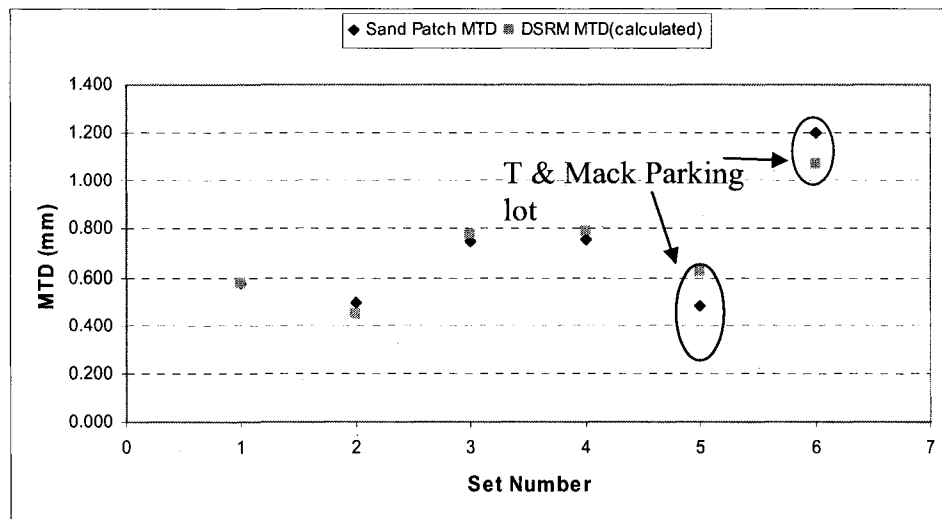


Figure 5.5 Parking lot DSRM and Sand Patch Test Results

A significant correlation was found between the DSRM and sand patch parking lot data. Figure 5.6 shows the correlation of DSRM and sand patch parking lot data. Regression analysis were conducted on the parking lot data and showed that the slope was statistically significant ( $p = 0.00359$ ) but the intercept was not significant ( $p = 0.1570$ )

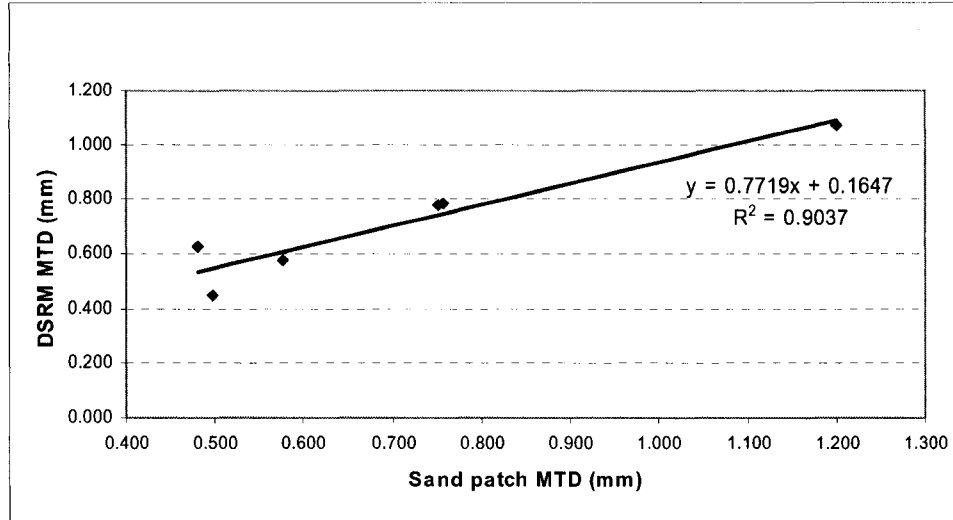


Figure 5.6 Correlation between DSRM and Sand Patch Parking Lot Data

### 5.3 13 Sampling Sites Results

61 total sand patch and approximately 244 DSRM measurements were made on three major road categories, local, collector and minor arterial. Some DSRM readings provided out-of-range results on pavements with values of MTD exceeding 1.2 mm. Those results were discarded according to the DSRM user manual's instructions.

The four DSRM sub-spot MTDs were averaged to compute spot-mean MTDs that could be directly compared to the ASTM E 965 sand patch values.

shows DSRM and sand patch comparisons of all 61 data points. Percentage deviation of sand patch results from DSRM was calculated from following formula.

$$\% \text{ Deviation} = \frac{\text{DSRM MTD} - \text{Sand patch MTD}}{\text{Sand patch MTD}} \times 100\% \quad (5.1)$$

Results showed that 57 data pairs out of 61 data pairs had within 10% agreement between the sand patch MTD and DSRM MTD. More than 10% deviations are highlighted (Table 5.2). DSRM MTDs were higher than sand patch MTDs for 22

measurements and 29 data pairs had higher DSRM MTD than the sand patch MTD. Ten data pairs had shown the same results for DSRM and sand patch MTD.

Uncertainties in sand patch test for each spot were calculated using the Root Mean Square (RMS) uncertainty analysis method (Holman, 2001). Uncertainties in the sand patch MTD were calculated using uncertainty in area of the “pancake” and the uncertainty in volume of the “pancake”. DSRM uncertainties for each spot were calculated using standard deviation for four measurements on each sub-spot. Sand patch MTD uncertainties range from 1% to 10% where as uncertainty for DSRM measurements range from 0% to 35 %

Table 5.2 Sand Patch MTD & DSRM MTD Results for All Data-points

Site Name	Sand Patch MTD	DSRM MTD	Sand Patch Uncertainty	DSRM Uncertainty	% Deviation
Evergold & Coral Sea	0.623	0.450	3%	2%	-28%
Ann Rd & San Mateo	1.601	1.314	5%	4%	-18%
Ann Rd & San Mateo	1.514	1.296	9%	8%	-14%
Maryland & Westminster	1.155	1.062	7%	12%	-8%
Armacost & Calmar	0.830	0.786	2%	2%	-5%
Veterans Memorial Blvd (South end)	0.961	0.911	5%	9%	-5%
Armacost & Calmar	0.754	0.720	3%	2%	-4%
Ann Rd & San Mateo	1.228	1.175	7%	9%	-4%
Sapphire light & Emerald Stone	0.780	0.748	3%	3%	-4%
Armacost & Calmar	0.761	0.730	3%	4%	-4%
Sapphire light & Emerald Stone	0.855	0.831	4%	4%	-3%
Crestdale & Covington Cross 2	0.646	0.628	3%	6%	-3%
Sapphire light & Emerald Stone	0.640	0.630	1%	7%	-2%
Pabco & Tabony	0.676	0.667	2%	4%	-1%
Ione & Coral Sea	0.910	0.898	5%	5%	-1%

Site Name	Sand Patch MTD	DSRM MTD	sand patch uncertainty	DSRM uncertainty	% Deviation
Pabco & Tabony	0.689	0.681	3%	6%	-1%
Evergold & Coral Sea	0.539	0.533	5%	7%	-1%
Veterans Memorial Blvd (South end)	0.640	0.633	2%	5%	-1%
Veterans Memorial Blvd (South end)	0.882	0.873	3%	8%	-1%
Crestdale & Covington Cross 1	0.743	0.737	4%	6%	-1%
Burkholder & Cabrillo	0.873	0.866	7%	19%	-1%
Crestdale & Covington Cross 1	0.682	0.678	4%	4%	-1%
Ione & Coral Sea	0.765	0.762	6%	4%	0%
Duneville & Oakey	0.804	0.801	2%	4%	0%
Sapphire light & Emerald Stone	0.634	0.632	1%	9%	0%
Ione & Coral Sea	0.765	0.763	2%	5%	0%
Veterans Memorial Blvd (South end)	0.743	0.742	1%	13%	0%
Maryland & Westminster	1.473	1.471	8%	35%	0%
Duneville & Oakey	0.591	0.592	10%	5%	0%
Duneville & Oakey	0.961	0.963	10%	23%	0%
Maryland & Westminster	1.198	1.202	7%	14%	0%
Pabco & Tabony	0.682	0.686	2%	4%	0%
Crestdale & Covington Cross 2	0.652	0.655	3%	5%	1%
Burkholder & Cabrillo	0.708	0.714	5%	13%	1%
Duneville & Oakey	1.114	1.127	4%	7%	1%
Goldhill & Richmar	0.562	0.569	2%	4%	1%
Evergold & Coral Sea	0.412	0.417	2%	1%	1%
Silver Spring & Spring Hill	0.780	0.790	5%	8%	1%
Silver Spring & Spring Hill	0.765	0.775	3%	10%	1%
Crestdale & Covington Cross 2	0.623	0.634	4%	3%	2%
Crestdale & Covington Cross 2	0.664	0.675	3%	29%	2%

Site Name	Sand Patch MTD	DSRM MTD	sand patch uncertainty	DSRM uncertainty	% Deviation
Veterans Memorial Blvd (South end) Crestdale &	0.750	0.763	3%	12%	2%
Covington Cross 2 Goldhill & Richmar	0.640	0.651	4%	13%	2%
Duneville & Oakey Veterans Memorial Blvd (Tower) Crestdale &	0.544	0.553	2%	7%	2%
Covington Cross 2 Veterans Memorial Blvd (South end)	0.464	0.473	1%	6%	2%
Ione & Coral Sea Veterans Memorial Blvd (Tower)	0.634	0.649	1%	2%	2%
Ione & Coral Sea Veterans Memorial Blvd (Tower)	0.695	0.711	3%	11%	2%
Ione & Coral Sea Burkholder & Cabrillo	0.736	0.753	3%	2%	2%
Ione & Coral Sea Veterans Memorial Blvd (Tower)	0.715	0.732	4%	6%	2%
Ione & Coral Sea Veterans Memorial Blvd (Tower)	0.629	0.643	5%	1%	2%
Ione & Coral Sea Burkholder & Cabrillo	0.652	0.671	3%	4%	3%
Ione & Coral Sea Veterans Memorial Blvd (Tower)	0.722	0.743	6%	8%	3%
Ione & Coral Sea Veterans Memorial Blvd (Tower)	0.670	0.691	4%	6%	3%
Ione & Coral Sea Veterans Memorial Blvd (Tower)	0.676	0.699	2%	2%	3%
Goldhill & Richmar Sapphire light & Emerald Stone	0.581	0.603	1%	5%	4%
Crestdale& Covington Cross 1	0.629	0.654	3%	9%	4%
Silver Spring & Spring Hill	0.629	0.655	2%	4%	4%
Veterans Memorial Blvd (Tower)	1.028	1.076	2%	16%	5%
Silver Spring & Spring Hill	0.602	0.640	1%	0%	6%
Silver Spring & Spring Hill	0.993	1.080	4%	15%	9%
Duneville & Oakey	0.493	0.550	1%	1%	12%



Table 5.3 Average DSRM and Sand Patch MTD (mm) Results

Site name	Roadway Type	Sand Patch MTD (mm)	Sand Patch dev	Std	DSRM MTD (mm)	DSRM dev	Std
Armacost & Calmar	Local	0.782	0.042		0.746	0.035	
Burkholder & Cabrillo	Local	0.768	0.091		0.774	0.081	
Evergold & Coral sea	Local	0.525	0.106		0.467	0.060	
Goldhill & Richmar	Local	0.562	0.019		0.575	0.026	
Sapphire light & Emerald Stone	Local	0.634	0.006		0.639	0.013	
Crestdale & Covington Cross 1	Collector	0.685	0.057		0.690	0.043	
Crestdale & Covington Cross 2	Collector	0.664	0.027		0.665	0.042	
Duneville & Oakey	Collector	0.960	0.155		0.964	0.163	
Ione & Coral sea	Collector	0.813	0.084		0.808	0.078	
Pabco & Tabony	Collector	0.682	0.006		0.678	0.010	
Veterans Memorial Blvd (South end)	Collector	0.792	0.078		0.793	0.070	
Veterans Memorial Blvd (Tower)	Collector	0.635	0.031		0.658	0.028	
Ann Rd & San Mateo	Minor Arterial	1.448	0.195		1.262	0.076	
Maryland & Westminster	Minor Arterial	1.275	0.172		1.245	0.208	
Silver Spring & Spring Hill	Minor Arterial	0.892	0.138		0.930	0.170	

Table 5.3 shows the average MTD of 13 sites. There were some rough sites and some smooth sites among the 13 sampling sites. The Ann Rd and San Mateo site (minor arterial) was found to be the roughest, and Evergold and Coral Sea (local) was found to be the smoothest road by both DSRM and sand patch techniques.

Ann Rd & San Mateo and Maryland & Westminster are both minor arterial roads and exhibited the highest mean texture depths. Evergold & Coral Sea and Goldhill & Richmar are both local roads and exhibited the lowest mean texture depths. Figure 5.7 shows the average sand patch MTD for 3 different road categories and Figure 5.8 shows the pavement texture measured by DSRM for 3 roadway types. Average MTDs were 0.71 mm, 0.69 mm and 1.28 mm for local, collector and minor arterial respectively.

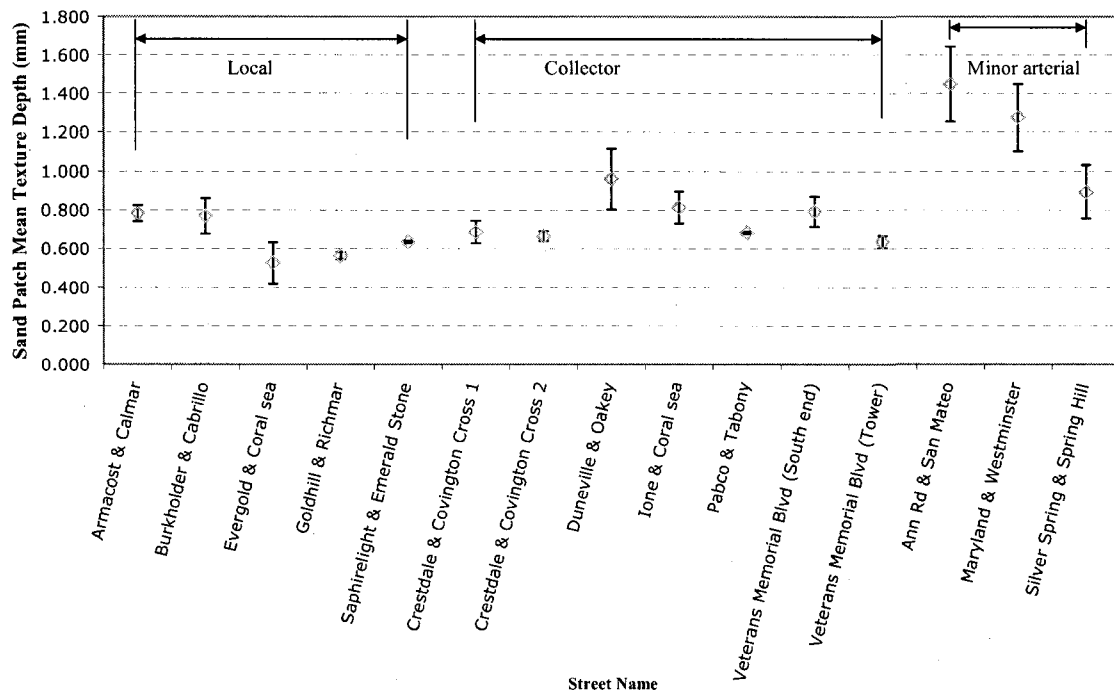


Figure 5.7 Pavement Texture Measured by Sand Patch (ASTM E965, 2001) at Different Roadway Category

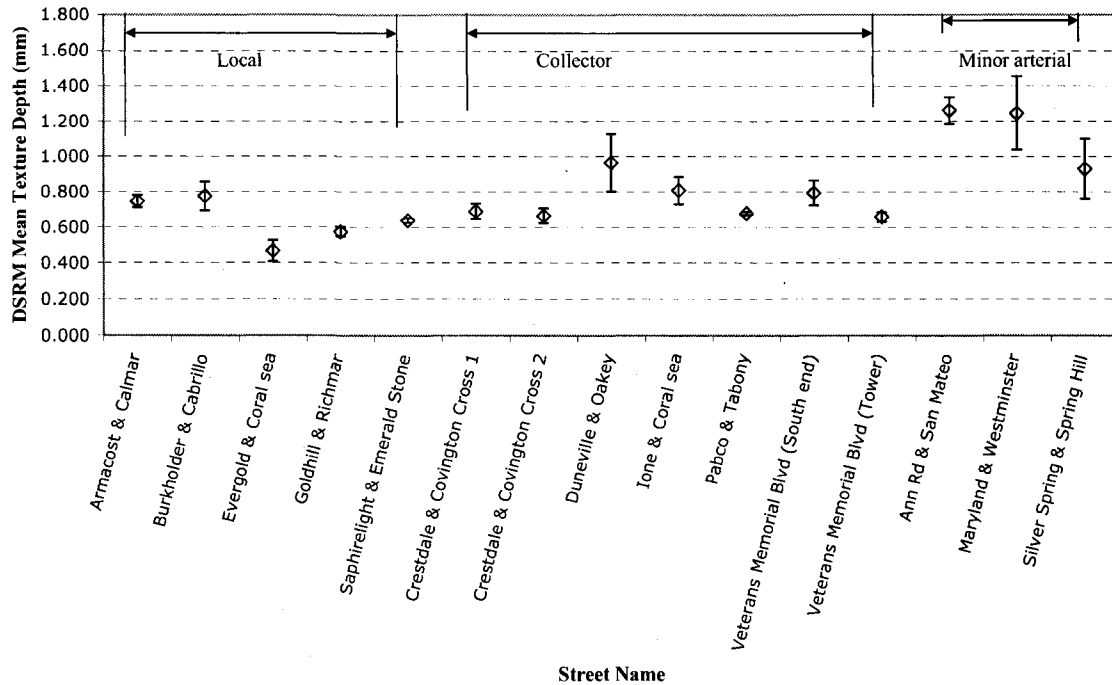


Figure 5.8 Pavement Texture Measured by DSRM at Different Roadway Category

Statistical analyses were performed for DSRM MTD and sand patch MTD results of different road surfaces. Least squares linear regression analysis was conducted using all 61 data pairs. Table 5.4 shows the regression output. Results indicate both slope and intercepts are statistically significant. The slope of 0.867 indicates that the DSRM slightly under measures MTD compared to sand patch.

Table 5.4 Regression Output for All Data Points

	Coefficients	P-value	Lower 95%	Upper 95%	r <sup>2</sup>
Intercept	0.094	2.65E-05	0.053	0.136	0.952
Sand Patch MTD	0.867	1.79E-40	0.816	0.918	

Figure 5.10 represents the DSRM and sand patch correlation results of all 13 sites and 61 measurements. Results indicated significant ( $p < 0.05$ ) correlation between sand patch and DSRM results. The coefficient of determination is ( $r^2$ ) 0.952. Figure 5.9 shows significant correlation but at the higher end of range there are few data points which are widely scattered and tend to above the regression line. ANOVA single factor results of total 61 data points indicate that DSRM and sand patch MTD are not significantly different.

One-way ANOVA analyses were made on measurements of tire wear at four sites to compare the on-tire and between-tire pavement surface textures. Results showed that there were no significant differences between-tire-worn and on tire-worn pavements textures at Veterans (South end), Ione & Coral Sea and Crestdale & Covington Cross 2. A significant difference on pavement texture was observed at Duneville and Oakey (local) pavement surface by both sand patch method ( $p = 0.0104$ ) and DSRM method ( $p = 0.013$ ). Figure 5.9 shows the graphical comparison between on tire and between tire pavement textures by sand patch method.

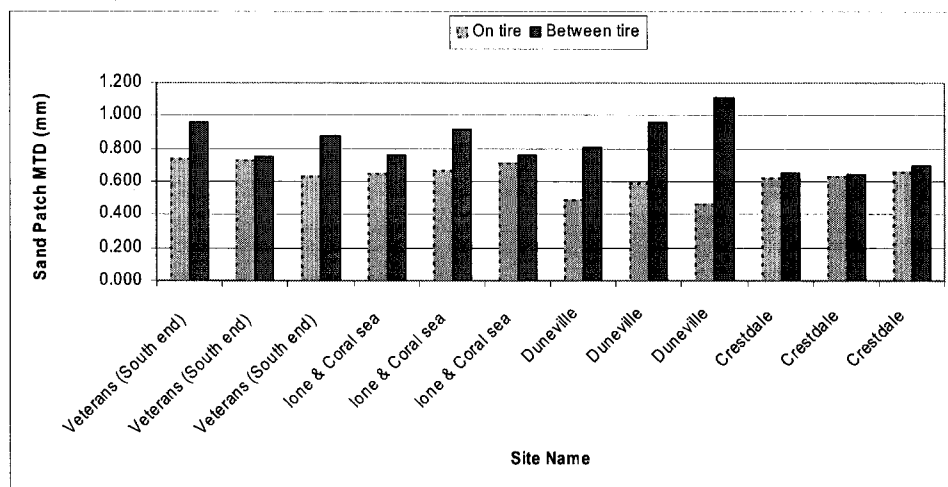


Figure 5.9 On Tire and Between Tire Sand Patch Mean Texture Depth

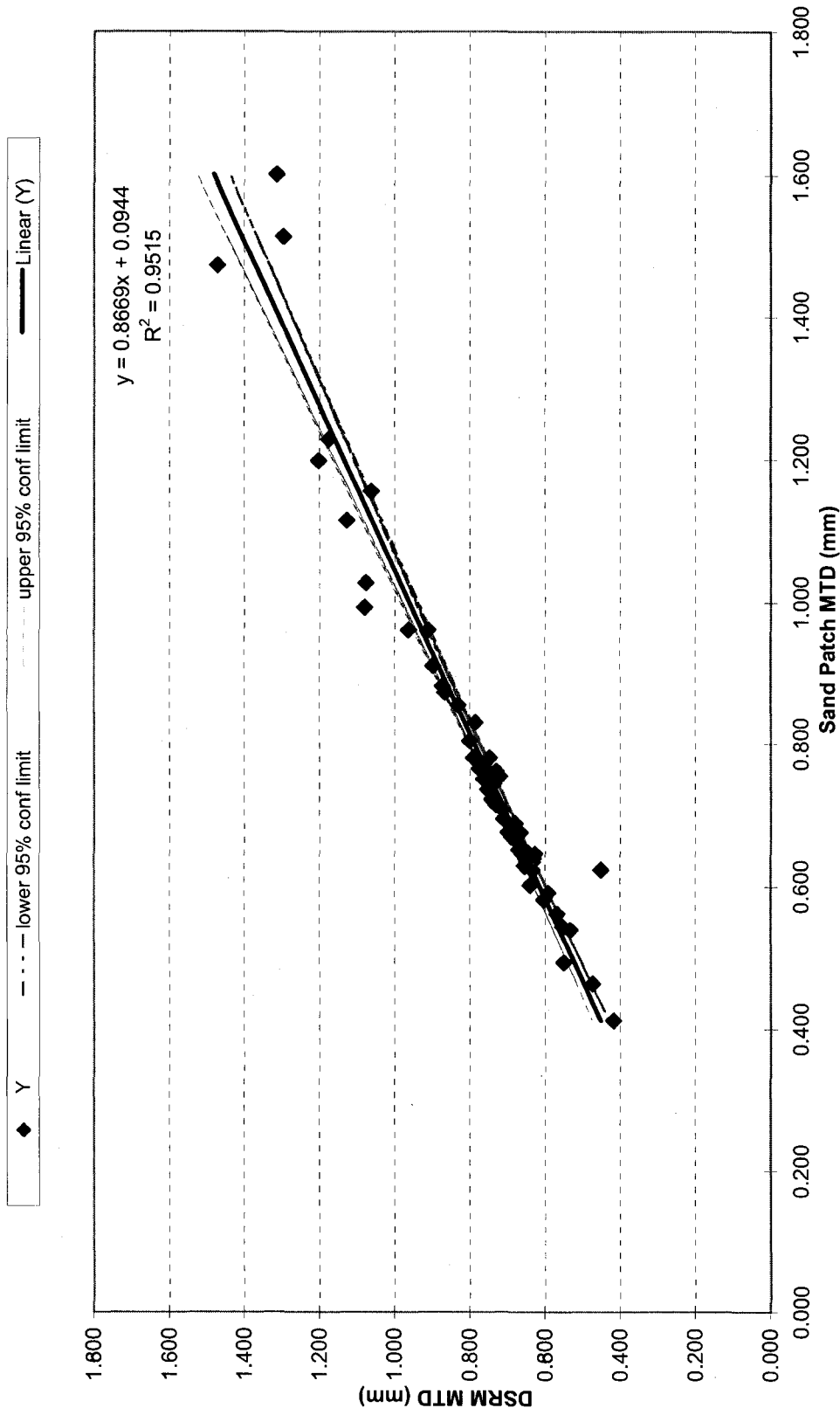


Figure 5.10 DSRM MTD and Sand Patch MTD with 95% Confidence Limit, n=61

## CHAPTER 6

### PM<sub>10</sub> EMISSION RESULTS

#### 6.1 Data Reduction and Processing

The Labview™ software (National Instruments) provides several outputs from the Mini-PI-SWERL™ experiment, such as time, target RPM, real RPM, volumetric flow of the blower (L/min), PM<sub>10</sub> concentration (mg/m<sup>3</sup>) measured by TSI DustTrak, instant emission rate(μg/s), step accumulated PM<sub>10</sub> (μg) and test accumulated PM<sub>10</sub>(μg). The Labview™ software records data every half second. The data were reduced to every second using a data filter in Microsoft Excel. Table 6.1 shows an example of the Labview™ software output after time was reduced to every second.

The time constant in TSI DustTrak was set to one second, meaning that raw PM<sub>10</sub> concentration data were recorded by LabView™. Figure 6.1 is an example of the raw output data from Labview™ software.

Average PM<sub>10</sub> background concentrations were calculated using a time-weighted average of the pre-shear and post-shear TSI data. The Mini PI-SWERL™ blade starts spinning 90 seconds after the ventilation fan started. The initial background PM<sub>10</sub>

concentration first increases due to mobilization of fine dust inside the Mini-PI-SWERL™ and then falls off (Figure 6.1). This initial “spike” decays to background values in the first 30 seconds of fan operation, so the background concentration was estimated using the 60 seconds of ventilation before the blade starts spinning and last the 20 seconds before the fan turns off. The Mini PI-SWERL™ blade stops 60 seconds before the fan turns off, so the last 20 seconds of fan operation takes place 40-60 seconds after the blade has stopped. The duration of background concentration measurements is 80 seconds. The time-weighted average background concentration is calculated as

$$\text{Background concentration} = \left( \frac{60 \text{ seconds}}{(60 \text{ seconds} + 20 \text{ seconds})} \right) * (\text{average concentration over 60 seconds before blade starts spinning}) + \left( \frac{20 \text{ seconds}}{(60 \text{ seconds} + 20 \text{ seconds})} \right) * (\text{average concentration for last 20 seconds after blade stops spinning})$$

The background data was subtracted from the TSI DustTrak concentrations measured during the five blade spin stages.

Table 6.1 Sample Output Data from Mini-PI-SWERL™ (Duneville & Oakey P2S2 Controlled Soil)

Date and Time	Site Name	Target RPM	Real RPM	DT	PM <sub>10</sub> (mg/m <sup>3</sup> )	Flow Rate(L/Min)	Instant Rate(µg/s)	Emission Rate(µg/s)
10:48:26	Duneville P2S2 Soil	2000	2000	0.024	176.4	176.4	0.071	0.071
10:48:27	Duneville P2S2 Soil	2000	1993	0.018	176.4	176.4	0.053	0.053
10:48:28	Duneville P2S2 Soil	3000	1998	0.011	182.6	182.6	0.033	0.033
10:48:29	Duneville P2S2 Soil	3000	2015	0.017	176.4	176.4	0.050	0.050
10:48:30	Duneville P2S2 Soil	3000	2073	0.025	174	174	0.073	0.073
10:48:31	Duneville P2S2 Soil	3000	2160	0.006	197.2	197.2	0.020	0.020
10:48:32	Duneville P2S2 Soil	3000	2284	0.011	197.2	197.2	0.036	0.036
10:48:33	Duneville P2S2 Soil	3000	2406	0.009	176.4	176.4	0.026	0.026
10:48:34	Duneville P2S2 Soil	3000	2520	0.016	174	174	0.046	0.046
10:48:35	Duneville P2S2 Soil	3000	2614	0.05	165.4	165.4	0.138	0.138
10:48:36	Duneville P2S2 Soil	3000	2697	0.114	182.6	182.6	0.347	0.347
10:48:37	Duneville P2S2 Soil	3000	2773	0.229	185	185	0.706	0.706
10:48:38	Duneville P2S2 Soil	3000	2848	0.358	172.8	172.8	1.031	1.031



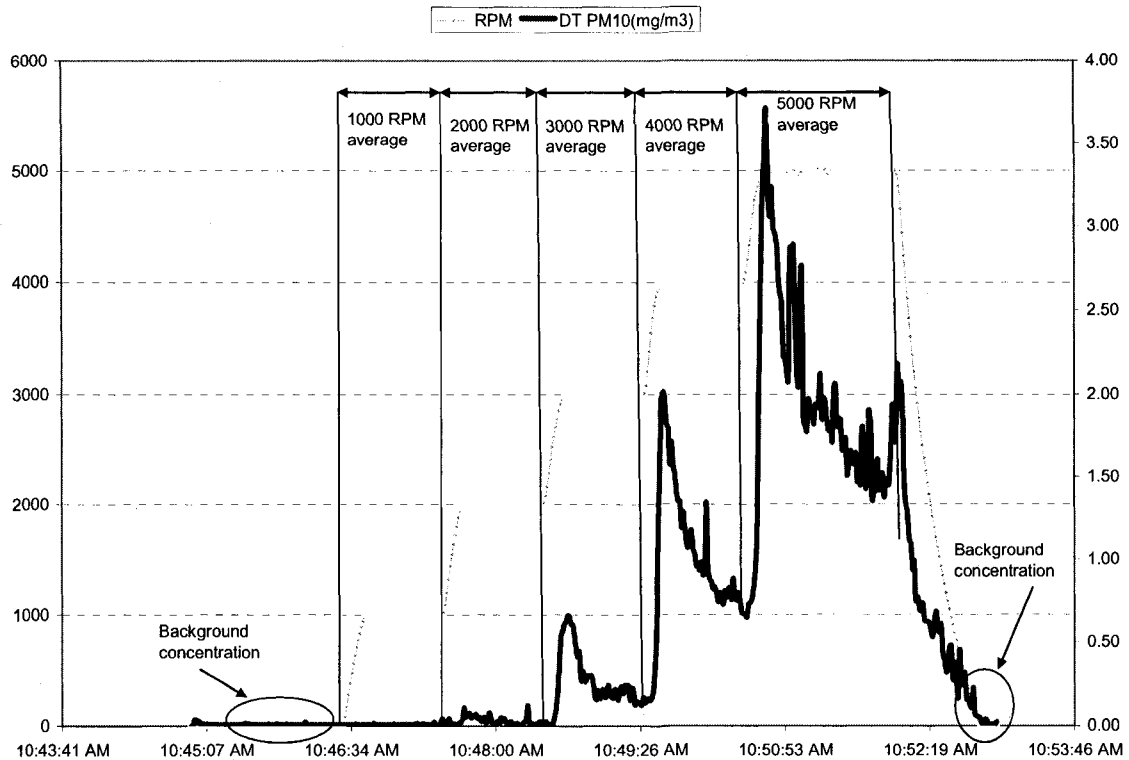


Figure 6.1 PM<sub>10</sub> Concentration Raw Data collected every second (Duneville & Oakey P2S2 Soil)

The average PM<sub>10</sub> emission rate (mg/min) was calculated by multiplying the average PM<sub>10</sub> concentration (mg/m<sup>3</sup>) by the average flow (L/min). Average emitted mass was calculated by multiplying average PM<sub>10</sub> emission rate (mg/min) by the duration (min). Each rpm step continued for 60 seconds except 5000 rpm step. The 5000 rpm step continued for 90 seconds. Figure 5.1 and Figure 5.2 show an initial “spike” in PM<sub>10</sub> concentration at each RPM step. Normally, in the 1000 rpm and 2000 rpm steps the spike is not prominent. The PM<sub>10</sub> concentration decreases through the duration of each rpm step due to depletion of surface reservoir.

The Mini PI-SWERL™ shear rate increases with blade rpm, and, generally, more mass is emitted from the pavement surface as shear rate increases. Shear produced by the

Mini-PI-SWERL™ was calculated using the equation provided by G.Nikolich from DRI to G. Rodrigues in 2006 shown below, where shear in N/m<sup>2</sup> (Nikolich, personal communication, 2006 as cited in Rodrigues, 2006).

$$\text{Shear} = -4 \times 10^{-12} \times (\text{rpm})^3 + 5 \times 10^{-8} \times (\text{rpm})^2 - 2 \times 10^{-5} \times (\text{rpm}) + 0.0351 \quad (6.1)$$

The average shear stress was calculated for each rpm. Table 6.2 shows an example of average emitted mass and average shear calculation.

Figure 6.2 shows an example of the least squares quadratic fit of time averaged mass-emission rate to applied shear. More mass was emitted when the shear rate was high.

Figure 6.3 shows an example of the power fit average PM<sub>10</sub> mass to shear force.

Table 6.2 Emitted Mass and Shear Calculation for Duneville & Oakey P2S2 Controlled Experiment

RPM Step	Avg RPM	Average Flow(L/min)	Avg Net PM <sub>10</sub> Concentration (mg/m <sup>3</sup> )	Avg PM10 Emission Rate (mg/Min)	Avg Mass Emissions (mg)	Avg Shear Stress (Pa)
1000	828	178.1	0.000	0.000	0.000	0.056
2000	1843	177.7	0.000	0.000	0.000	0.151
3000	2837	178.7	0.218	0.039	0.039	0.299
4000	3847	178.1	0.919	0.164	0.164	0.480
5000	4891	176.3	1.849	0.326	0.494	0.671

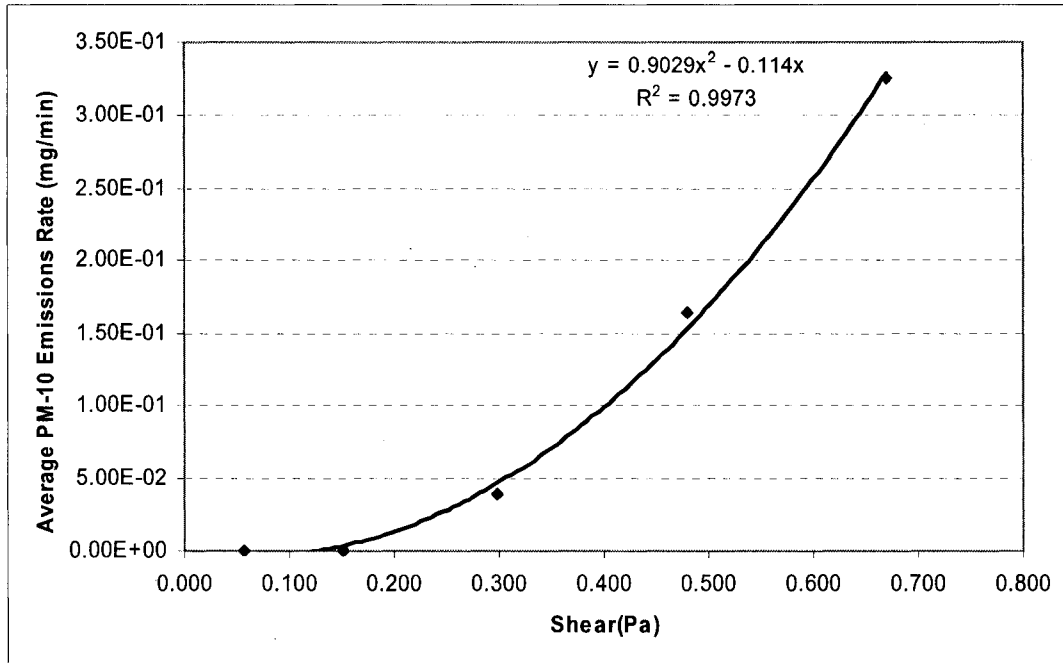


Figure 6.2 Average Emitted Mass vs Shear for Duneville & Oakey P2S2

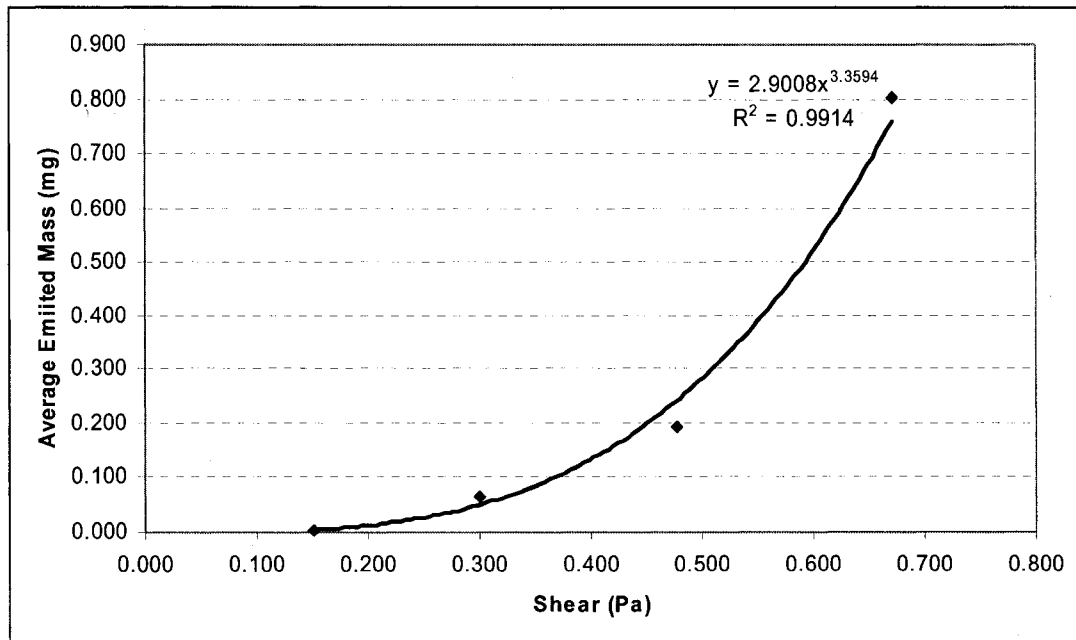


Figure 6.3 Average Emitted Mass vs Shear for Burkholder & Cabrillo P2S1 Soil

## 6.2 Pavement Texture and PM<sub>10</sub> Emissions

### 6.2.1 Ambient Condition Experiments

The pavement texture measurements results for the sand patch method and the DSRM were explained in Chapter 5. Silt loadings were calculated using the silt fraction from AP-42 silt recovery sampling for each plot at every site (Chapter 4). It is hypothesized that (1) equilibrium silt loading on pavement surface could depend on pavement texture, (2) emissions depend on silt loading and (3) normalized emissions from pavement surfaces depends on pavement surface texture. In order to test the first hypothesis, silt loading was plotted against pavement texture (Figure 6.4). The sand patch MTD was used for comparisons because the sand patch is the ASTM (E 965, 2001) standard method for pavement macrotexture measurement.

Visual inspection and regression analysis of the data set show that there is no significant relationship between silt loading and Sand Patch MTD.

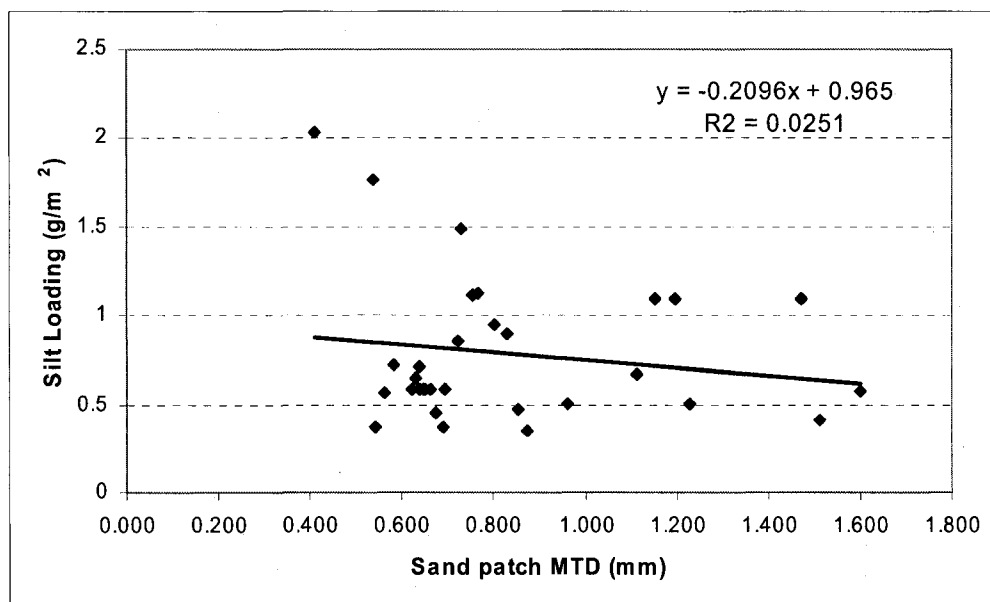


Figure 6.4 Silt Loading vs Sand Patch MTD

The apparent low silt loadings at high (MTD > 1.000) textures shown in Figure 6.4 are a consequence of these loadings all being measured from minor arterial roads, where lower equilibrium silt loadings are expected due to higher vehicle speeds and a larger proportion of heavy vehicles. It is possible that measured silt was not in equilibrium because of recent depositions from external sources.

To test second hypothesis, ambient mass for all rpms were summed (sum of all RPM mass = mass emitted at 1000 rpm+ mass emitted at 2000 rpm + mass emitted at 3000 rpm + mass emitted at 4000 rpm + mass emitted at 5000 rpm). Next silt loading and emitted mass for sum of all rpm was plotted in Figure 6.5. The least squares quadratic regression indicated a significant correlation ( $r^2 = 0.895$ ) was between  $PM_{10}$  mass emitted from the pavement surface and silt loading. The p value for linear term was 0.04 and p value for the quadratic was  $6.069 \times 10^{-6}$ .

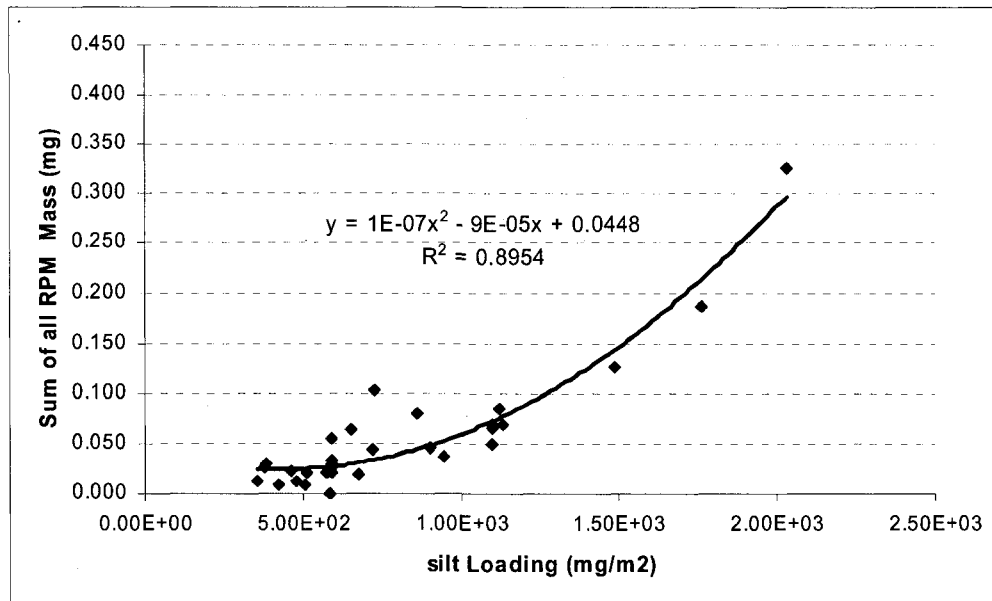


Figure 6.5 Ambient  $PM_{10}$  Mass Emissions vs silt loading

To test the third hypothesis, emitted mass was then plotted against the sand patch MTD. Figure 6.6 shows that the emitted mass are high for lower texture range from 0.4 mm to 0.8 mm and emitted mass are low when the sand patch MTD range from 1.2 mm to 1.6 mm. The linear regression results show that the coefficient of determination is not high ( $r^2=0.158$ ) but is statistically significant ( $p = 0.0267$ ) (Figure 6.6 a).

The sand patch mean texture depth (MTD) was compared with mass emitted by the Mini-PI-SWERL™ at 2000, 3000, 4000 and 5000 rpm. The 1000 rpm mass was neglected because in most of the cases very little mass was emitted at 1000 rpm. Figure 6.6 compares several different least-square fits that were used to test various functional correlations of summed mass with sand patch MTD. The power fit and the exponential fit did a better job of explaining the relationship between the summed ambient emissions and texture.

Figure 6.7 and 6.8 (a and c) show the relationship of emitted mass with pavement texture at 2000 rpm, 3000 rpm , 4000 rpm and 5000 rpm. Figure 6.7 and 6.8 (b and d) depict the same relationship but shown in an expanded scale.

As discussed earlier the emission from pavement surface depends on silt loading. Silt loadings were not same for all the test sites, so the decision was made to normalize the emitted mass by silt loading (6.2).

$$\text{Normalized mass} = \frac{\text{Actual emitted mass}(mg)}{\text{Silt loading}(mg / m^2) \times \text{Test area}(m^2)} \quad (6.2)$$

Normalized mass was plotted against the sand patch MTD to investigate if there was any strong relation between mass emissions from the pavement surface by Mini-PI-SWERL™ with pavement surface texture.

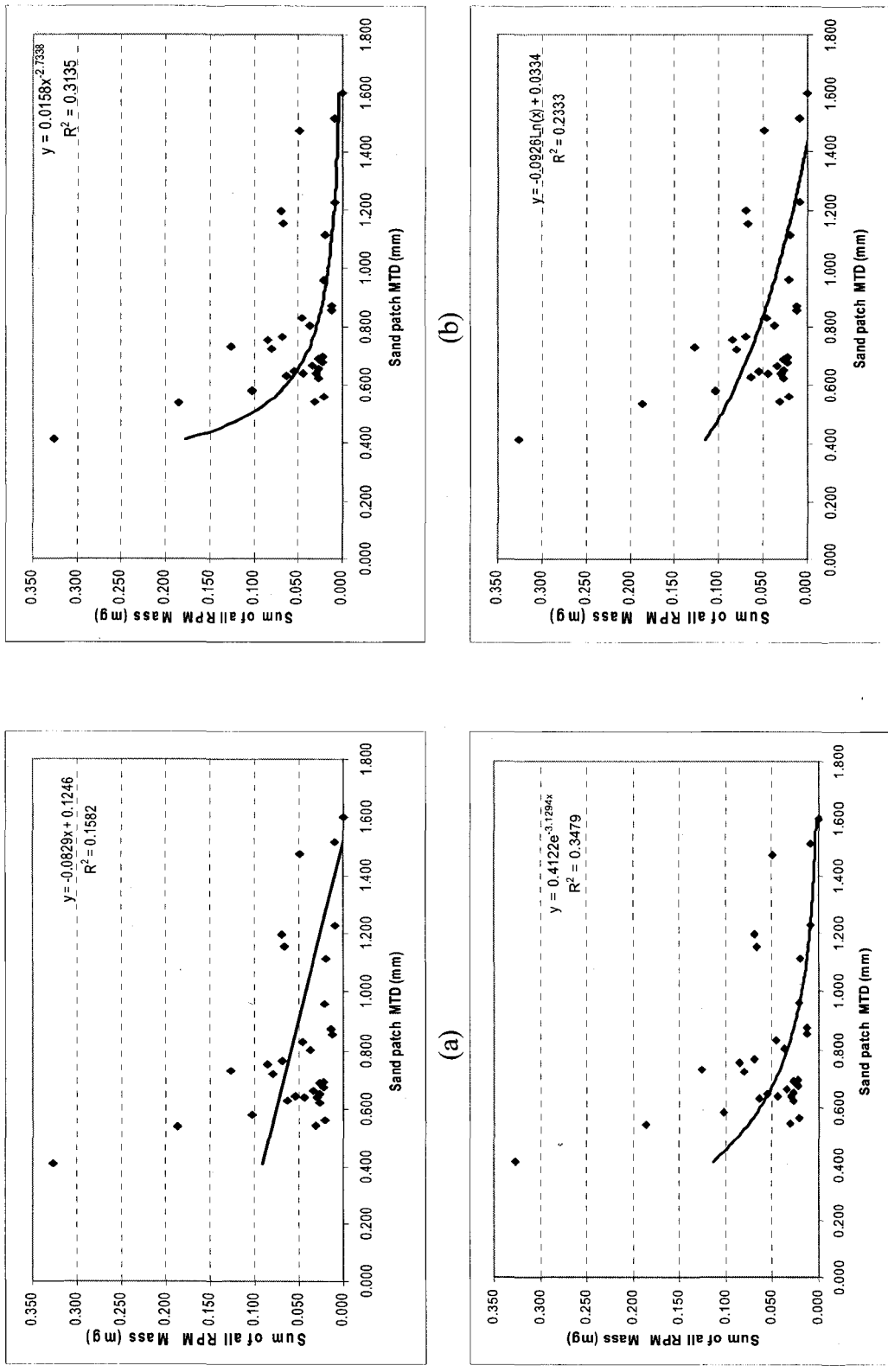


Figure 6.6 (a) Linear fit (b) Power fit, (c) Exponential fit, (d) Logarithmic fit (All are Ambient Condition and Summed Actual Emitted Mass)

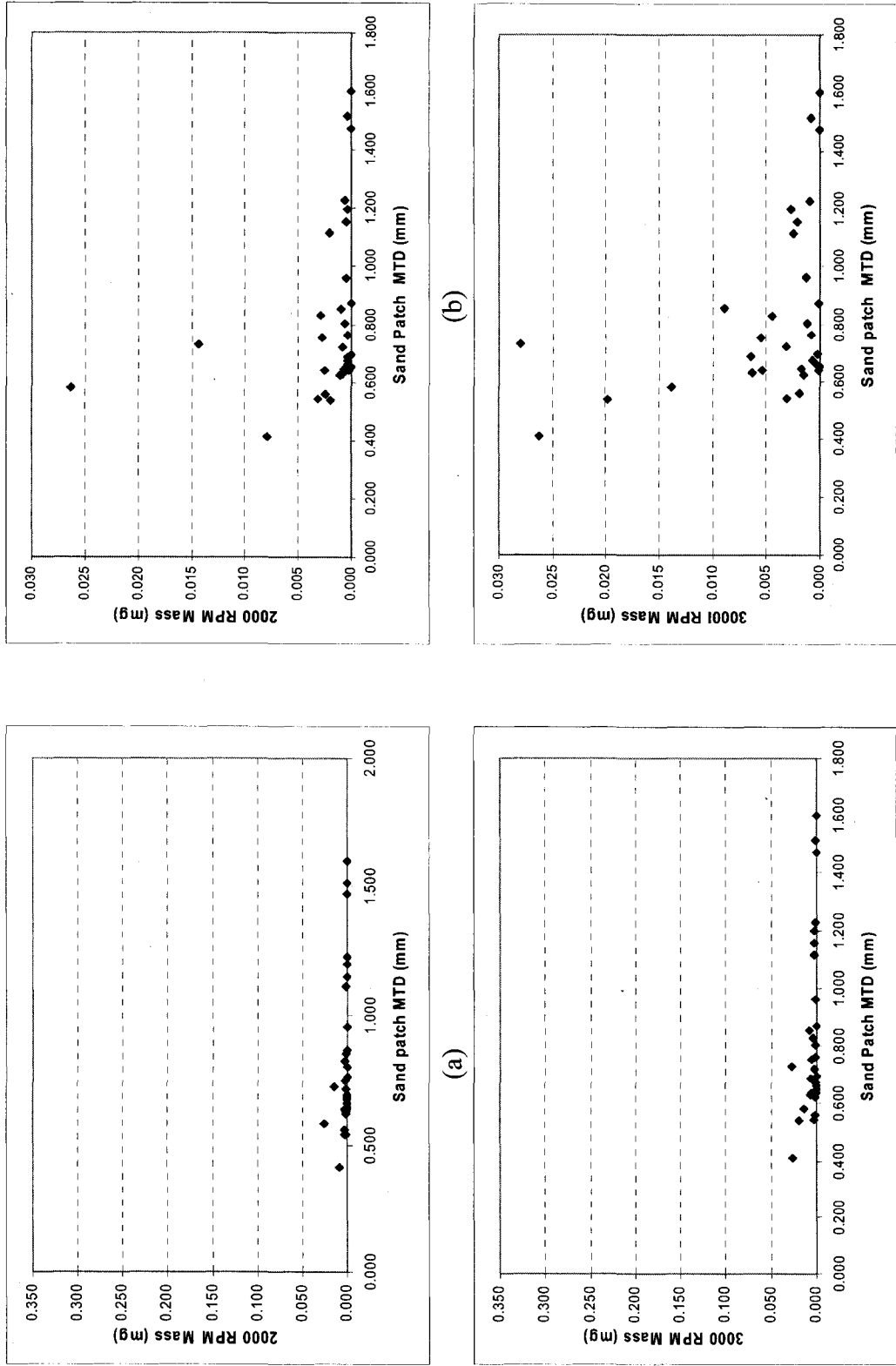


Figure 6.7 (a) 2000 RPM Mass, (b) 2000 RPM Mass with Expanded Scale, (c) 3000 RPM Mass, (d) 3000 RPM Mass with Expanded Scale (All are Ambient Condition and Actual Emitted Mass)



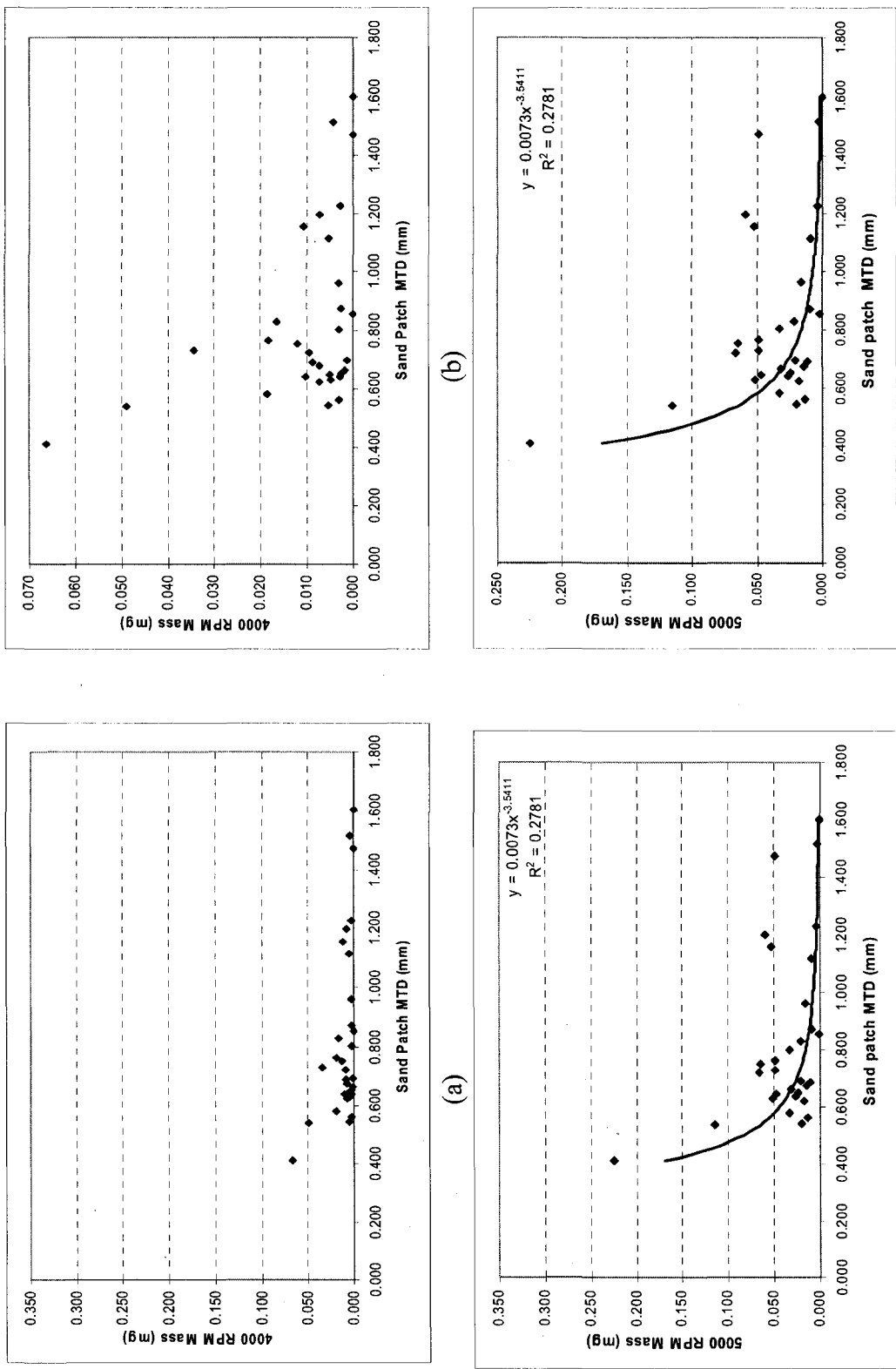


Figure 6.8 (a) 4000 RPM Mass with Expanded Scale, (b) 4000 RPM Mass with Expanded Scale, (c) 5000 RPM Mass, (d) 5000 RPM Mass with Expanded Scale (Ambient condition)

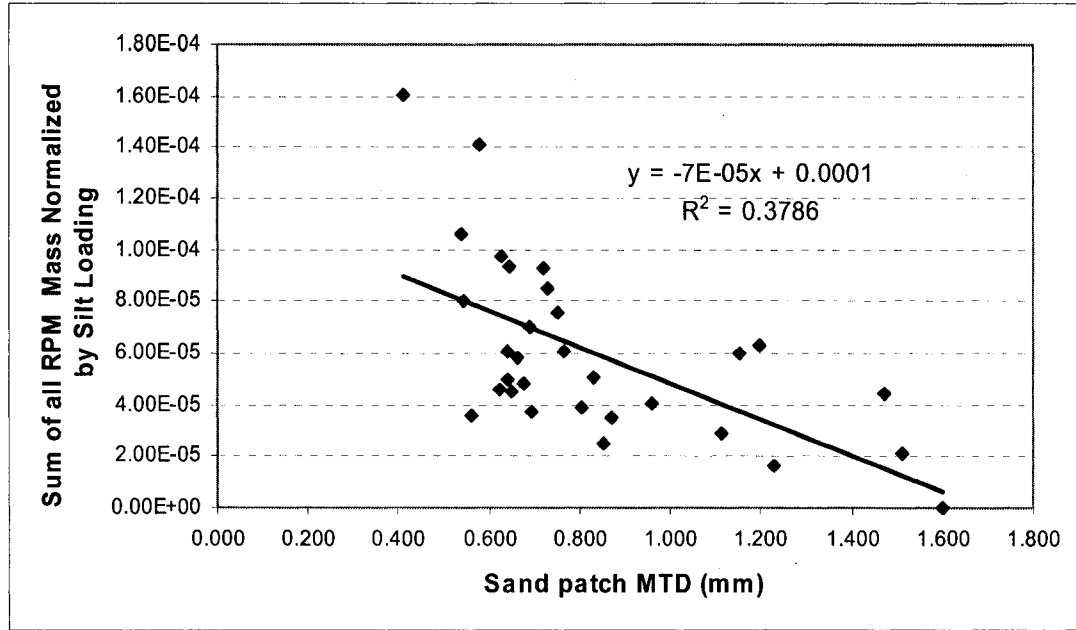


Figure 6.9 Normalized Sum of all RPM Ambient Mass Emissions vs Sand Patch MTD

Figure 6.9 shows that the correlation ( $r^2 = 0.379$ ) for normalized ambient mass with pavement texture is better than the correlation without normalization. The correlation suggests that there might be a relationship between normalized  $PM_{10}$  mass emission rates and pavement surface texture. The correlation is statistically significant ( $p = 0.001$ ).

Figure 6.10 (a & c) show the normalized mass and pavement texture plots for 2000, 3000 rpm. Figure 6.11 (a & c) show 4000 and 5000 rpm at different MTD. Effects of texture on ambient  $PM_{10}$  emissions are suggested but are not distinct at the lower (2,000, 3000, 4,000 rpm) shear rates. Ambient  $PM_{10}$  mass emitted at 5000 rpm strongly indicates that the higher  $PM_{10}$  masses are emitted when pavement textures are low and lower masses are emitted when pavement textures are high. Several data points also indicate that emissions were high although pavement texture was high.

Figure 6.10 (b & d) and Figure 6.11 (b & d) showed the segmented curve with slope “break” (<0.9 mm and > 0.9 mm). When segmented linear fits are performed, Figure 6.10 (b & d) data pairs don’t show any kind of pattern. Figure 6.11(d) at 5000 rpm suggests that there may be break point in the slope of ambient emissions with texture. After that break point, the rate of change of emission rate with texture is small, except for several data points.

An apparent break in ambient mass emitted at 5000 rpm seems to line up with an apparent break in the mode of the road surface texture. Figure 6.12 shows the dependency of mode on pavement texture. Emitted mass were plotted against mode at 2000, 3000, 4000 and 5000 rpm (Figure 6.13, a, b, c and d). The “break” didn’t appear when emitted mass were plotted against mode. The linear least square regression shows that there are partial effects of pavement texture on mode for  $PM_{10}$  emission for ambient condition.

Overall, emitted ambient  $PM_{10}$  mass strongly depends on silt loading, and may depend on pavement surface macrotexture. Controlled experiments with a soil on fixed composition might better explain the relationship between pavement texture and emissions because ambient soil had different particle size distribution at different site. As threshold friction velocity depends on particle size mode, so threshold friction velocity of particle will vary from site to site. Thus the effect of pavement surface macrotexture on  $PM_{10}$  emissions can’t be separated from varying threshold friction velocities of soils from different sites.

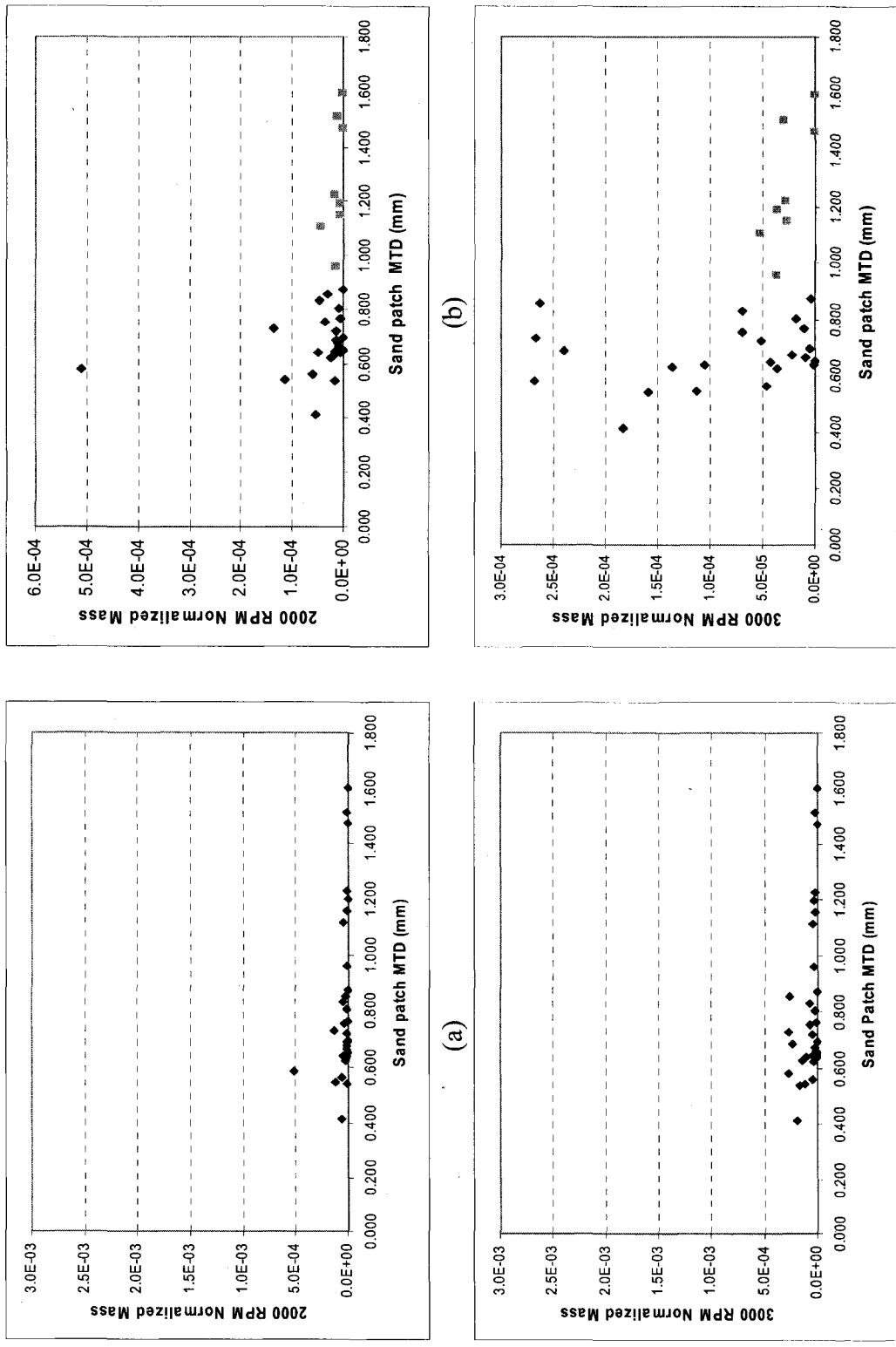


Figure 6.10 (a) 2000 RPM Mass, Segmented plot (b) 2000 RPM Mass, Segmented plot (c) 3000 RPM Mass, Segmented plot (d) 3000 RPM Mass Segmented plot (Normalized Mass by Silt Loading), (Diamonds represent  $<0.9\text{ mm}</math>, and Squares represent  $>0.9\text{ mm}</math>)$$

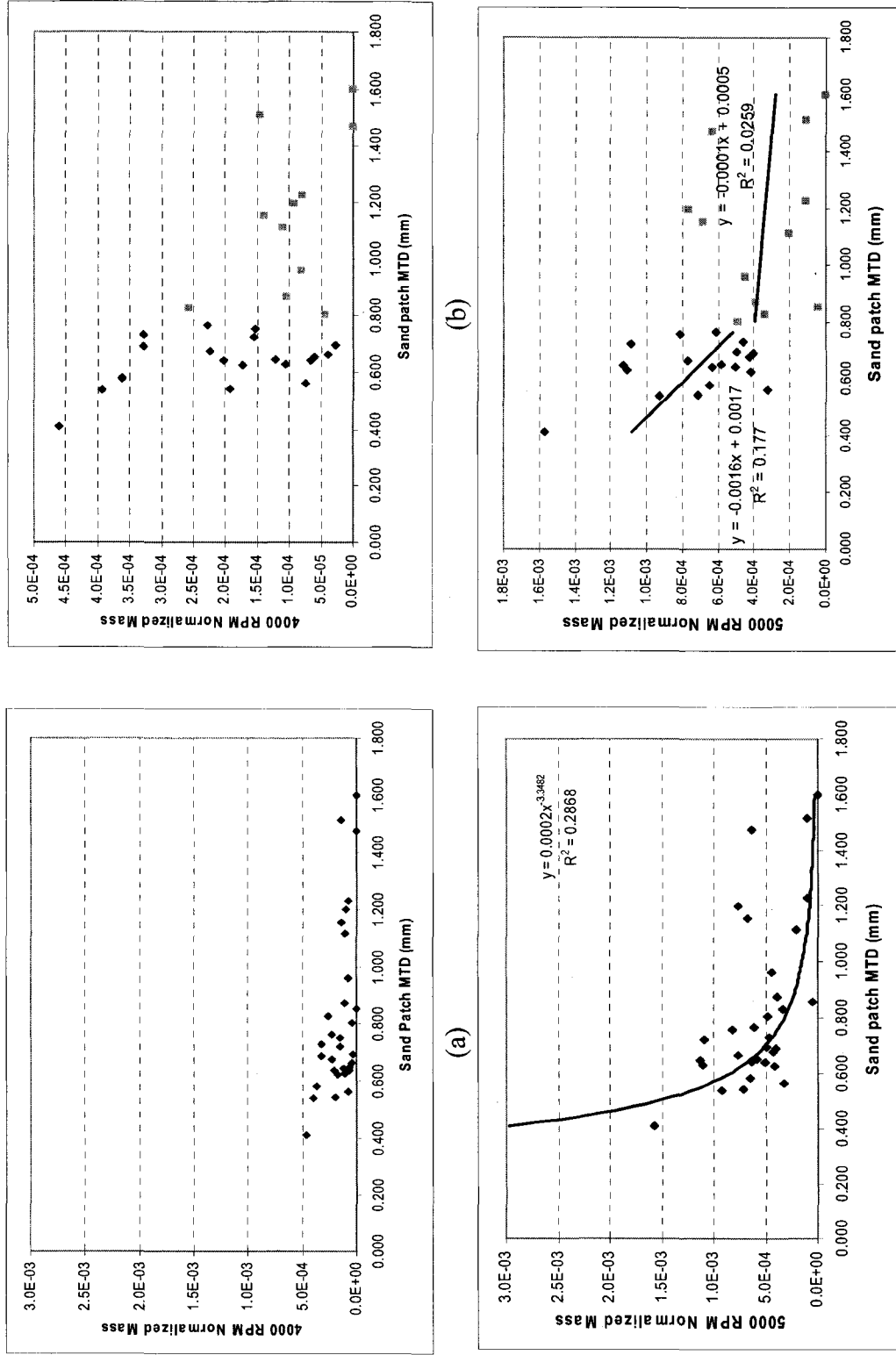


Figure 6.11 (a) 4000 RPM Mass, (b) 4000 RPM Mass with Segmented plot, (c) 5000 RPM Mass, (d) 5000 RPM Mass with Segmented plot (Normalized Mass), (Diamonds represent <0.9 mm, and Squares represent >0.9 mm)

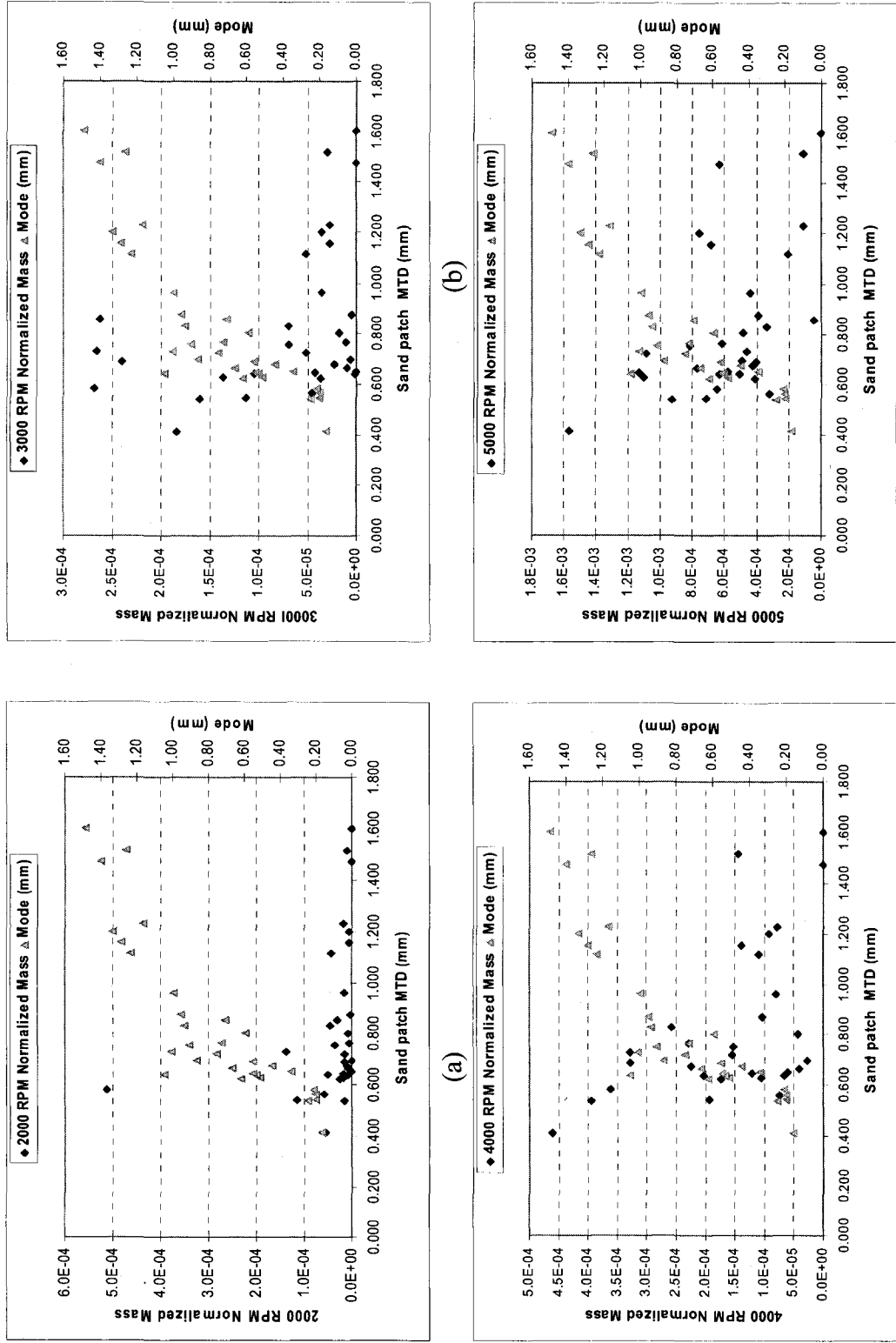
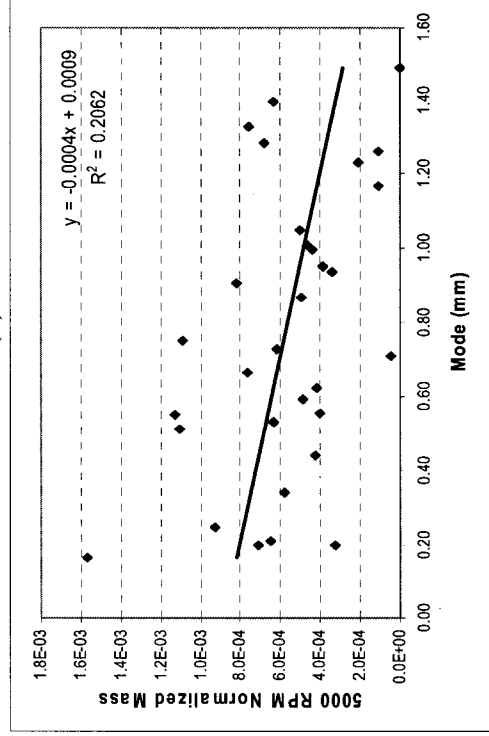
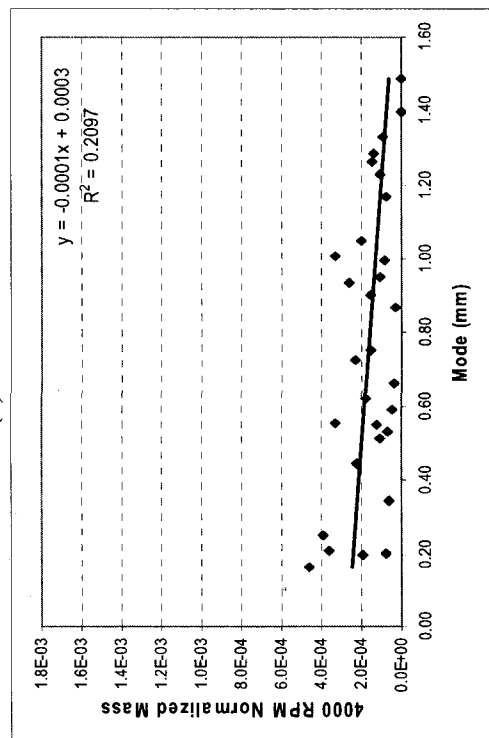
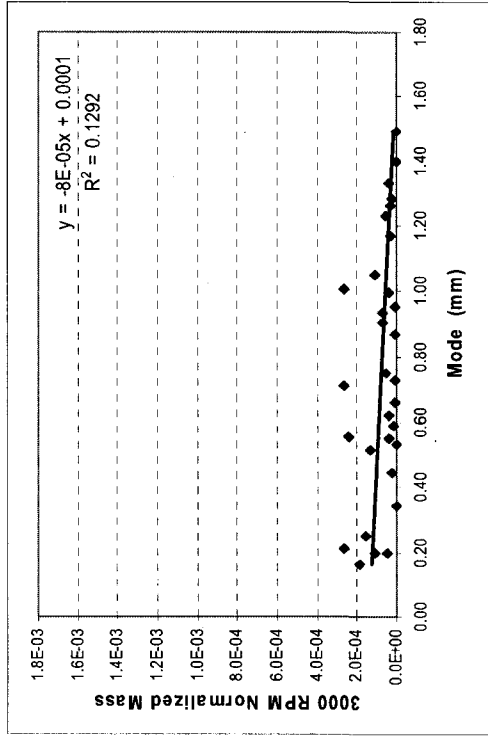
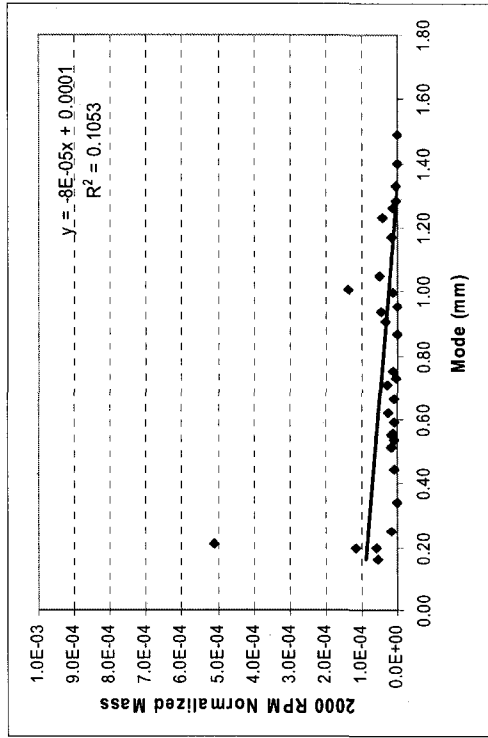


Figure 6.12 2000 RPM Mass, (b) 3000 RPM Mass, (c) 4000 RPM Mass, (d) 5000 RPM Mass with Mode (mm) and MTD(mm) (Ambient Condition and Normalized Mass By Silt Loading)



(a) 2000 RPM Mass, (b) 3000 RPM Mass, (c) 4000 RPM Mass, (d) 5000 RPM Mass vs Mode (mm) (Ambient Condition and Normalized Mass By Silt Loading)

## 6.2.2 Controlled Experiments

The controlled experiment (described in Chapter 3) data were used for mass emissions comparisons with MTD. For each Mini PI-SWERL speed, emitted mass was tabulated and plotted against the sand patch MTD. Figure 6.16 (a) and (c) show the relationship between the mass emitted at 2000 rpm and 3000 rpm vs sand patch MTD respectively and Figure 6.16 (b) and (d) show the same data using an expanded scale. Figure 6.17(a) and (c) show the relationship between mass emitted at 4000 rpm and 5000 rpm vs sand patch MTD respectively, and Figure 6.17 (b) and (d) show the same data using an expanded scale.

At each rpm (shear) level, emissions were highest at the low MTDs and lowest at the high MTDs. Applied shear at 1,000 rpm is nearly always below the threshold to initiate erosion, and 2,000 rpm shear is often below the threshold to initiate erosion, with some sites with MTD < 0.80-0.90 mm emitting, and all sites above 0.80-0.90 mm MTD not emitting. Results also show dependency of PM<sub>10</sub> mass emission on the pavement macrotexture for shear rates of 3,000, 4,000 and 5,000 rpm. . Emitted mass was always much higher for MTD's < 0.80-0.90 mm than for MTD's > 0.90 mm.

Table 6.3 shows the Mini PI-SWERL emitted mass at 5000 rpm and the texture at different site locations. Data for 2000, 3000 and 4000 rpm are tabulated in Appendix A. At 5000 rpm, the highest mass (1.518 mg) emitted at Evergold & Coral Sea site at Plot 3 Spot1 (P3S1) location had the second lowest measured MTD (0.539 mm). The lowest mass was emitted from Ann & San Mateo site (P1S1) which had the highest sand patch MTD (1.601 mm).



Table 6.3 Mini PI-SWERL™ Emitted Mass at 5000 RPM and Sand Patch MTD

Site Name	Location	DSRM		5000	(Clean)
		(MTD) mm	Sand patch MTD) mm	RPM Mass(mg)	5000 RPM Mass(mg)
Evergold & Coral Sea	P2S1	0.417	0.412	1.441	0.023
Evergold & Coral Sea	P3S1	0.533	0.539	1.518	0.037
Goldhill & Richmar	P3S1	0.553	0.544	1.207	0.000
Goldhill & Richmar	P2S1	0.569	0.562	1.063	0.027
Goldhill & Richmar	P1S1	0.603	0.581	1.083	0.019
Crestdale	P1S1	0.634	0.623	0.887	0.023
Sapphire Light	P3S1	0.654	0.629	0.883	0.102
Sapphire Light	P2S2	0.63	0.64	0.885	0.074
Crestdale	P2S1	0.651	0.640	0.858	0.042
Crestdale	P2S2	0.628	0.646	0.890	0.044
Crestdale	P1S2	0.655	0.652	0.747	0.045
Crestdale	P3S1	0.675	0.664	0.844	0.041
Pabco & Tabony	P2S1	0.667	0.676	0.888	0.000
Pabco & Tabony	P1S1	0.681	0.689	0.782	0.024
Crestdale	P3S2	0.711	0.695	0.766	0.031
Burkholder	P2S1	0.743	0.722	0.801	0.075
Armacost & Calmar	P3S1	0.761	0.730	0.661	0.085
Armacost & Calmar	P2S1	0.720	0.754	0.722	0.027
Silverspring & Spring Hill	P1S2	0.775	0.765	0.497	0.001
Silverspring & Spring Hill	P2S2	0.790	0.780	0.448	0.023
Duneville & Oakey	P1S2	0.801	0.804	0.559	0.031
Armacost & Calmar	P1S1	0.786	0.830	0.416	0.002
Sapphire Light & Emerald Stone	P1S1	0.831	0.855	0.462	0.025
Burkholder	P3S1	0.866	0.873	0.568	0.058
Duneville & Oakey	P2S2	0.963	0.961	0.494	0.039
Silverspring & Spring Hill	P2S1	1.076	1.028	0.447	0.015
Duneville & Oakey	P3S2	1.127	1.114	0.436	0.002
Maryland & Westminster	P2S1	1.062	1.155	0.713	0.086
Maryland & Westminster	P3S1	1.202	1.198	0.587	0.064
Ann Rd	P2S1	1.175	1.228	0.200	0.019
Maryland & Westminster	P1S1	1.471	1.473	0.558	0.100
Ann Rd	P3S1	1.296	1.514	0.227	0.018
Ann Rd	P1S1	1.314	1.601	0.119	0.014

Several different least-square fits were attempted to correlate emitted mass at different rpms with sand patch MTD. Figure 6.14 show an example of the fitting process for a power fit to the 5000 rpm data. This speed and fit were chosen for detailed display because the data exhibited the highest coefficient of determination,  $r^2=0.72$ . Ninety-five percent confidence limits were computed on the least square linear regression slope and intercept of the log-log transformed data, then applied to compute the confidence limits on the entire regression for the transformed data (Figure 6.14) and then back transformed to illustrate the 95% confidence limits for the power fit (Figure 6.15). Although the power fit explains a significant portion of the variance, and illustrates the overall data trend, it appears to fail in two zones. Results show that a “pocket” of data lies outside the confidence limits at an MTD of about 0.800 mm. Additionally, five of seven data pairs lie outside the 95% confidence limits for MTD’s exceeding 1.2 mm.

Power fits summaries without the 95% confidence limits are shown in Figure 6.16 (d) (3000 rpm), Figure 6.17(b) (4000 rpm), and Figure 6.17(d) (5000 rpm). The coefficients of determination ( $r^2$ ) range from 0.60 to 0.72 Figure 6.18 shows an example of the exponential fit of pavement surface macrotexture and emitted mass. The power fits indicate that the rate of mass emissions on pavement surface texture increases nonlinearly with increasing shear rate. The exponent on shear rate (x) were calculated to be 3.6 for 3,000 rpm, 1.9 for 4,000 rpm and 1.4 for 5000 rpm A power fit was not possible for 2000 rpm as no mass was emitted for many of the cases.

Table 6.4 shows the summary for different fits of emitted mass on sand patch MTD. Exponential and power fits to sand patch MTD both do an adequate job explaining variance in data except for highest values of MTD. The results indicate that the

exponential fit is better for 3000 and 4000 rpm, but the power fit (0.721) was better at 5000 rpm. Scatter above the regression line at high MTD is due to the Maryland & Westminster site, which shows a higher amount of mass emitted although the pavement surface texture at all three tested locations was high. A possible explanation for this anomaly is discussed later.

The expanded plots (Figure 6.16b and d, 6.17b and c) of mass emitted at 2000, 3000, 4000 and 5000 rpm vs MTD show a breakpoint in the slope of emissions vs MTD at somewhere in the range of 0.8 mm to 0.9 mm. Before this break, emission rates decrease rapidly with increase of MTD but after the breakpoint, the observed slope of emission rates vs. MTD may actually be flat.

To evaluate this observation, a segmented linear plot was developed using 0.9 mm break point. Figure 6.19 shows the segmented linear fits. Results are summarized in Table 6.4. The first half of the segment (<0.9 mm MTD) shows coefficients of determination exceeding 0.50 for 3,000 and 5,000 rpm. On the second, flatter half of the segment, only the 4,000 rpm speed has a  $r^2$  value exceeding 0.5.

Table 6.4 Comparing  $r^2$  for Different Fits-Soil Mass Emitted vs Sand Patch MTD

RPM	Power	Exponential	Segmented Linear	
			<0.9 mm	>0.9 mm
2000	NA	NA	0.034	0.002
3000	0.634	0.676	0.511	0.283
4000	0.604	0.656	0.114	0.527
5000	0.721	0.699	0.854	0.254

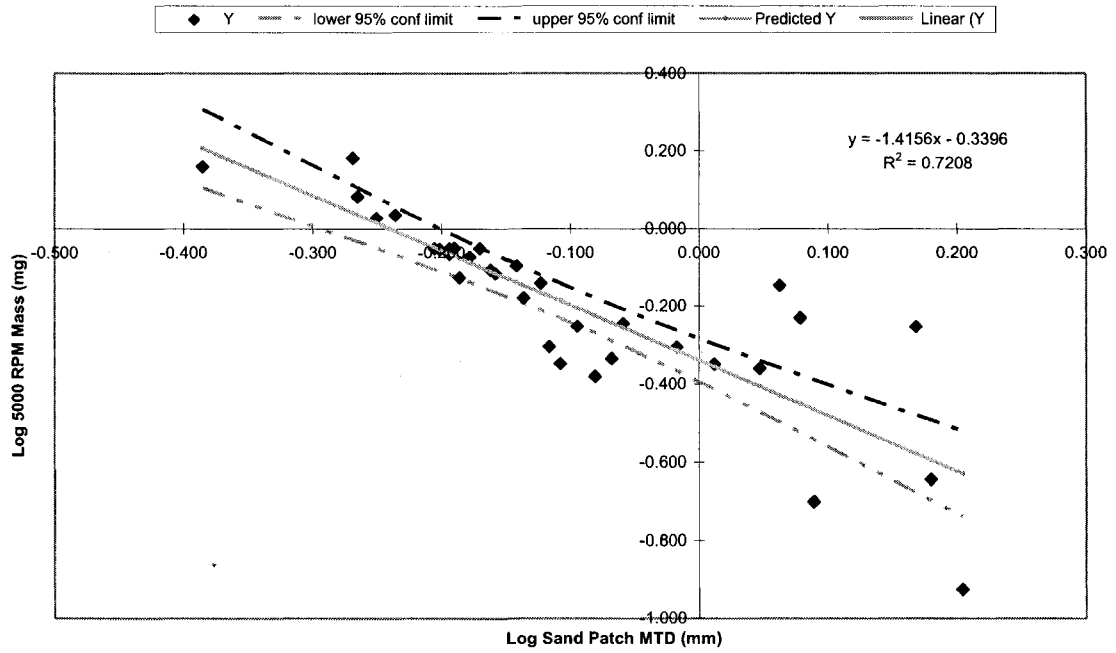


Figure 6.14 5000 rpm power fit log-log plot with 95% Confidence Limit (before back transform)

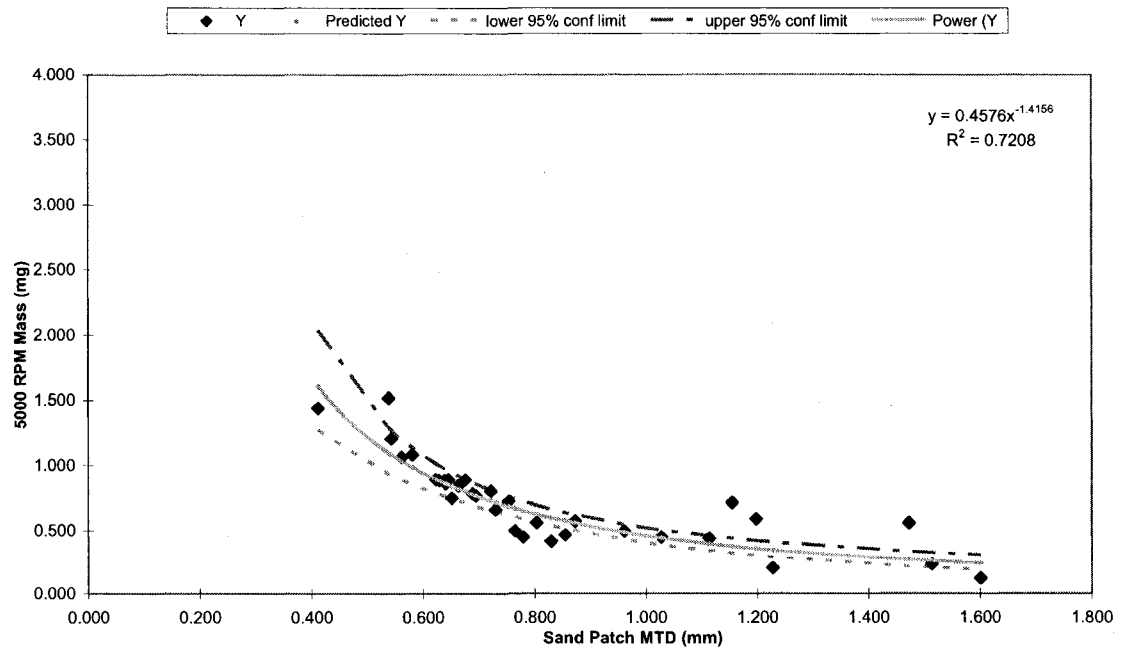


Figure 6.15 5000 rpm power fit with 95% Confidence Limit (after back transform)

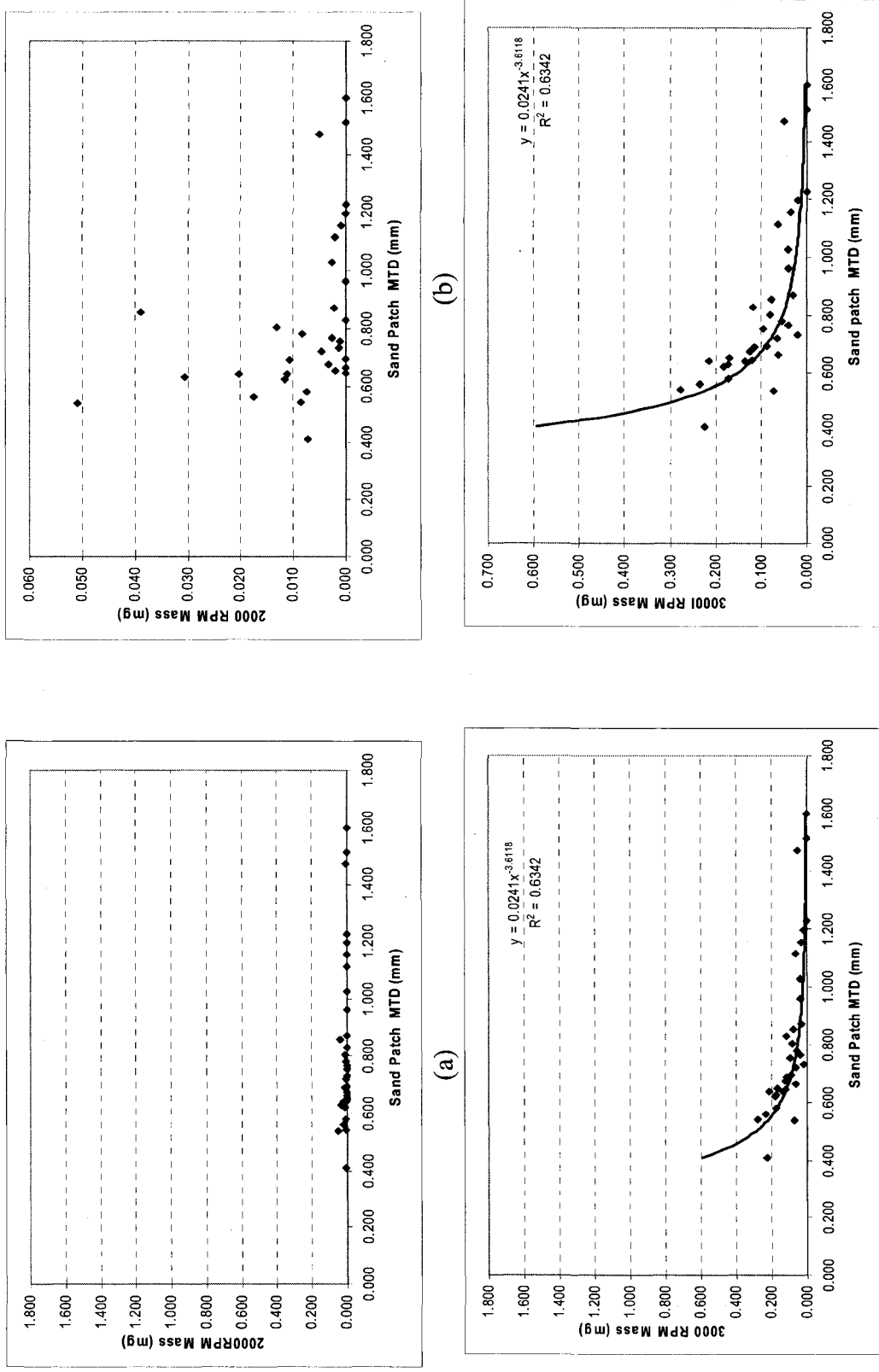
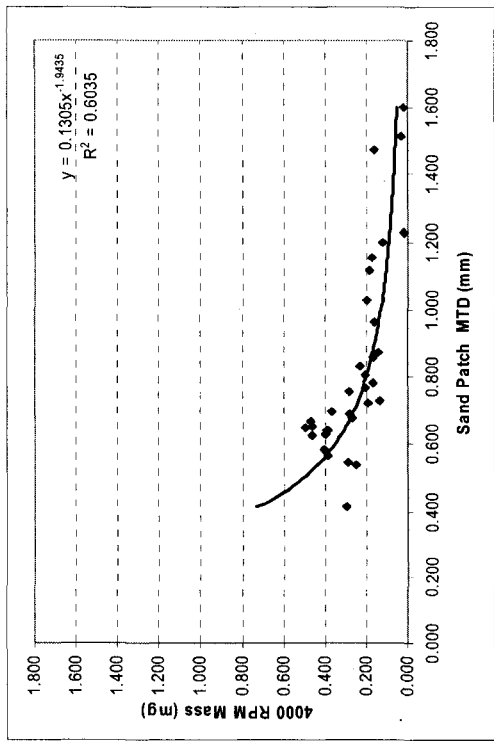
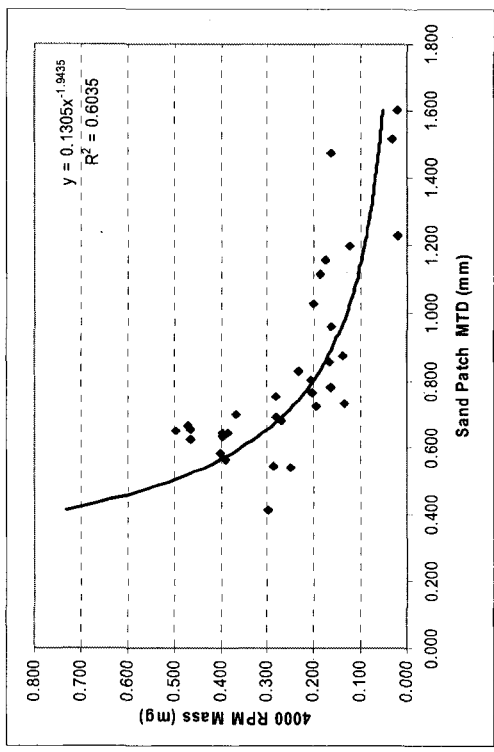


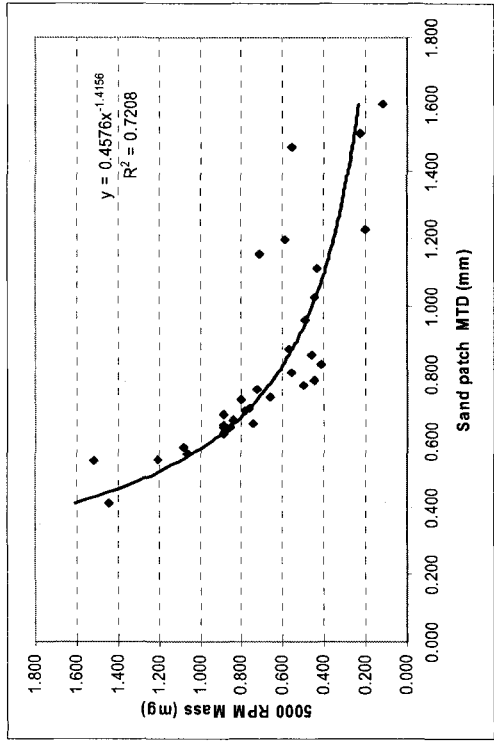
Figure 6.16 (a) 2000 RPM Mass with Expanded Scale, (b) 2000 RPM Mass with Expanded Scale, (c) 3000 RPM Mass with Expanded Scale, (d) 3000 RPM Mass with Expanded Scale



(a)



(b)



(c)

Figure 6.17 (a) 4000 RPM Mass with Expanded Scale, (b) 4000 RPM Mass vs Sand Patch MTD, (c) 5000 RPM Mass vs Sand Patch MTD

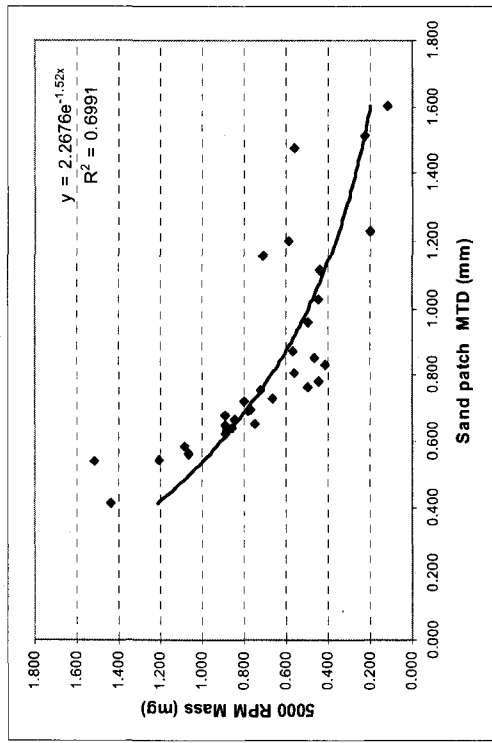
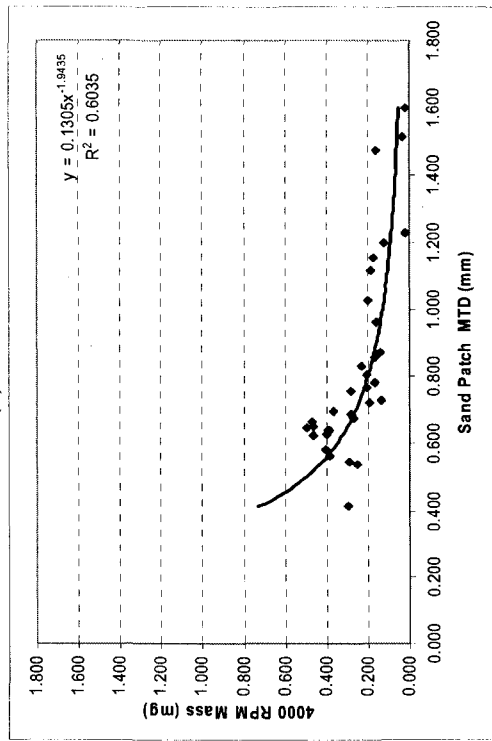
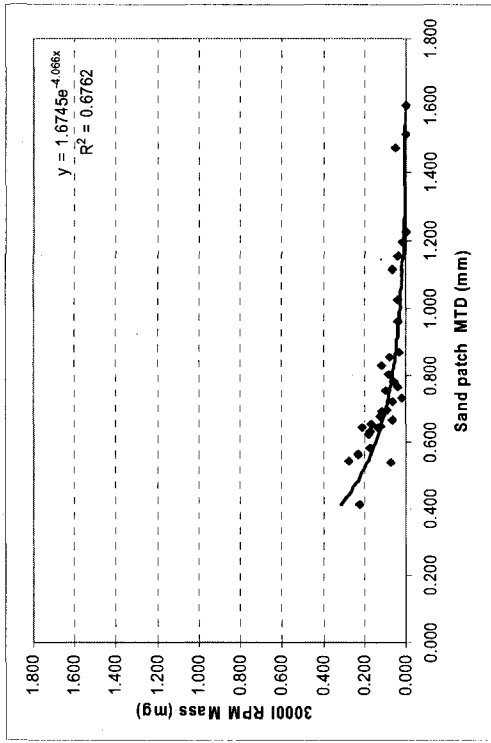
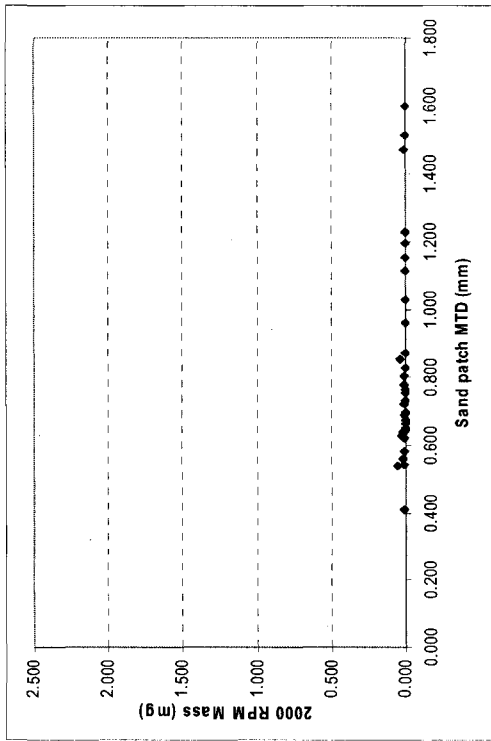
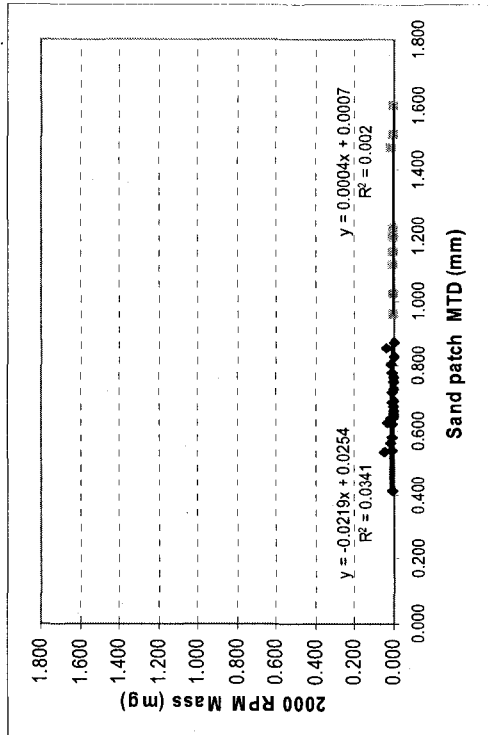
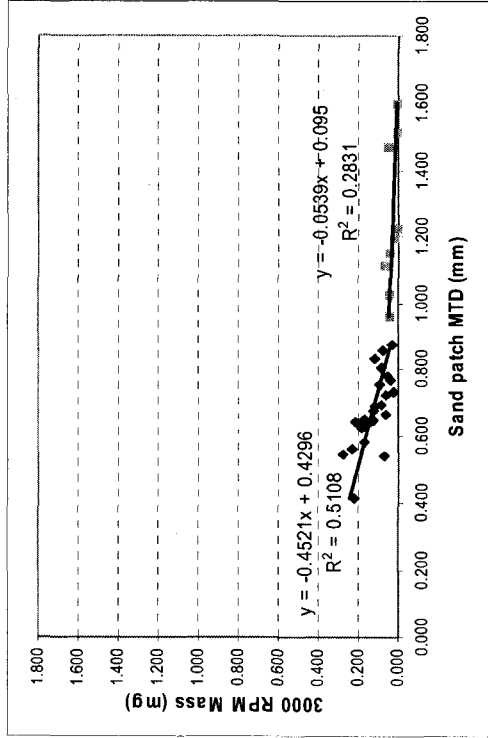


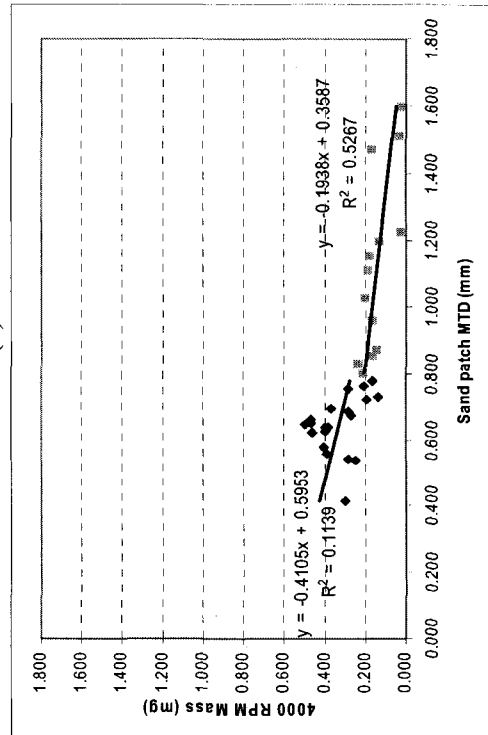
Figure 6.18 (a) 2000 RPM Mass, (b) 3000 RPM Mass (c) 4000 RPM Mass, (d) 5000 RPM Mass with Exponential Fit



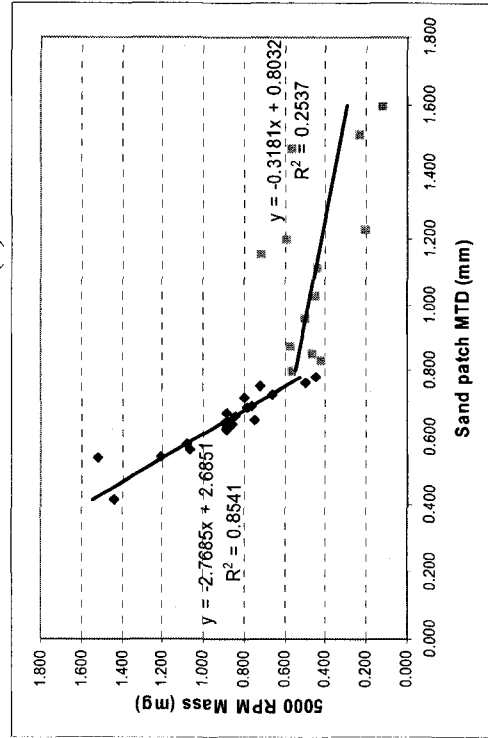
(a)



(b)



(c)



(d)

Figure 6.19a) 2000 RPM Mass, (b) 3000 RPM Mass (c) 4000 RPM Mass (d) 5000 RPM Mass with Segmented Linear Fit



### 6.3 Two-way Frequency Distribution and Photographic Analysis

At high MTD values, Ann & San Mateo had significantly lower PM<sub>10</sub> emissions than predicted by the simple regressions of PM<sub>10</sub> emitted mass on texture, and Maryland and Westminster had significantly higher emissions than predicted by the simple regressions. Since many other sites closely followed the regression, it was decided to further investigate the physical characteristics of these sites in more detail.

#### 6.3.1 Close-up Photographic Analysis

Close-up digital photos and DSRM data were evaluated to determine if either site had unique peak and valley topography in the pavement macrotexture that could shelter or expose erodible material.

Figure 6.20 shows a close-up photo of the Maryland/Westminster site. The high resolution macro lens was not available at the time this field site was visited. The photo was taken before Mini-PI-SWERL™ control experiment. Unfortunately no photo was taken after the controlled experiments.

Figure 6.20 shows that aggregate size distribution are not uniform for Maryland /Westminster pavement surface. Relatively small aggregates are lying between big aggregates which might be responsible for exposed areas for PM<sub>10</sub> particles.

Close-up photos of the Ann and San Mateo were first taken immediately after AP-42 recovery of silt from the surface and before the controlled experiment (Figure 6.21) and then recorded in approximately the same location after application of a controlled silt loading and shear by the Mini-PI-SWERL™(Figure 6.22).

Figure 6.21 shows that the aggregates are exposed and not sealed and that there is very little sediment sheltering in the pits of the cleaned surface.

Figure 6.22 shows residual silt particles located in the pits that were not removed at shear rates applied by the Mini PI-SWERL™, i.e. that the silt particles were “sheltered” in the pits. Shear applied by the Mini-PI-SWERL™ couldn’t scour silt from the deep valleys at the highest applied shear rate (5000 rpm or 0.68 N/m<sup>2</sup>). This might be the reason for the lower-than-expected PM<sub>10</sub> emissions from the Ann & San Mateo pavement surface.

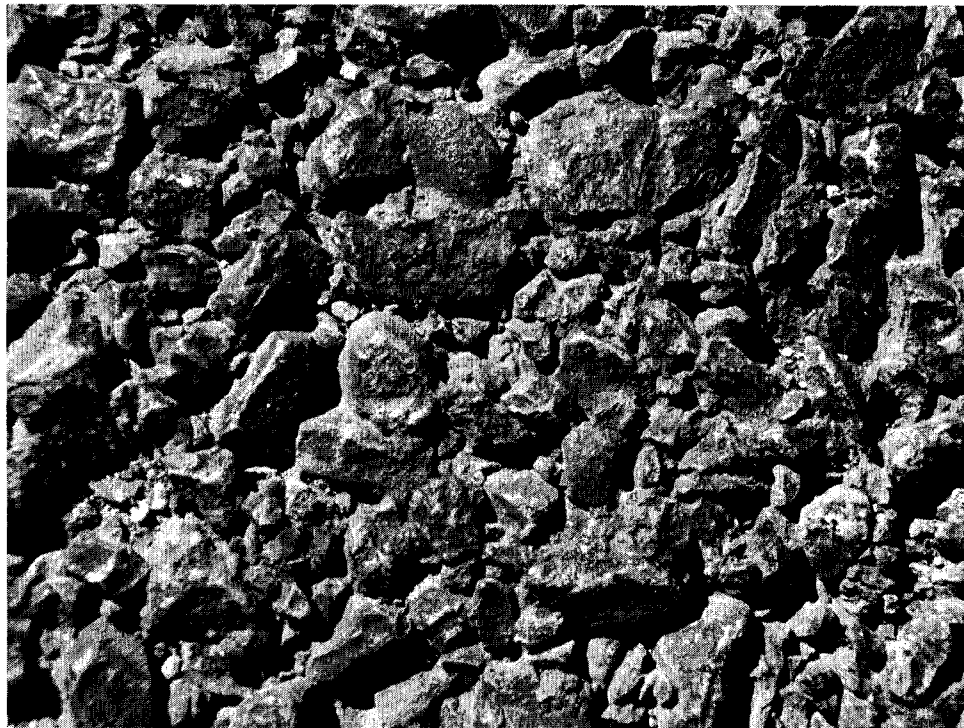


Figure 6.20 Before Mini-PI-SWERL™ Control Experiment at Maryland/ Westminster



Figure 6.21 Before Mini-PI-SWERL™ Control Experiment (Ann Rd & San Mateo)

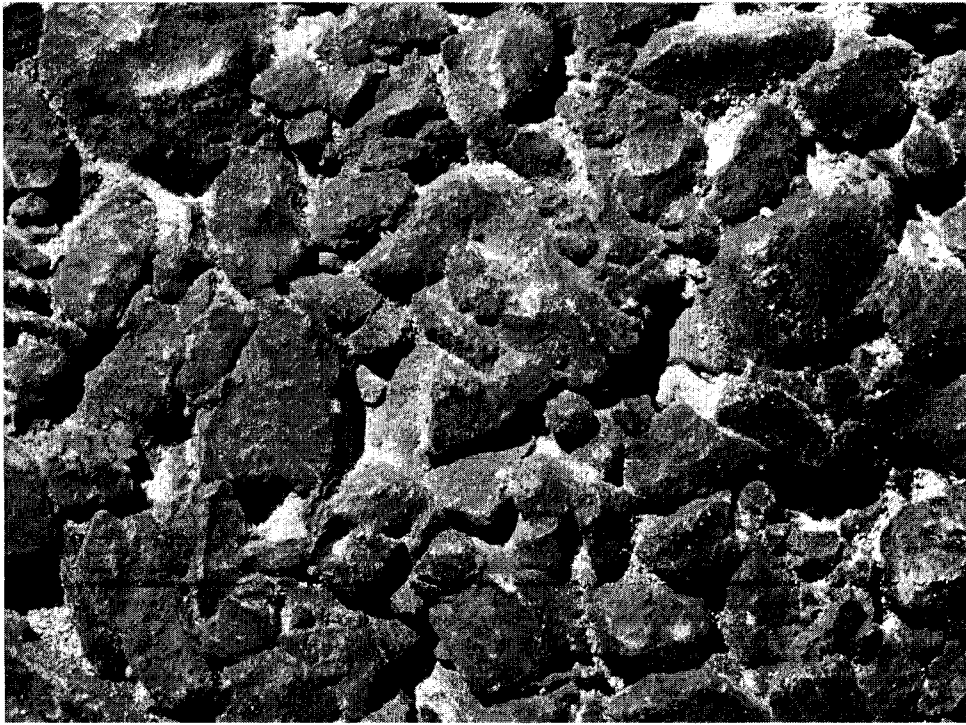


Figure 6.22 After Mini-PI-SWERL™ Control Experiment (Ann Rd & San Mateo)

### 6.3.2 Two-way Frequency Distribution Analysis

Road pavement surface topography was analyzed by identifying, counting and classifying the number of peak and valleys and the magnitudes of their widths and depths to see if there were differences in the relative number of sheltered or exposed zones at the Ann Road/San Mateo and Maryland/Westminster sites. Two-way frequency distributions were computed from the DSRM pixel data to determine the width and depth distributions of the peaks and valleys at these sites. The DSRM provides five lines of measurement and 630 data points on each line to generate 3,150 data points in each 5.0 cm x 5.0 cm measurement square.

Figure 6.23 shows an example of the raw pixel data from DSRM when pixel data for all 5 lines are plotted. Surface “waves” on these plots appears to vary in both amplitude and in frequency. There are several regions where profiles appear to be similar, for example the middle of lines 3 and 4, but in many cases the individual waves are unique to each of the five profile lines. There are obvious broad “valleys,” such as the middle of line 1, or broad high “mesas”, such as the left-hand side of line 5. There are also regions where valleys are deep and narrow, such as on the right hand side of lines 2, 3 and 4.

The widths and heights or depths of the peak or valleys were calculated using the raw pixel data and the vertical and horizontal resolution (0.08 mm per pixel) of the DSRM. Figure 6.24 shows the pavement surface profile for line 3 of one of the Ann Rd & San Mateo sites. The figure shows the pavement surface maximum peak height at about  $x = 2.3$  cm, and maximum valley depth at about  $x = 3.5, 3.7, 4.3$  and  $4.8$  cm. The width of each feature is identified on the horizontal axis, but it doesn't represent the magnitude of the width of each peak or valley at each interval when it crosses zero line.

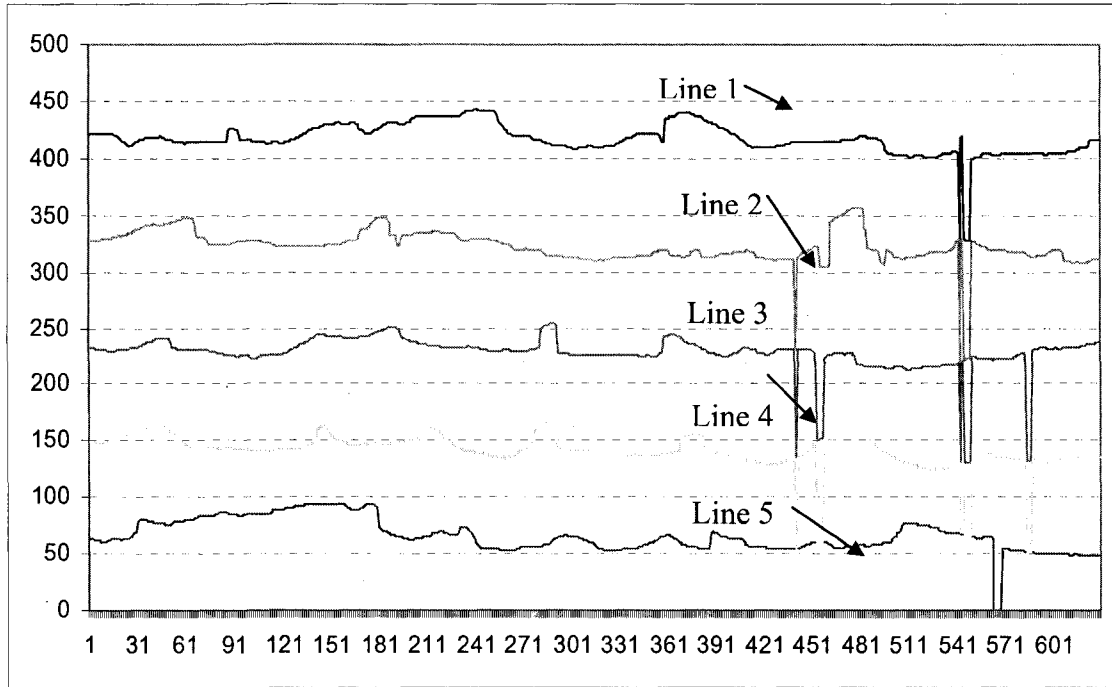


Figure 6.23 DSRM Raw Pixel Data (Ann Rd & San Mateo, P3S1)

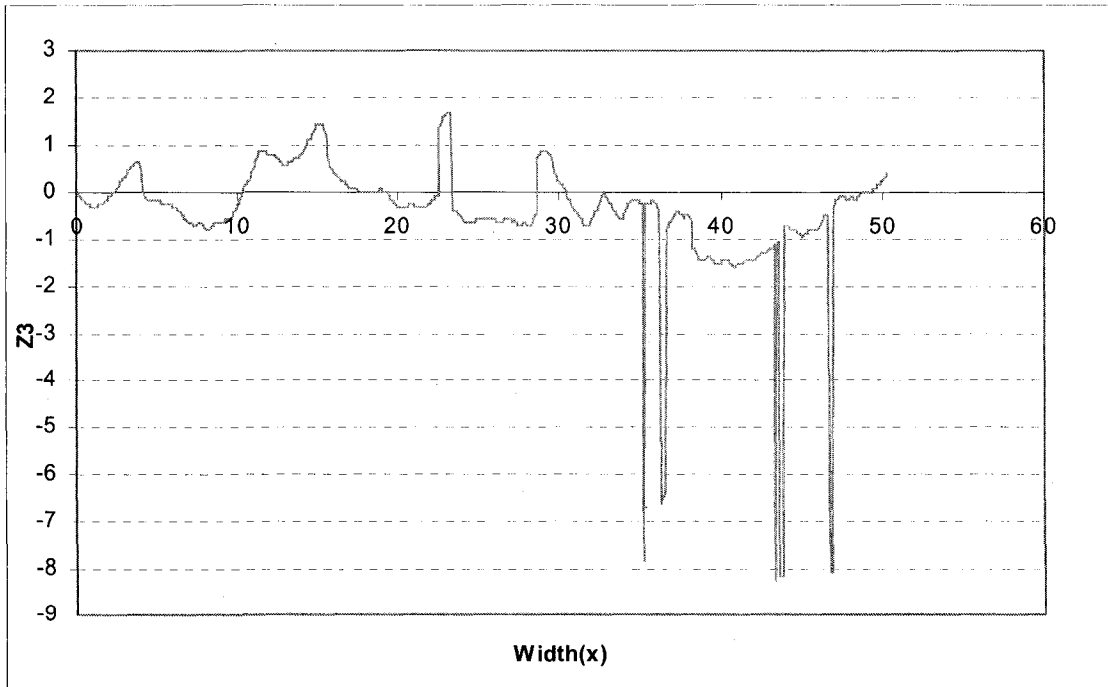


Figure 6.24 Pavement Surface Profile (Ann Rd & San Mateo, P3S1, line 3)

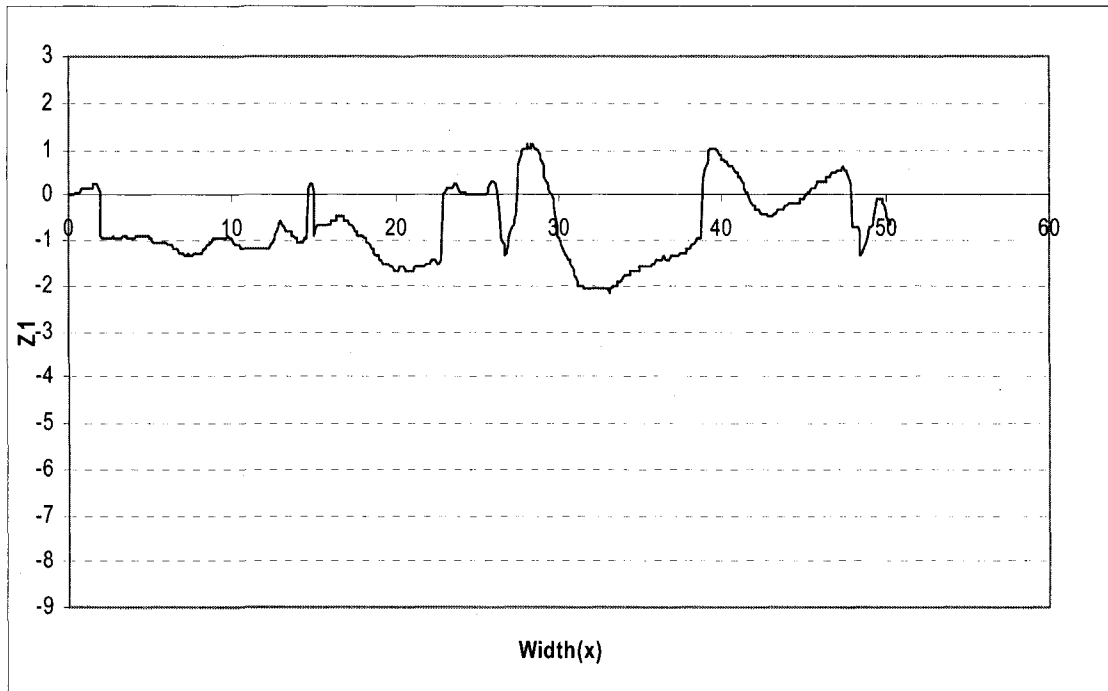


Figure 6.25 Pavement Surface Profile (Maryland & Westminster, P3S1, line 1)

In order to find the width of each feature, and its corresponding average or maximum height or depth, an algorithm was developed in Microsoft Visual C++® 6.0. The algorithm is capable of finding the width and the maximum and average height or depth of each feature in a given set of data. The detailed code for the algorithm is attached in Appendix B.

Figure 6.26 and 6.27 show the summary results of the algorithm's calculations for peak and valley heights along two different profiles of the Ann Rd & San Mateo site. Figure 6.28 and 6.29 show results for Maryland and Westminster. The height or depth of each feature is depicted on the vertical axis, and the corresponding width of that feature is shown on the x-axis. Figure 6.29 and Figure 6.27 distinctly show that Ann Rd & San Mateo site had a large number of deep valleys which could act to shelter silt from aerodynamic shear. Figure 6.26 and Figure 6.27 shows six and 10 valleys deeper than 6

millimeters, respectively. Figure 6.28 and Figure 6.29 summarize analyses of Maryland & Westminster site's pavement topography. They show no valleys and three valleys deeper than 6 millimeters, respectively, much less than the counts developed from the Ann Rd & San Mateo site.

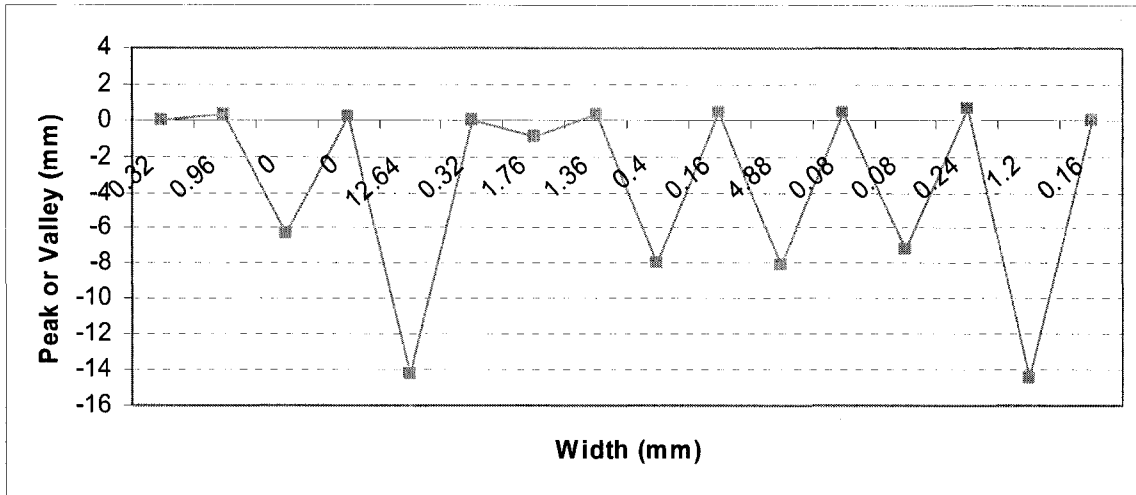


Figure 6.26 Peak or Valley vs Width (Ann Rd & San Mateo, P3S1, line 3)

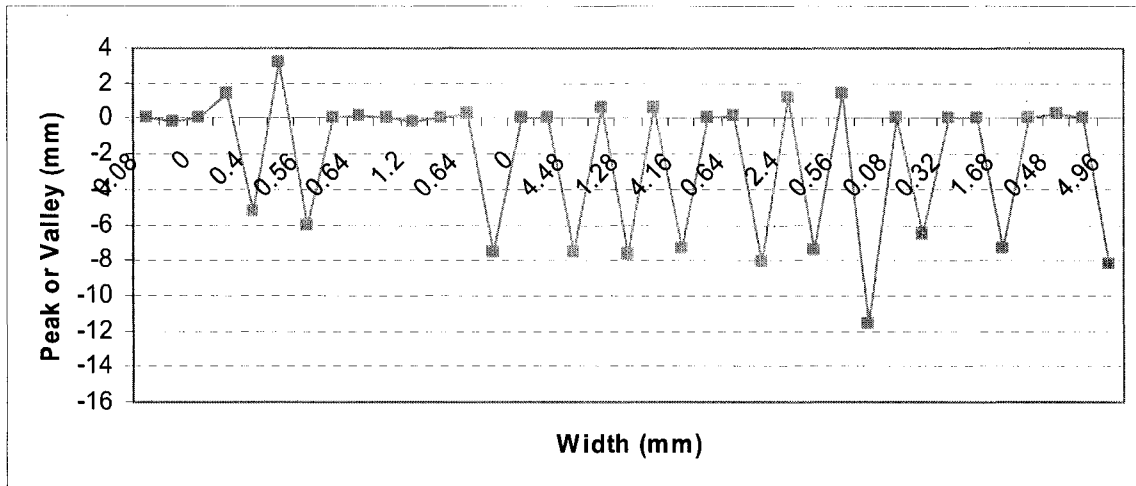


Figure 6.27 Peak or Valley vs Width (Ann Rd & San Mateo, P3S1, line 2)

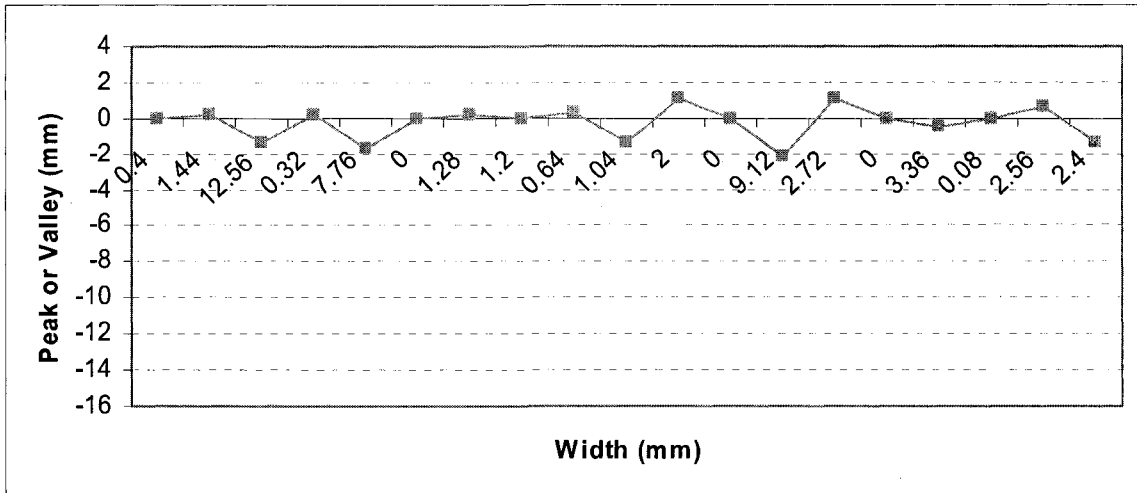


Figure 6.28 Peak or Valley vs Width (Maryland & Westminster, P1S1, line 1)

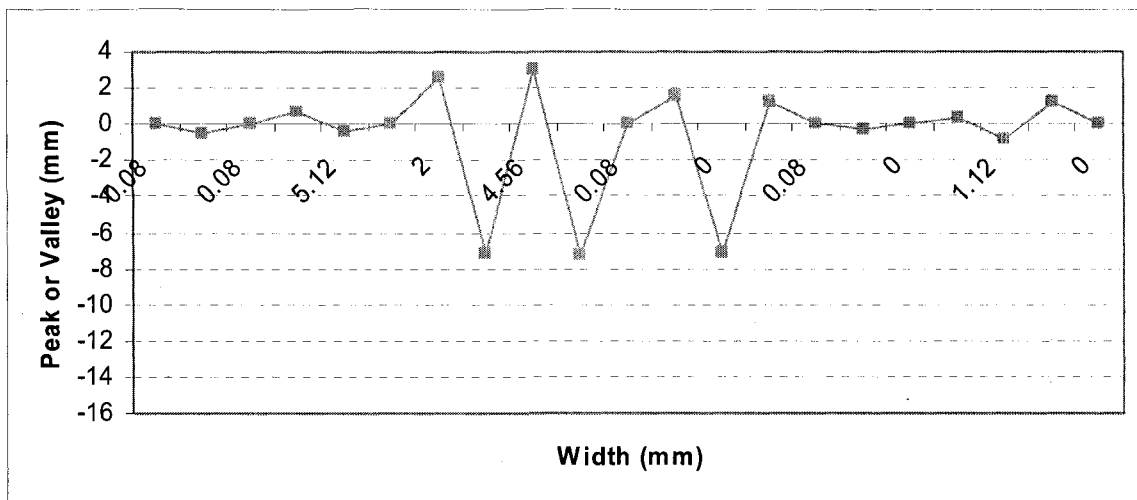


Figure 6.29 Peak or Valley vs Width (Maryland & Westminster, P3S1, line 1)

Summary files containing peak and valley widths and depths/heights were manually classified into 2-way frequency tables to estimate the percentage of features that could be categorized as either (1) deep and narrow, (2) flat medium, and (3) high and wide. These frequency tables were plotted, and the resulting graphs inspected for differences in the patterns of the peak and valley frequency distributions.



Figure 6.30 is an example of a two-frequency distribution for the Ann Rd and San Mateo site where the percentage of deep narrow pits was easy to visually distinguish. Figure 6.31 is an example of a two-way frequency distribution for Maryland & Westminster site where the percentages of flat/medium features are distinct.

The Ann Rd and San Mateo plot (Figure 6.30) shows a denser “cluster” of deep narrow valleys (widths less than 2 mm and depths  $> 2$  mm) than the Maryland and Westminster site (Figure 6.31). The Maryland and Westminster example plot (Figure 6.31) shows a “cluster” of wide (widths 8 mm to 14 mm and depths -1 mm to -5 mm) valleys (upper left quadrant of the figure) and another cluster of peaks (widths 0.8 – 2 mm and heights 2-5 mm) that are much more dense than found in the Ann Road and San Mateo plot (Figure 6.30).

It is hypothesized that sites with higher percentages of flat/medium ( $-1\text{mm} < \text{depth} < 1\text{mm}$  and  $3\text{mm} < \text{width} < 5$  mm) or high/wide (heights exceeding 1 mm and widths exceeding 5 mm) features would have more  $\text{PM}_{10}$  exposed, and subject to rapid wind erosion. Sites with higher percentages of deep narrow features (depths  $< -1$  mm and widths less than 3 mm) would have more  $\text{PM}_{10}$  sheltered. To test the hypothesis, the two-way frequency distribution percentages were summarized for each of the above ranges and tabulated in Table 6.5. Results show that percentages of deep narrow pits were higher in Ann Rd & San Mateo site than the Maryland & Westminster site (Table 6.5). Percentages of flat/medium features were somewhat higher in Maryland & Westminster site than the Ann Road and San Mateo site. Comparisons of the high-wide data were inconclusive. Although two Ann Road sites had no high-wide features, one site had a large percentage of them. At Maryland and Westminster, one site had no high-wide

features, and two sites had small percentages. The most distinct difference between the Ann and Maryland sites was the relative frequency of narrow deep pits.

Table 6.5 Two-way Frequency Distribution Summary

Site name	Location	Deep narrow (%)	Flat medium (%)	High wide (%)
Ann Rd & San Mateo	P2S1	15.8	2.6	0
Ann Rd & San Mateo	P3S1	18.9	10.8	0
Ann Rd & San Mateo	P1S1	14.9	6.4	19.1
Maryland & Westminster	P2S1	6.3	9.4	3.1
Maryland & Westminster	P3S1	9.5	21.4	0
Maryland & Westminster	P1S1	5.3	7.9	5.3

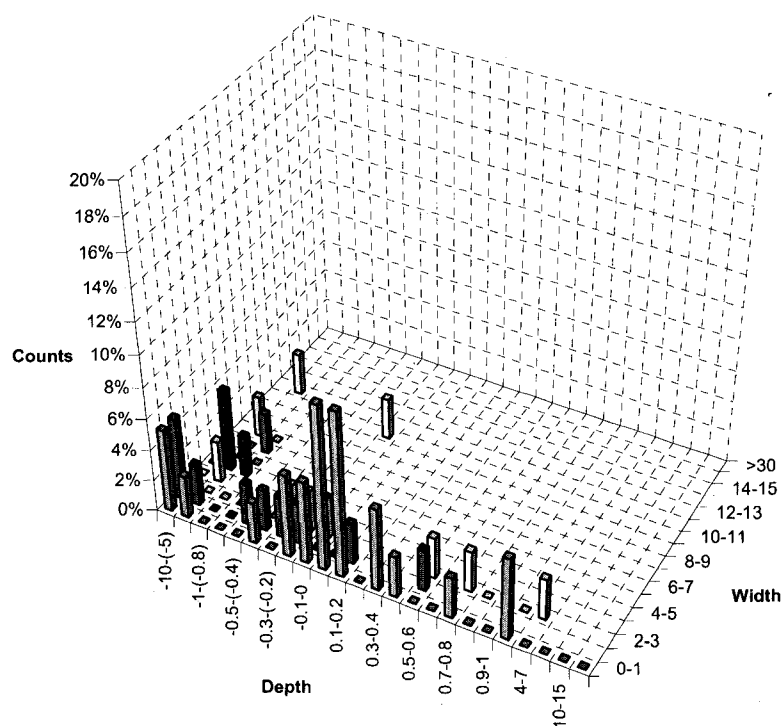


Figure 6.30 Two-way Frequency Distribution of Ann Rd & San Mateo site (P2S1)

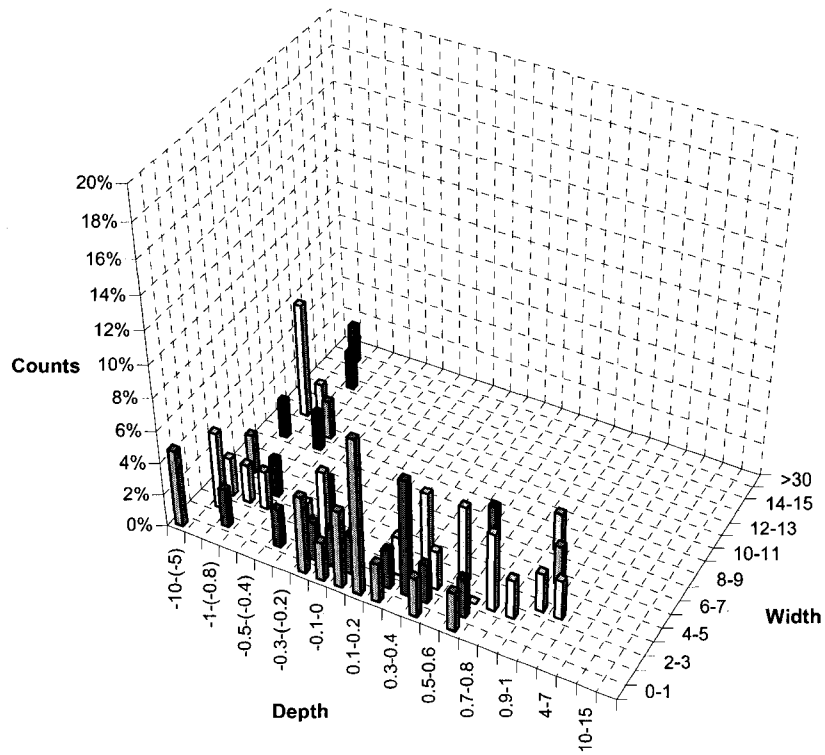


Figure 6.31 Two-way Frequency Distribution of Maryland & Westminster site (P3S1)

The distinctly different percentages of deep narrow valley and the possibly different percentages of flat/medium features indicate likelihood that:

- 1) a larger proportion of the applied silt was sheltered from applied shear in the deep narrow valleys at Ann and San Mateo than at Maryland and Westminster, and
- 2) a larger proportion of applied silt may have been exposed to moderate shear at Maryland and Westminster than at Ann and San Mateo. Higher percentages of deep narrow pits sheltered the silt and contributed to lower  $PM_{10}$  emissions in Ann Rd and San Mateo site.

## 6.4 Aggregate Size Mode and PM<sub>10</sub> Emissions

### 6.4.1 Average Aggregate Size and Mode Calculation

Aggregate size distributions were estimated by counting the number of aggregates and their sizes across a plastic ruler with 1.0 mm gradations.

Figure 6.32 shows an example of the different aggregate sizes and their distribution. Table 6.6 shows an example of aggregate size distribution. Aggregate mode is the aggregate size class with the maximum frequency. Average aggregate size of the Maryland & Westminster (P2S1) was calculated from the Table 6.6. The maximum number of aggregates was between 4-5 mm in length and the mode of the aggregate size was computed to be 4.5 mm.



Figure 6.32 Aggregate Size Distributions (Maryland & Westminster, P2S1)

For sites with aggregates less than 1 mm in size, the frequency analysis was conducted on the consolidated width data output from the 2-way frequency analysis Microsoft Visual C++® 6.0 program written by the author. The maximum number of frequency gave the mode of the aggregate size. For example the mode of the aggregate from a photo was less than 1 mm for Evergold & Coral Sea. The mode of the aggregate was found to be 0.625 for Evergold & Coral Sea site using Visual C++® program output data.

Table 6.6 Mean Aggregate Size and Mode Calculation (Maryland & Westminster P2S1)  
Maryland & Westminster (P2S1)

Category	Count(f)	Percent	Cumulative%
<1mm	0	0.000	0.000
1-2mm	2	0.133	0.133
2-3mm	2	0.133	0.267
3-4mm	3	0.200	0.467
4-5mm	5	0.333	0.800
5-6mm	1	0.067	0.867
6-7mm	1	0.067	0.933
7-8mm	1	0.000	0.933
8-9mm	0	0.000	0.933
9-10mm	0	0.000	0.933
Total	15	0.933	

Although this method gives an estimate horizontal size mode for the aggregates, the aggregates are embedded in the binder, so it is not feasible to judge the degree of embedding in the binder from the close-up photos. The visual photo mode was therefore corrected using the ratio of sand patch MTD and mean aggregate size.

Table 6.7 shows the average aggregate size, mode and corrected mode for all the site locations. The data showed a significant correlation between mean photographic

aggregate size and MTD (Figure 6.33). Furthermore, photographic aggregate mode size also correlated well with MTD (Figure 6.34)

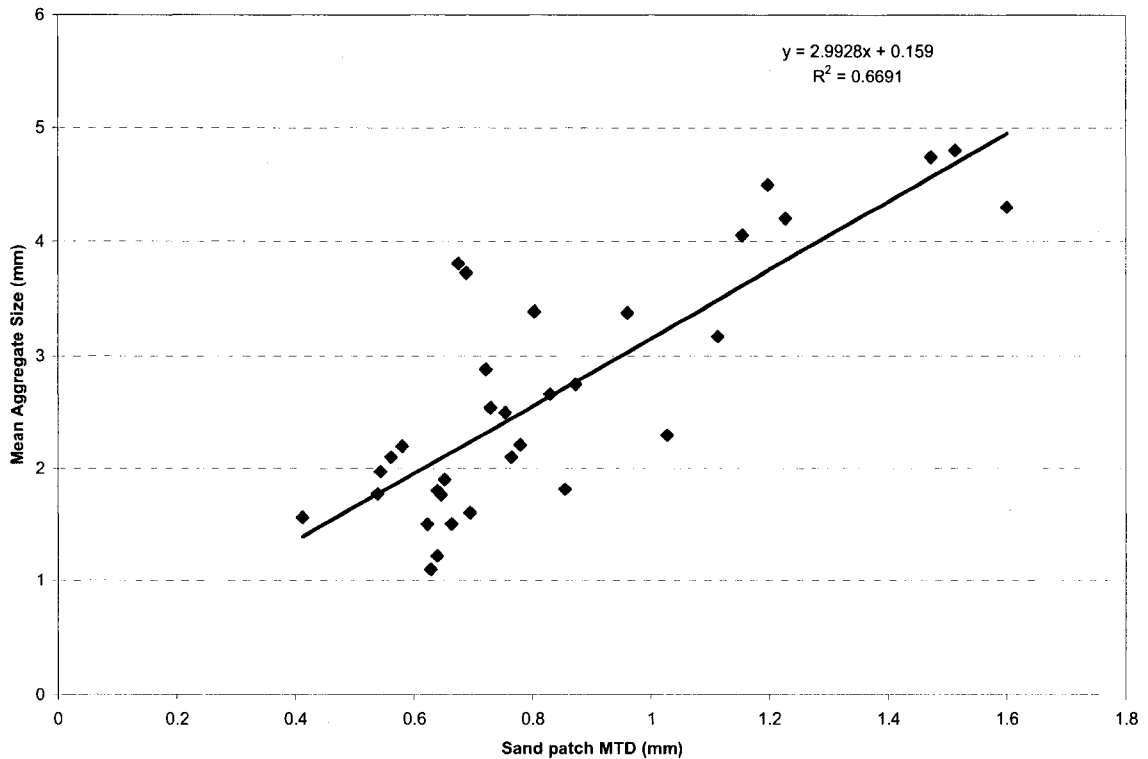


Figure 6.33 Mean Aggregate Size vs Sand Patch MTD

It was found that Ann Rd & San Mateo (P1S1) had the highest sand patch MTD (1.601 mm), had the biggest corrected aggregate mode. The Evergold & Coral Sea (P2S1) had the lowest MTD (0.412 mm) and had the smallest corrected mode of 0.165 mm. Figure 6.34 shows the MTD and mode relation. Aggregates are embedded on the pavement surface with binder (Figure 6.35). The mode of each sample was corrected by multiplying it by the ratio of sand patch MTD to macrophoto aggregate mean size (Equation 6.3). A plot of corrected mode vs MTD is shown in Figure 6.36. Although logarithmic fits do a reasonable and statistically significant job of describing the trends in

mode size vs MTD and corrected mode size vs MTD, the raw data show a break from steep slope below MTD of 0.80 mm to a shallower slope for MTD > 0.80 mm.

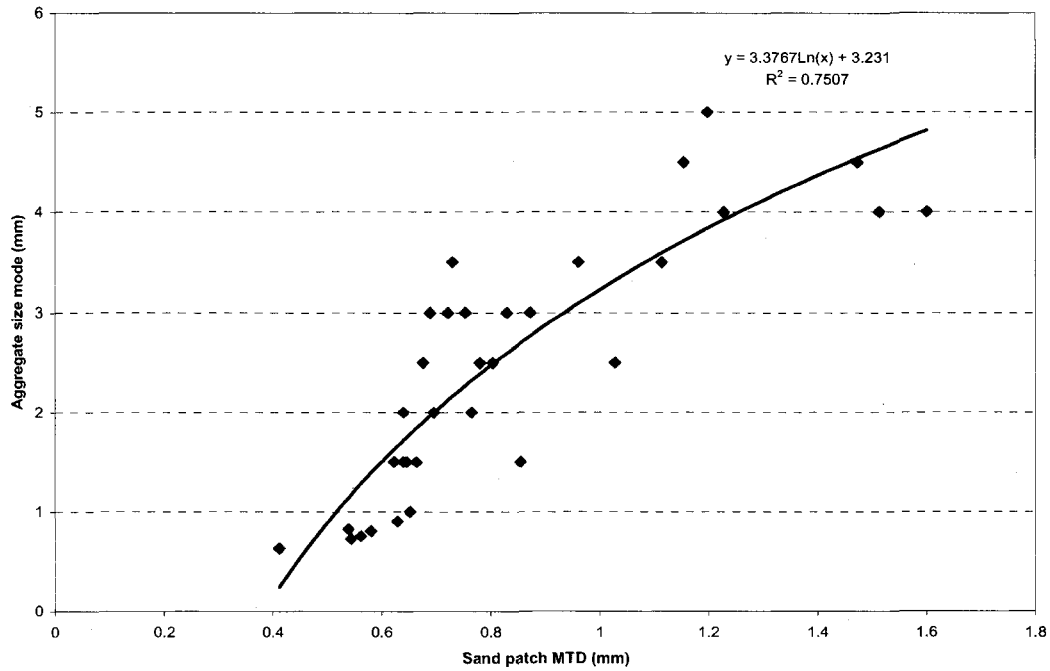


Figure 6.34 Aggregate Size Mode vs Sand Patch MTD

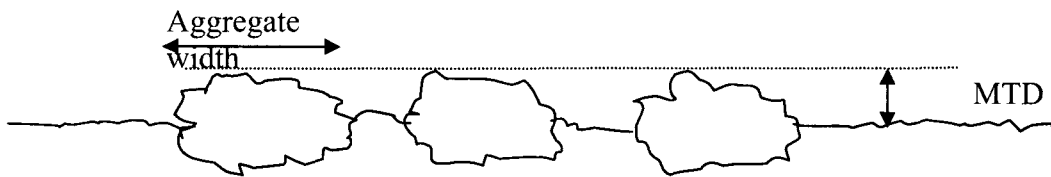


Figure 6.35 Aggregate Mode Size Correction

$$\text{Corrected vertical mode}_i = \frac{\text{Observed horizontal mode}_i}{\text{Aggregate width}_i / \text{MTD}_i} \quad (6.3)$$

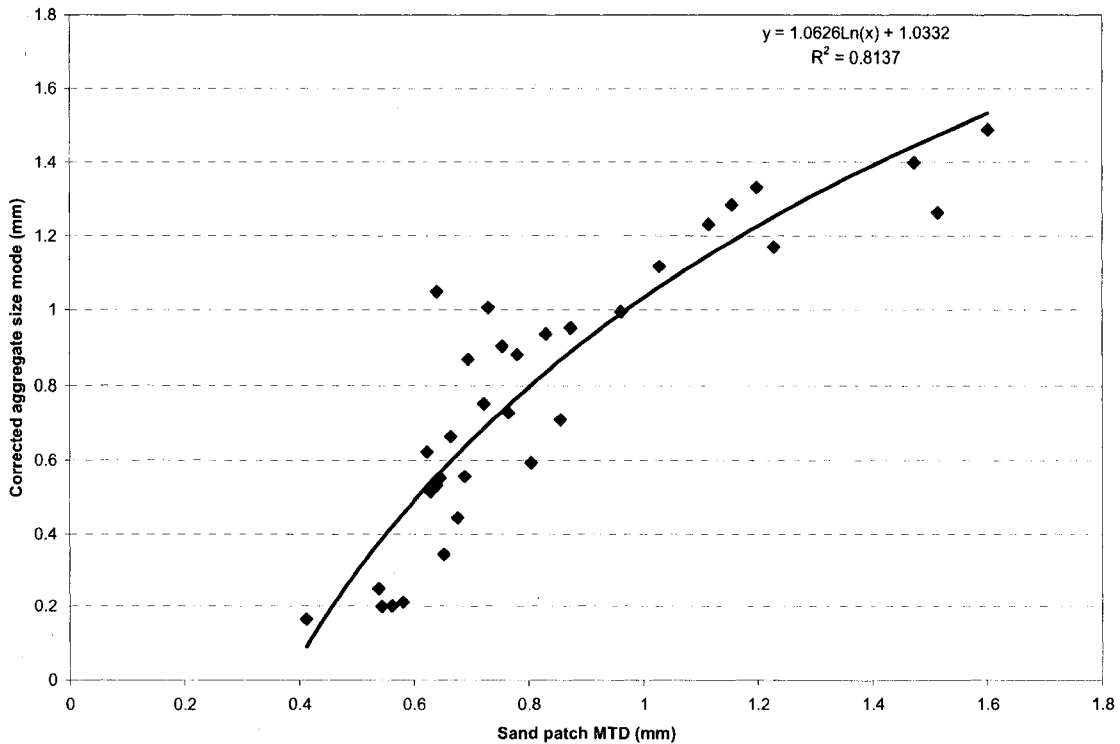


Figure 6.36 Corrected Aggregate Size Mode vs Sand patch MTD

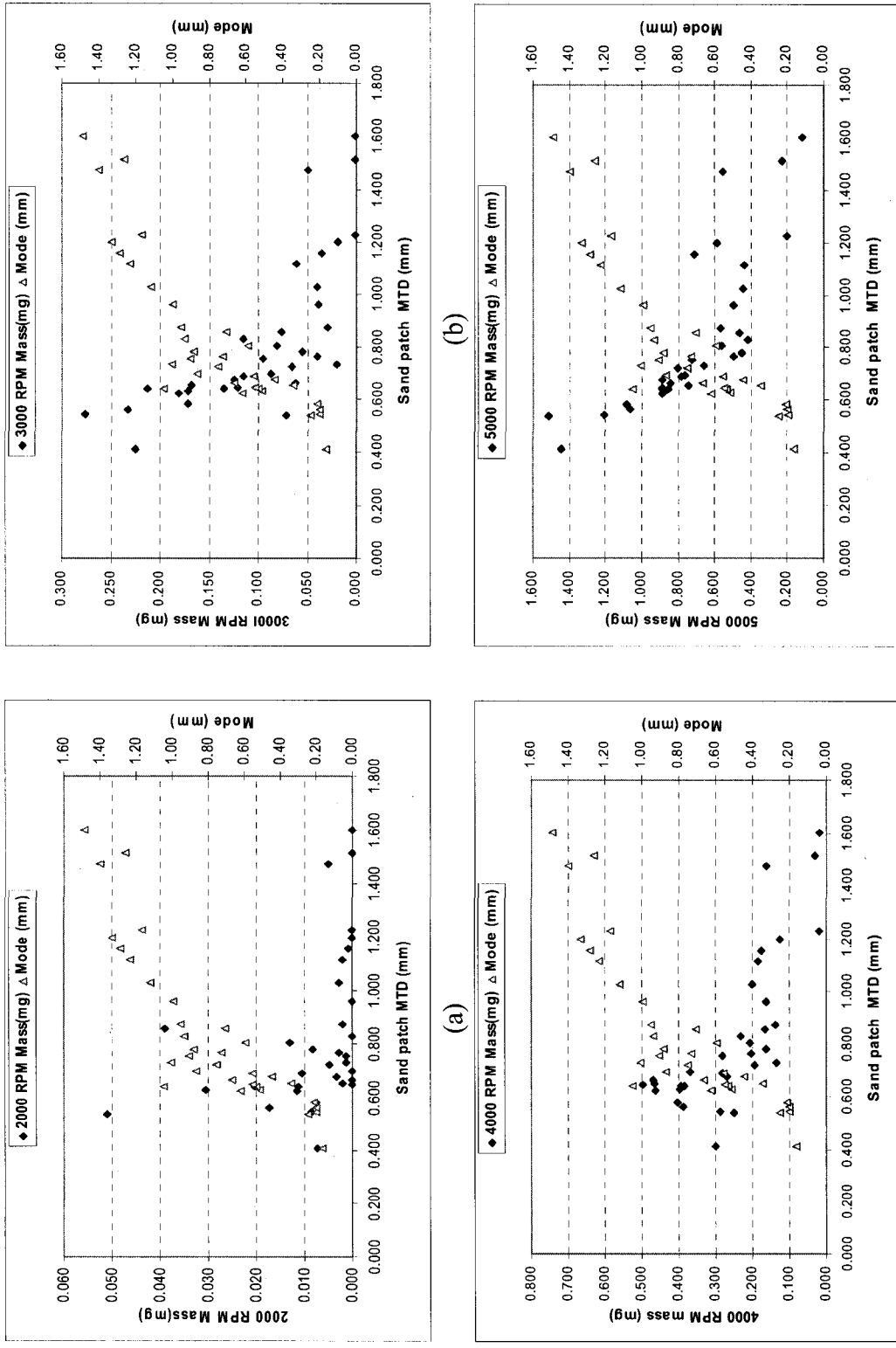
PM<sub>10</sub> mass emissions and corrected mode size were both plotted against sand patch MTD to see if a statistically significant correlation could be established (Figure 6.37). “Breaks” in the slope of PM<sub>10</sub> emissions vs MTD are seen to occur at similar values of MTD, 0.80-0.90 mm, compared to a similar slope “break” in the plot of corrected aggregate mode vs MTD (Figure 6.37a, b, c and d)

PM<sub>10</sub> mass emissions were then plotted directly against corrected mode size for each shear value. Results (Figure 6.38a, b, c and d) show a linear relationship between PM<sub>10</sub> emissions and mode. The slope “breaks” are now absent, and coefficients of determination for PM<sub>10</sub> mass vs corrected mode are better than the segmented linear fits of PM<sub>10</sub> emissions on MTD.

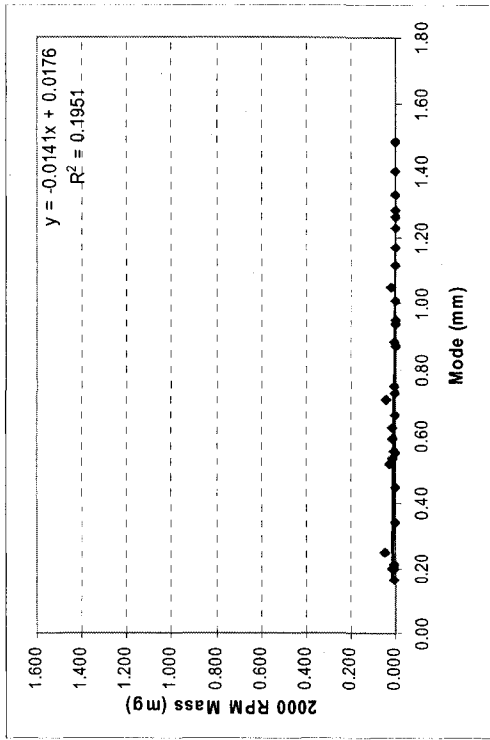


Table 6.7 Average Aggregate size and Mode Correction

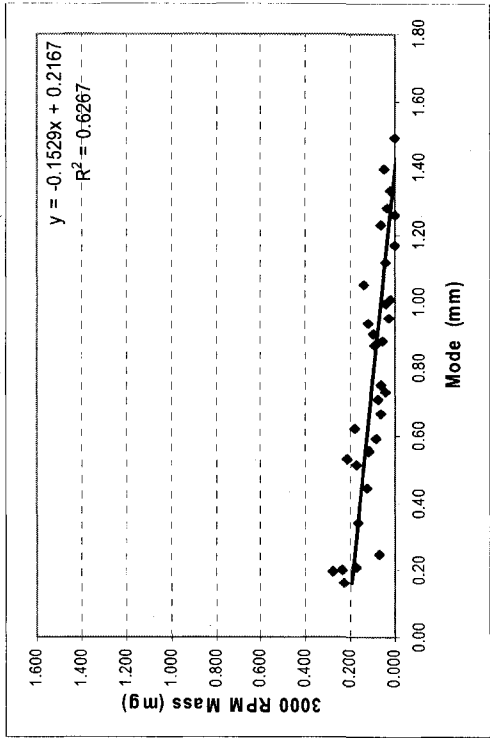
Site Name	Location	Sand patch (MTD)	Average Aggregate Sizes (mm)	Ratio MTD/Mean aggregate size	Mode (mm)	Corrected Mode (mm)
Evergold	P2S1	0.412	1.56	0.263	0.625	0.165
Evergold	P3S1	0.539	1.77	0.304	0.82	0.249
Goldhill	P3S1	0.544	1.97	0.276	0.72	0.199
Goldhill	P2S1	0.562	2.10	0.268	0.75	0.201
Goldhill	P1S1	0.581	2.20	0.264	0.8	0.211
Crestdale	P1S1	0.623	1.50	0.415	1.5	0.623
Sapphire Light	P3S1	0.629	1.1	0.572	0.9	0.515
Sapphire Light	P2S2	0.640	1.22	0.525	2.0	1.049
Crestdale	P2S1	0.640	1.80	0.356	1.5	0.533
Crestdale	P2S2	0.646	1.76	0.368	1.5	0.552
Crestdale	P1S2	0.652	1.90	0.343	1	0.343
Crestdale	P3S1	0.664	1.50	0.442	1.5	0.664
Pabco	P2S1	0.676	3.8	0.178	2.5	0.445
Pabco	P1S1	0.689	3.72	0.185	3.0	0.556
Crestdale	P3S2	0.695	1.60	0.434	2	0.869
Burkholder	P2S1	0.722	2.88	0.251	3	0.752
Armacost	P3S1	0.730	2.54	0.288	3.5	1.006
Armacost	P2S1	0.754	2.50	0.301	3	0.904
Silverspring	P1S2	0.765	2.10	0.364	2	0.728
Silverspring	P2S2	0.780	2.21	0.353	2.5	0.882
Duneville	P1S2	0.804	3.39	0.237	2.5	0.593
Armacost	P1S1	0.830	2.66	0.312	3	0.936
Sapphire Light	P1S1	0.855	1.81	0.472	1.5	0.709
Burkholder	P3S1	0.873	2.75	0.317	3	0.952
Duneville	P2S2	0.961	3.38	0.284	3.5	0.995
Silver Spring	P2S1	1.028	2.3	0.447	2.5	1.117
Duneville	P3S2	1.114	3.17	0.352	3.5	1.231
Maryland	P2S1	1.155	4.05	0.285	4.5	1.283
Maryland	P3S1	1.198	4.5	0.266	5	1.331
Ann Rd	P2S1	1.228	4.2	0.292	4	1.170
Maryland	P1S1	1.473	4.74	0.311	4.5	1.398
Ann Rd	P3S1	1.514	4.8	0.315	4	1.262
Ann Rd	P1S1	1.601	4.3	0.372	4	1.489



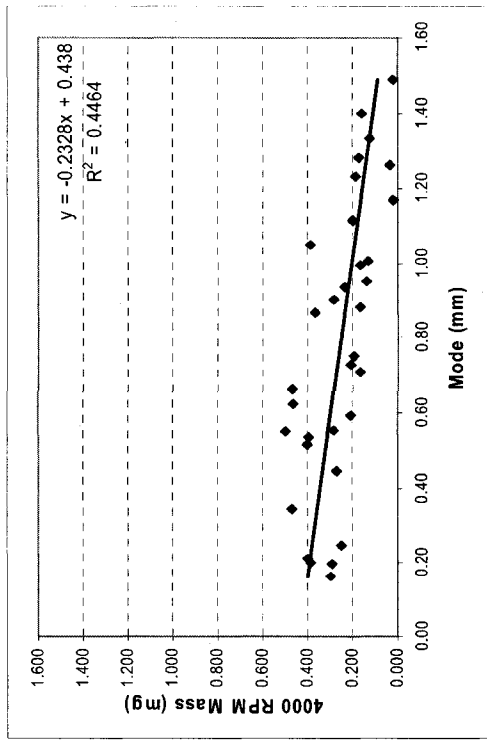
(a) 2000 RPM Mass, (b) 3000 RPM Mass, (c) 4000 RPM Mass, (d) 5000 RPM Mass vs MTD(mm)



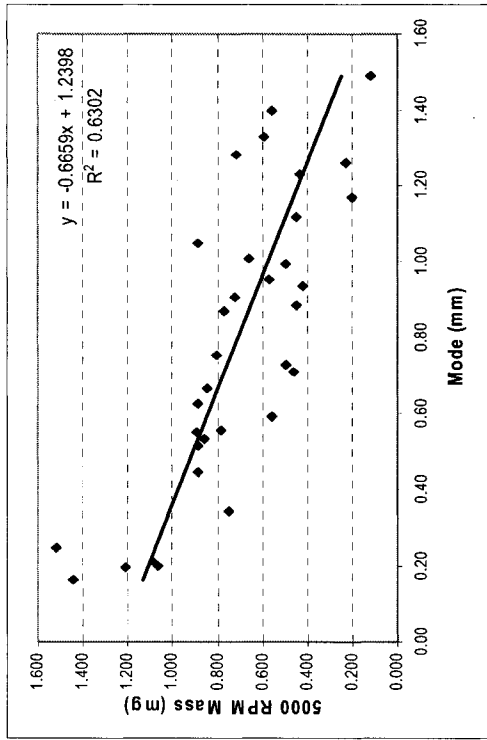
(a)



(b)



(c)



(d)

Figure 6.38 (a) 2000 RPM Mass, (b) 3000 RPM Mass (c) 4000 RPM Mass, (d) 5000 RPM Mass vs Mode (mm)

Regression analysis mass emitted on corrected mode at 5000 rpm showed PM<sub>10</sub> mass emission at 5000 rpm was significantly ( $p < 0.05$ ) correlated to corrected mode. The coefficient of determination was found to be 0.63. Regression on soil-clean mass showed better results ( $r^2 = 0.67$ ) and this is also statistically significant.

Results showed that relationship between PM<sub>10</sub> mass emissions and pavement texture was better for controlled mass than ambient mass. Coefficient of determination ( $r^2 = 0.206$  for ambient mass and 0.63 for controlled mass) showed better agreement between non-erodible aggregate mode size and emitted PM<sub>10</sub> mass at high shear rate for controlled experiments. The controlled experiments showed better results as uniform soil particles were used during experiments, so the threshold friction velocity was the same for the controlled study. The ambient soils had varied particle size mode, so soil particles had a range of threshold friction velocities.

## 6.5 Application of Wind Erosion Theory to Controlled Studies

Because Figure 6.38 results indicate a significant effect of asphalt aggregate corrected size mode, it was decided to test the data against classical wind erosion theory.

The near-surface wind profile for wind erosion is described as (US EPA, 1988),

$$u(z) = \frac{u^*}{k} \ln\left(\frac{z}{z_0}\right) \quad (6.4)$$

Where

$u$  = Wind speed, m/s

$u^*$  = Friction velocity, m/s

$z$  = Height above test surface, m

$z_0$  = Roughness height, m

$k$  = Von Karman's constant (0.4)

Also, near surface wind stress that causes erosion is defined as  $u^*$ , the friction velocity where  $u^*$  represents the wind speed at approximately 1.5x the aerodynamic roughness height

Wind erosion occurs when  $u^*$  exceeds a critical value for initiation of soil movement, defined as the threshold friction velocity,  $u^*t$  (See Chapter 2). Generally, horizontal flux of wind-eroded particles is thought to vary with either the square or cube of the difference between  $u^*$  and  $u^*t$ .

A decision was made to test the hypothesis that, for embedded asphalt aggregates,  $z_0$  would be a function of the corrected mode size of the asphalt aggregate, in a manner similar to that described in Gillette, 1980, as cited in US EPA, 1988.

Threshold friction velocity (TFV) would be a constant function of the mode size of the standard erodible soil in the controlled experiments, known to be 0.15 mm. Using Gillette's 1980 correlation, as described in US EPA, 1988, the TFV for the standard controlled soil would be 0.29 meter/second.

The critical height for applied wind shear was calculated by using  $z = 0.075$  mm, representing  $\frac{1}{2}$  the height of the mode of the erodible standard soil aggregate (See Figure 6.39 showing velocity vector pushing on rock  $\frac{1}{2}$  way up from bottom), second, using a height determined by the asphalt terrain, with the critical height being  $MTD/10$ . For the range of MTD's observed, 0.50mm to 1.6 mm, this would give heights for applied wind stress ranging from 0.5mm to 0.16 mm, values that put wind stress ranging from  $\frac{1}{3}$  the modal height of the soil aggregate ( $0.05$  mm/ $0.15$  mm = 0.30) to just above the modal

height (0.16 mm just greater than 0.15 mm). Both of these heights would exceed  $z_0$  for all studied cases. The specific relationship of wind speed to height is shown in Figure 6.39. Equation 6.5 and 6.7 was used for friction velocity calculation at MTD/10 mm and 0.075 mm.

$$u\left(\frac{MTD}{10}\right) = \frac{u^*}{k} \left[ \ln \frac{MTD}{10} - \ln(z_0) \right] \quad (6.5)$$

$$z_0 = \frac{\text{Corrected Aggregate Mode Size}}{30} \quad (6.6)$$

$$u(0.075) = \frac{u^*}{k} [\ln 0.075 - \ln z_0] \quad (6.7)$$

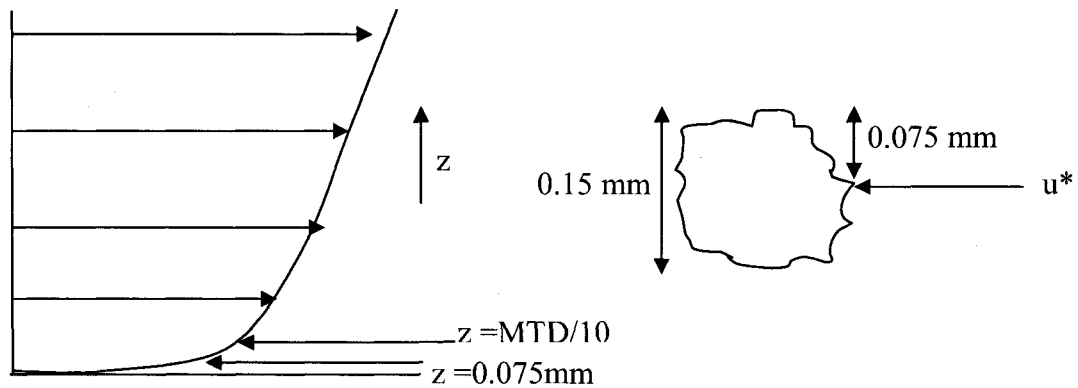


Figure 6.39 Relationship of Wind speed and Height

$u(0.075\text{mm})-u^*t$  and  $u((\text{MTD}/10))-u^*t$  was plotted against soil-clean emitted mass for each shear rate (Figure 6.40 and 6.41). For  $u(0.075)-u^*t$ , a linear relationship was found between  $\text{PM}_{10}$  mass emissions and friction velocity. A linear regression analysis shows that the relationship was not strong at 2000 rpm ( $r^2=0.173$ ) but statistically significant ( $p = 0.015$ ). For 3000 rpm, Figure 6.40b shows a significant correlation ( $r^2=0.638$ ,  $p = 0.000$ ) between  $\text{PM}_{10}$  mass emissions and  $u(0.075)-u^*t$ . Results suggests that the

threshold friction velocity for initiation of PM<sub>10</sub> mass removed occurred somewhere between 2000 rpm and 3000 rpm. The coefficient of determination increased with increasing shear rate, but at 4000 rpm lower  $r^2$  (0.315) value was found than 3000 rpm  $r^2$  value (0.638). The depletion effect at 3000 rpm could be a possible reason for this anomaly (Table 6.8).

When MTD/10 was the critical height for wind shear application, the same pattern was observed. The statistical analysis was tabulated in Table 6.9. Comparisons of the correlations for the two different heights showed that 0.075 mm was determined to be a better option (Table 6.8 and 6.9)

Table 6.8 Statistical Summary for (u0.075)-u\*t (controlled experiments)

RPM	Liner Coefficient	p	$r^2$
2000	0.010	1.59E-02	0.173
3000	0.088	2.49E-08	0.638
4000	0.166	6.86E-04	0.315
5000	0.265	2.22E-10	0.732

Table 6.9 Statistical Summary for (u(MTD/10))-u\*t (controlled experiments)

RPM	Liner Coefficient	p	$r^2$
2000	0.014	5.02E-02	0.118
3000	0.110	7.48E-05	0.402
4000	0.069	1.13E-01	0.079
5000	0.313	5.44E-05	0.413

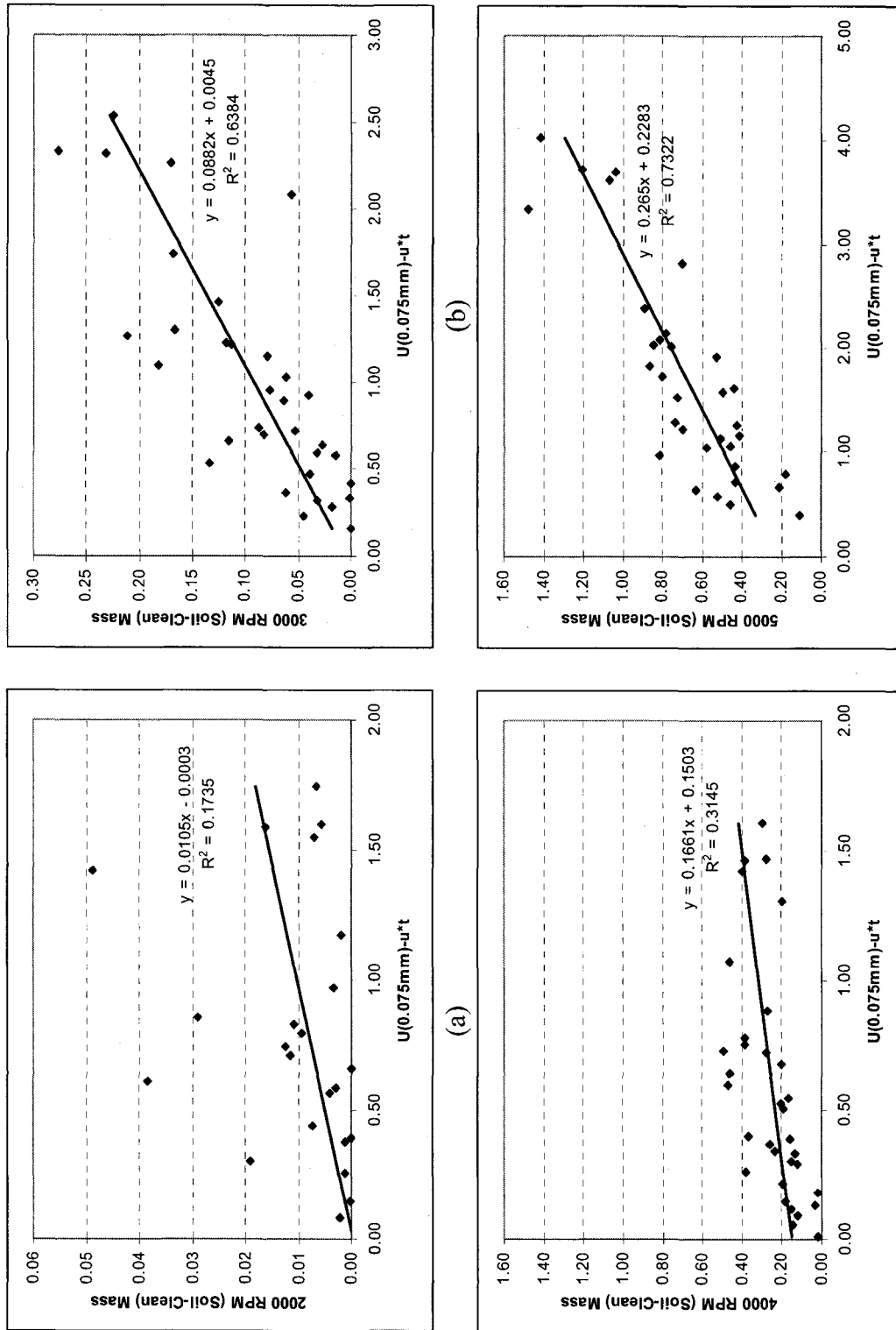


Figure 6.40 2000 RPM (a) 3000 RPM (b) 4000 RPM (c) 5000 RPM (Soil-Clean) Mass vs  $u(0.075\text{mm})-u*t$



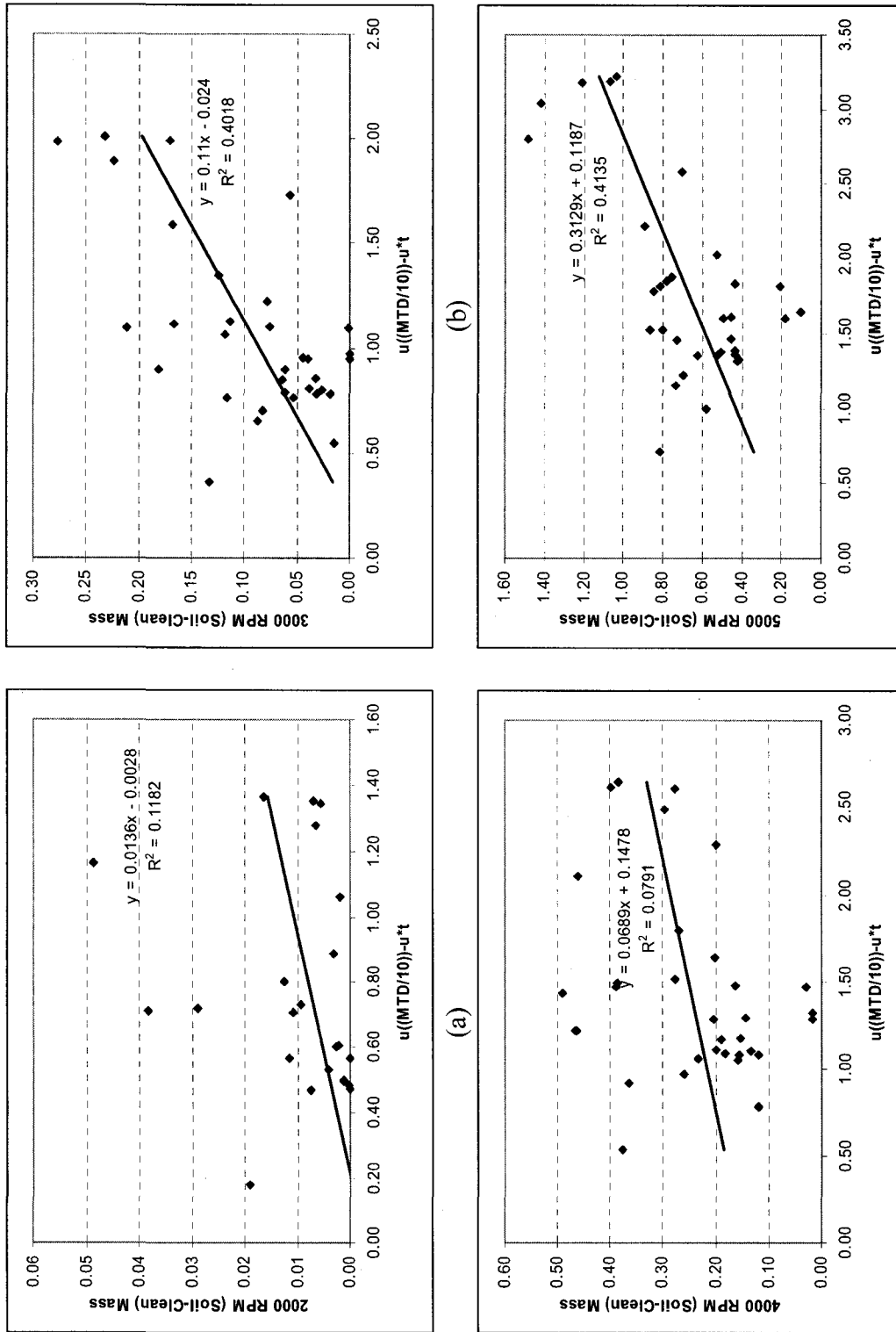


Figure 6.41 2000 RPM (a) 3000 RPM (b) 4000 RPM (c) 5000 RPM (Soil-Clean) Mass vs  $u((MTD/10))-u*t$  (d)

## 6.6 Thomas & Mack Parking Lot Depletion Study

The Thomas & Mack parking lot depletion study was conducted with the standard soil used in the controlled PM<sub>10</sub> experiments at the 12 Las Vegas Valley sites and with Mini-PI-SWERL™. The Mini-PI-SWERL™ tests were performed on the rough surface and smooth surface to compare the rates of PM<sub>10</sub> depletion for rough surface and smooth surface. Both surfaces had recently been sealed.

The sand patch test and DSRM were used to measure mean texture depth. The MTD of the smooth surface was found to be 0.48 mm and 0.625 with sand patch test and DSRM respectively. The MTD for the rough surface was found to be 1.2 mm and 1.07 mm by sand patch test and DSRM respectively.

The Mini-PI-SWERL™ was run on the rough surface for ambient conditions and then the pavement surface was cleaned with a vacuum cleaner. One gram of soil of known silt composition was spread under the 0.0707 m<sup>2</sup> footprint of the Mini-PI-SWERL™, creating an effective silt loading of 2 gram/m<sup>2</sup> (please see details in Chapter 3). The Mini-PI-SWERL™ was run twelve times on each surface without removing the Mini-PI-SWERL™ from the pavement surface.

The average mass emissions were calculated for every run and also at every shear rate. Table 6.10 and Table 6.11 show an example for emitted mass and cumulative emitted mass at the 5000 rpm shear rate from the smooth and rough surfaces, respectively.

Table 6.10 Mass Emitted at 5000 RPM from Smooth Surface

RPM	Run #	Mass (mg)	Emitted	Cumulative Mass Emitted (mg)
5000	1	1.038		1.038
5000	2	0.209		1.247
5000	3	0.122		1.369
5000	4	0.105		1.474
5000	5	0.115		1.589
5000	6	0.075		1.664
5000	7	0.068		1.732
5000	8	0.065		1.797
5000	9	0.057		1.853
5000	10	0.042		1.896
5000	11	0.040		1.936
5000	12	0.043		1.979

Table 6.11 Mass Emitted at 5000 RPM from Rough Surface

RPM	Run #	Mass (mg)	Emitted	Cumulative Mass
5000	1	0.659		0.659
5000	2	0.191		0.849
5000	3	0.101		0.950
5000	4	0.057		1.008
5000	5	0.045		1.053
5000	6	0.044		1.097
5000	7	0.026		1.123
5000	8	0.022		1.145
5000	9	0.024		1.169
5000	10	0.024		1.193
5000	11	0.022		1.214
5000	12	0.022		1.237

Mass removed for each 12 run were plotted for 3000 rpm, 4000 rpm, 5000 rpm and 3000+4000+5000 rpm shear rate (Figures 6.42, 6.43, 6.44 and 6.45). Plots showed that the maximum amount of mass was emitted at the first application of shear, and then

progressively decreasing amounts of mass were emitted during the remaining 11 runs. More mass was emitted at higher shear rates than lower shear rates.

Table 6.10 and 6.11 show that 0.66 mg of mass was removed at first run from the rough surface whereas 1.04 mg of mass was removed from the smooth surface (Figure 6.46). Total removed mass from run 1 to run 12 were calculated for each rpm. A total amount of 1.24 mg mass was removed at 5000 rpm for all 12 runs on the rough surface and 1.98 mg from smooth surface (Figure 6.47).

Cumulative mass removed at 3000 rpm, 4000 rpm, 5000 rpm and 3000+4000+5000 rpm were plotted in Figures 6.48, 6.49, 6.50 and 6.51. Cumulative emitted mass increased with increase of shear rate.

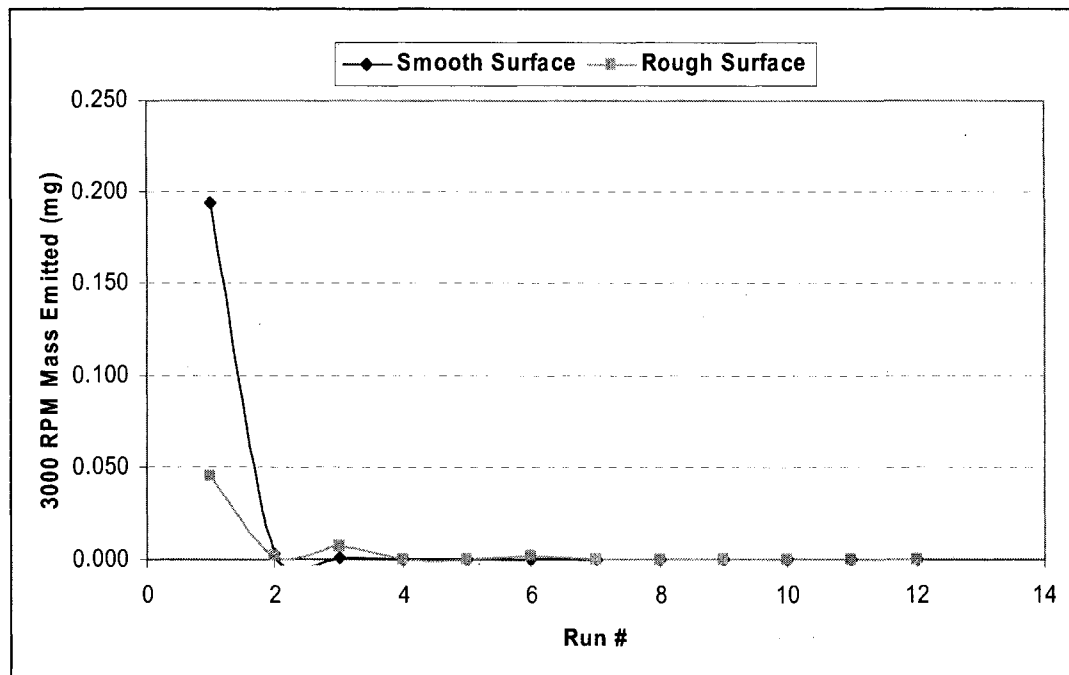


Figure 6.42 Mass Emitted at 3000 RPM at Different Run

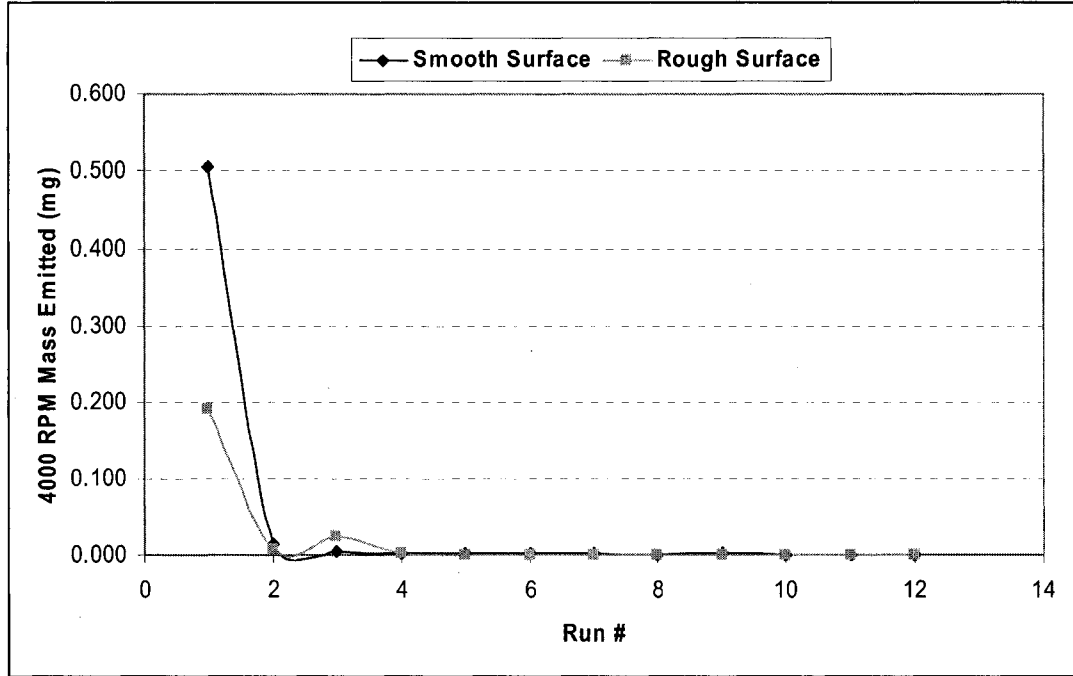


Figure 6.43 Mass Emitted at 4000 RPM at Different Run

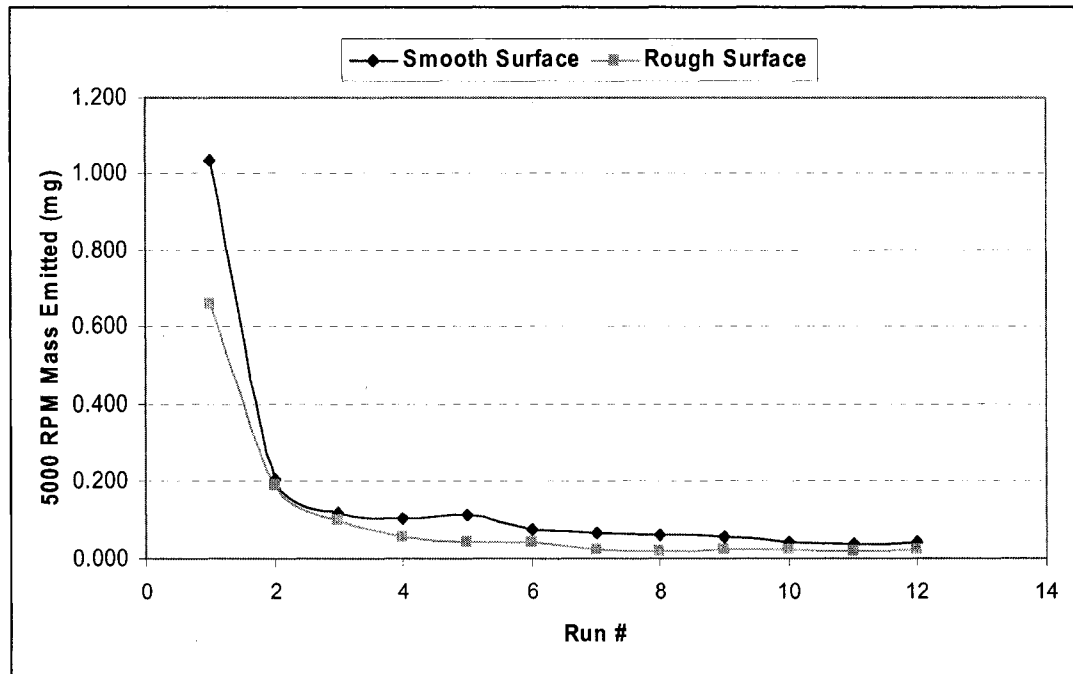


Figure 6.44 Mass Emitted at 5000 RPM at Different Run

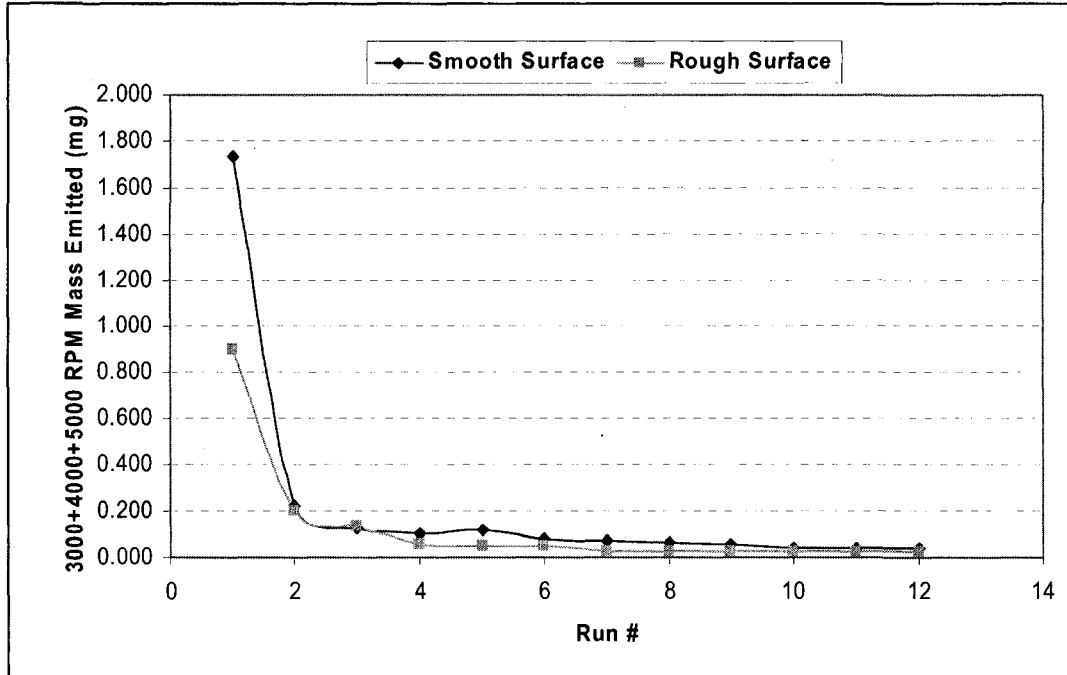


Figure 6.45 Mass Emitted at 3000+4000+5000 RPM at Different Run

Initial and total amounts of mass removed varied nonlinearly with the shear rate (Figure 6.46 and 6). The quadratic fit of mass removed at the first run to shear rate shows that the mass removal rate goes with the square of the applied shear (Figure 6.46). After the first run, the total amounts of mass removed at, 3000, 4000 rpm were negligible because the curves of cumulative mass vs the run number are flat (Figures 6.48 and 6.49), and that the only applied shear rate that removed more mass was 5,000 rpm (Figure 6.50). It was the increase in mass removed at 5000 rpm that contributed to the increase in total mass removed at the different speeds (Figure 6.51).

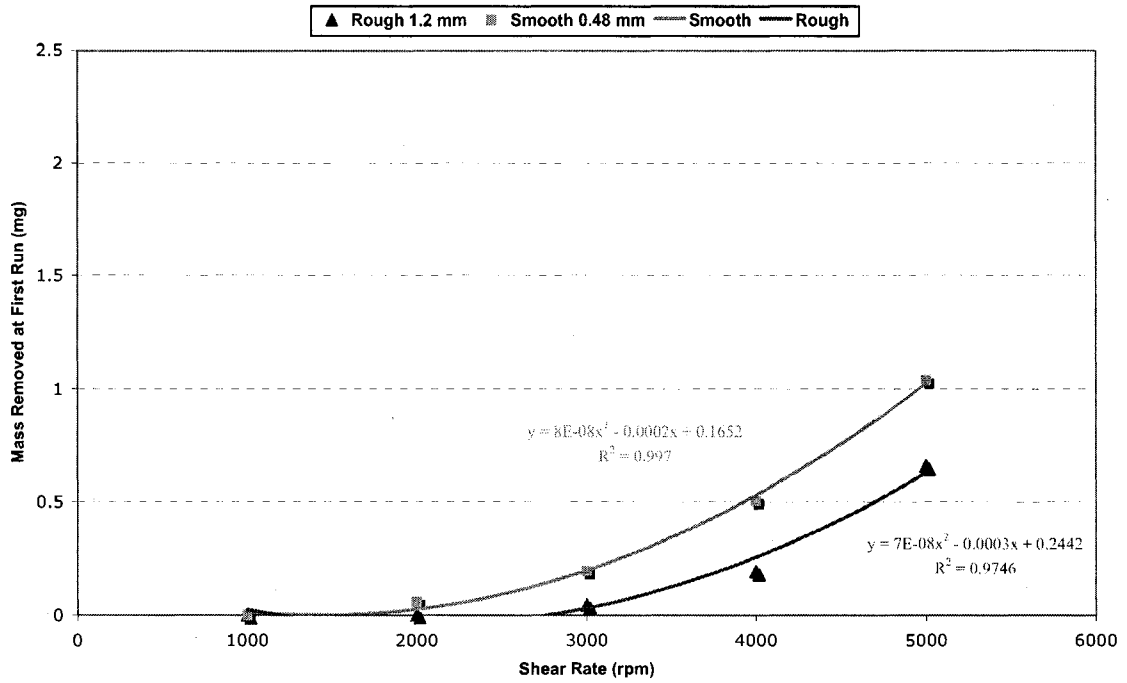


Figure 6.46 Mass Removed at First Run at Different Shear Rate

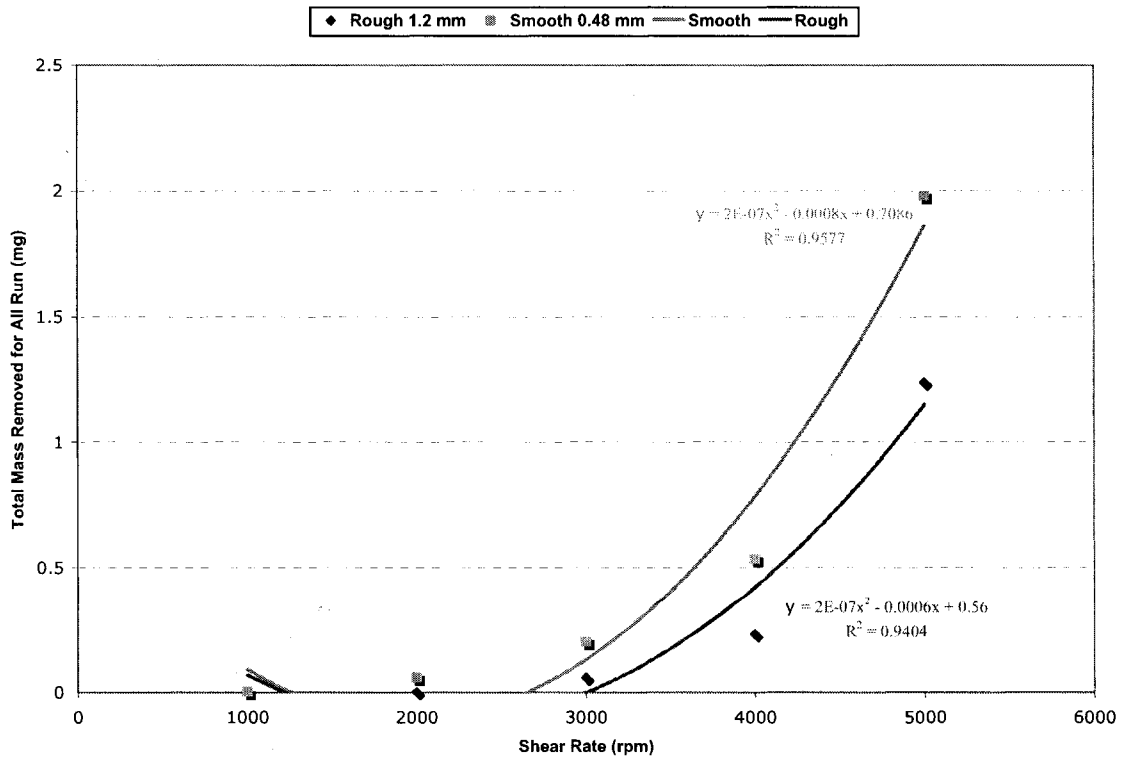


Figure 6.47 Total Mass Removed for All Run at Different Shear Rate

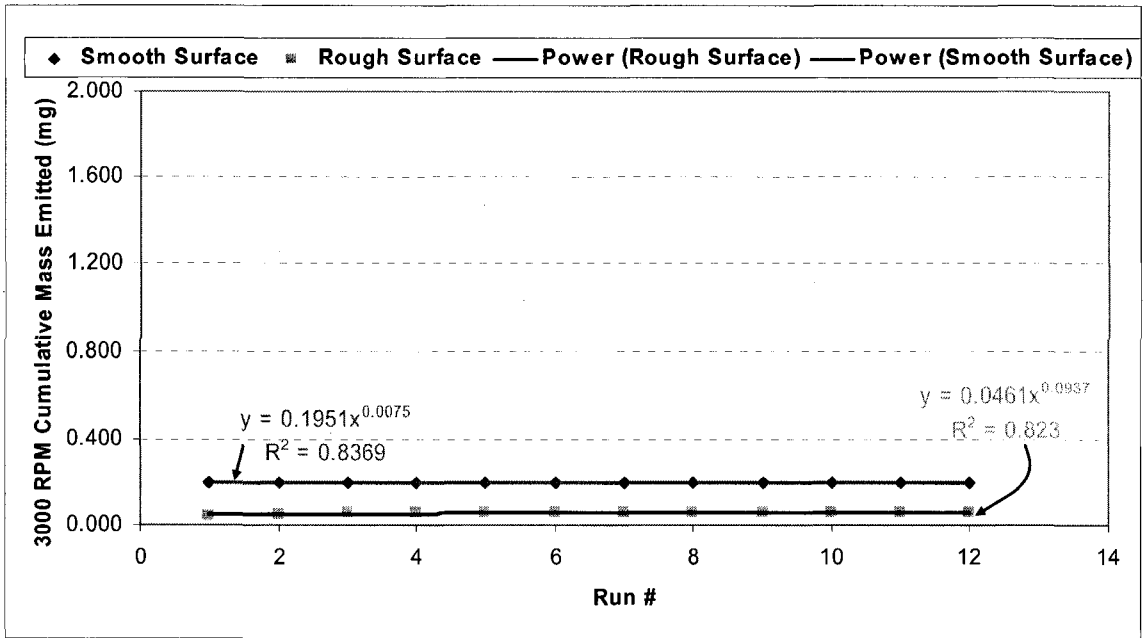


Figure 6.48 Cumulative Mass Removed at 3000 RPM Shear Rate

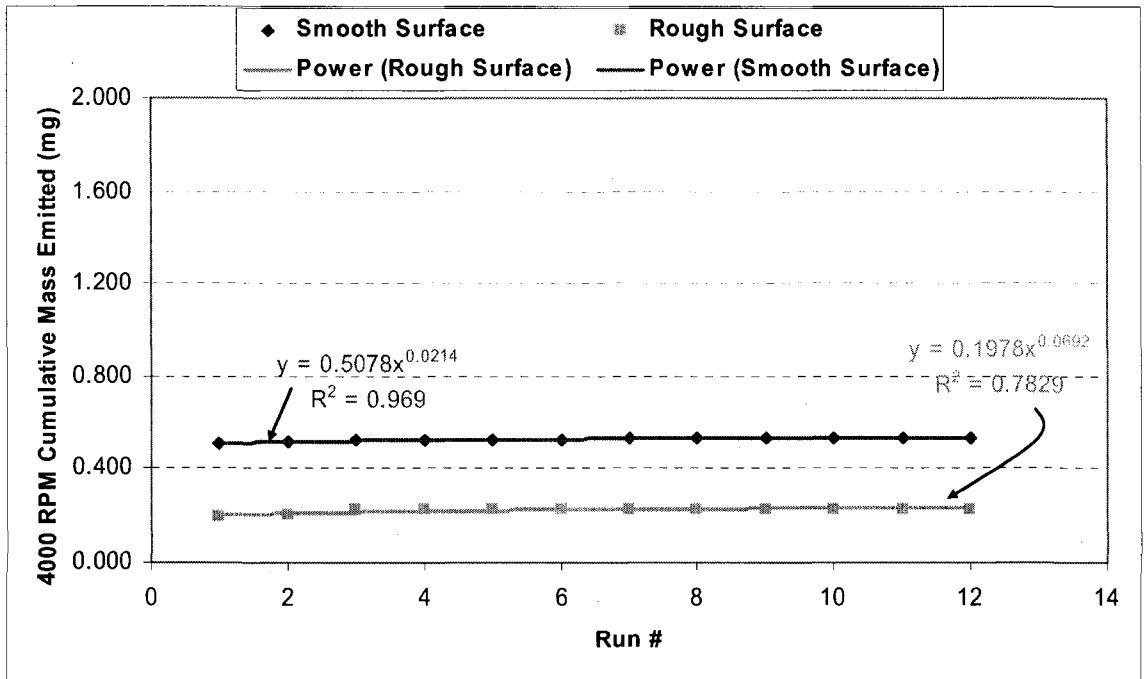


Figure 6.49 Cumulative Mass Removed at 4000 RPM Shear Rate



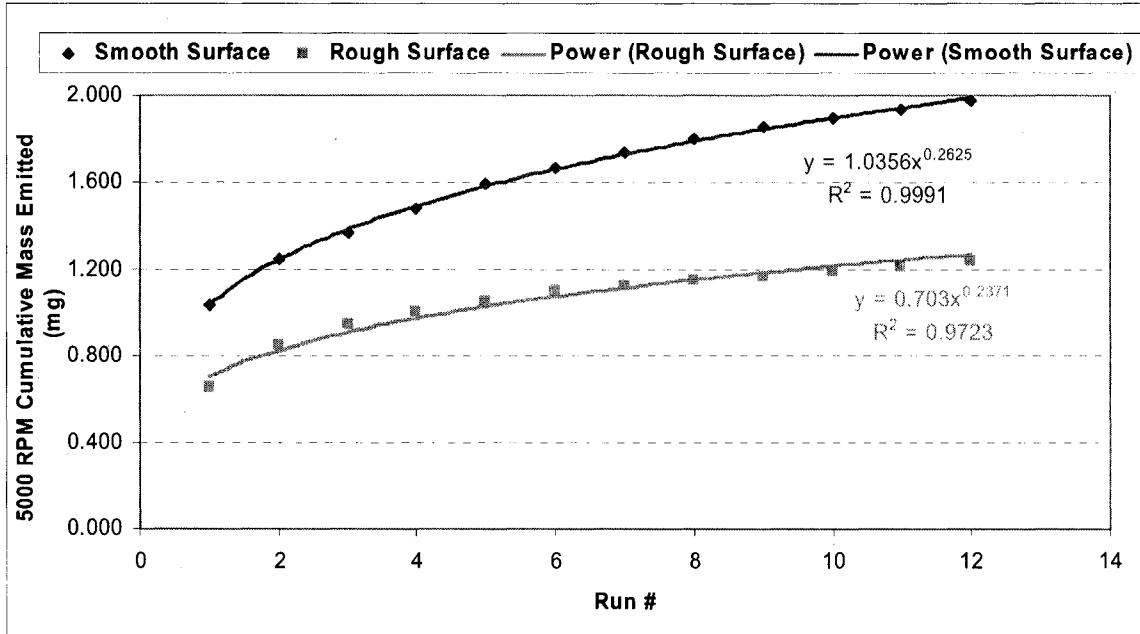


Figure 6.50 Cumulative Mass Removed at 5000 RPM Shear Rate

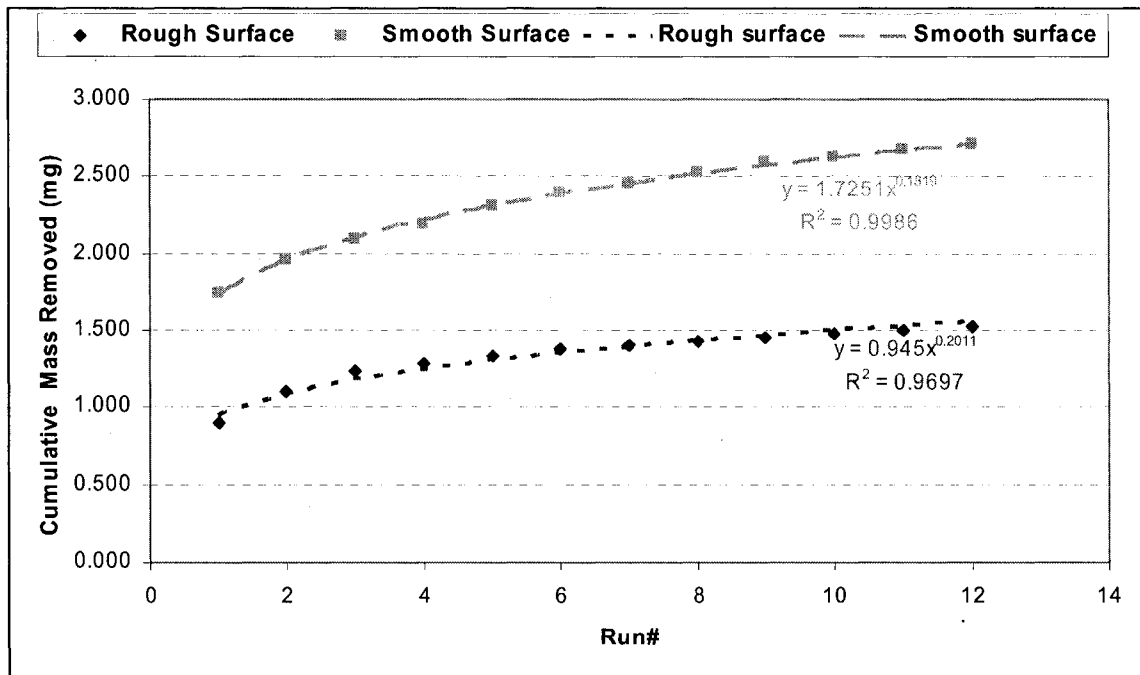


Figure 6.51 Cumulative Mass Removed at 3000+4000+5000 RPM Shear Rate

## CHAPTER 7

### CONCLUSIONS AND RECOMMENDATIONS

#### 7.1 Conclusions

AP-42 emission factors were estimated to update historical data. Recovered AP-42 silt loadings indicate that paved road dust  $PM_{10}$  emission factors measured in the first quarter of 2008 were higher than most recent sampling for 11 of 12 sampling sites. The lowest silt loading was found at Veterans Memorial Blvd, a collector road in Boulder City. Highest average silt loading was found in local roads, followed by minor arterial and collector.

Sand patch (ASTM E965, 2001) and DSRM measurements of road surface macrotexture were made to determine if a relationship existed between data obtained by the two methods. A strong correlation ( $r^2=0.90$ ) was found between DSRM and sand patch MTDs for initial measurements taken in the parking lot. A statistically significant correlation ( $r^2=0.95$ ) was found between the sand patch and DSRM measurements for 61 measurements taken at the 13 field sampling sites. Significant differences in pavement texture were found between tire-worn and non-worn road macrotexture at the Duneville and Oakey sampling site.

PM<sub>10</sub> emissions from the Mini-PI-SWRL™ were estimated at 13 field sites with a range of pavement surface macrotextures to determine if there was a relationship between PM<sub>10</sub> emissions and pavement macrotexture. Ambient PM<sub>10</sub> emissions were significantly related to silt loadings.

Ambient PM<sub>10</sub> emissions, normalized by silt loading were significantly correlated with road pavement macrotexture but partially explained the effect of PM<sub>10</sub> emissions on pavement macrotexture. PM<sub>10</sub> emission results from controlled experiments with an applied soil of constant composition showed a stronger correlation with pavement macrotexture.

Analysis of controlled PM<sub>10</sub> mass emissions from different pavement surfaces showed that there is a “break” in the slope of emitted PM<sub>10</sub> mass and pavement macrotexture that occurred at about 0.8 mm to 0.9 mm MTD. The “break” became more prominent at higher applied shear rates (4000 and 5000 rpm). When replacing MTD with an adjusted mode size, PM<sub>10</sub> emissions were found to linearly depend on an adjusted mode size of the pavement surface aggregate which indicates the dependency of PM<sub>10</sub> emission on pavement aggregate mode size.

Wind erosion theory was applied for PM<sub>10</sub> emissions from the asphalt pavement surface for the controlled experiment. The threshold friction velocity of soil particles was estimated from the mode of the applied soil. Paved road surface aerodynamic roughness height was estimated from the mode size of non-erodible asphalt aggregate. A critical threshold for initiation of PM<sub>10</sub> erosion was determined to occur between the 2000 rpm and 3000 rpm  $u^*$  values (0.31 m/s and 0.43 m/s). 0.075 mm was determined to be a reasonable critical height for wind shear application to explain the wind erosion theory.

A discrepancy was found in the PM<sub>10</sub> emissions vs pavement macrotexture relationship at the two highest MTD sites, Maryland & Westminster and Ann Rd & San Mateo. A two-way frequency distribution was developed from the DSRM data to describe the pavement's surface topography and then compared to the PM<sub>10</sub> emissions. A relatively higher frequency of deep narrow pits at Ann Rd & San Mateo site likely contributed to lower-than-expected PM<sub>10</sub> emissions because erodible particles could be sheltered from applied aerodynamic shear. A higher percentage of flat medium features at Maryland & Westminster site resulted in higher-than-expected emissions because more erodible particles were exposed to applied aerodynamic shear.

A depletion study conducted in the Thomas and Mack parking lot showed that the amount of PM<sub>10</sub> mass removed from smooth surface was higher than from a rough surface for the first run. The study concluded that over 12 runs, the cumulative mass removed at high shear rates from a smooth surface was higher than for a rough surface.

## 7.2 Recommendations for Air Quality Control

The following are the recommendations for reducing PM<sub>10</sub> emissions from paved roads based on the conclusions of this study.

- (a) Roads can be constructed with paving material that produces a mean texture depth exceeding 0.9 mm to reduce potential PM<sub>10</sub> emissions from paved roads.
- (b) Revisions of road maintenance procedures should be considered to resurface roads to textures exceeding 0.9 mm where tire polishing of pavement is

evident. Resurfacing to increase mean texture depth may increase safety for friction issues, and might increase road noise.

- (c) Uniform aggregate size distributions could be used for paving roads to reduce emissions. Aggregate mode size around 4.5 mm might be useful for creating both a mean texture depth exceeding 0.9 mm and pits in which road silt can be sheltered from tire and aerodynamic shear.
- (d) A new equation for emission factor measurement from paved road should be developed, and it should include pavement macrotexture as controlling variable.

### 7.3 Recommendations for Future Work

#### 7.3.1 Pavement Macrotexture Measurements

A three-line laser should be used for rougher texture (probably greater than 1.2 mm) as the five-line laser sometimes provided out-of-range data when texture exceeded 1.2 mm. Use of a three line laser may provide better correlation with the sand patch method for coarse texture pavement. The DSRM raw signal data from all sites could be subjected to additional analyses (such as Fourier Transforms, or direct determination of mode size) to characterize pavement surface profile more accurately.

#### 7.3.2 PM<sub>10</sub> Emissions

Additional sampling should be conducted on other types of pavement textures, (grooved pavement, concrete pavement, porous pavements) to determine the effect on PM<sub>10</sub> emissions. Close-up photographic analysis using a macro lens should be conducted for (1) ambient condition, (2) after vacuuming the pavement surface, (3) after the

application of soil, (4) after control experiments to find out “sheltering” and “exposed” features for ambient silt particles on pavement surface. Two-way frequency distributions (width and depth) for a range of pavement macrotextures should be studied more intensively to determine if there are significant differences in pavement topography that could affect  $PM_{10}$  emissions rates.

Lower than expected  $PM_{10}$  emissions at Veterans Memorial Blvd sampling site indicated that either additional analysis of road surface texture data, such as two-way frequency distribution of pavement surface profile, or additional controlled experiments may be needed at this site to explain the observed low emissions rates.

Aerodynamic roughness height can be calculated using ratios different from 30 and  $u(z)$  can be calculated at different heights. A parametric study of the existing controlled study data set, systematically varying the  $z$  used calculating for  $u(z)$ , the divisor used for calculating  $z_0$  and the soil mode size used to estimate  $u^*t$  could be performed to find the optimum combination for explaining variance in emissions data when plotting emissions vs  $u(z)-u^*t$ . Estimation of threshold friction velocity ( $u^*t$ ) for various soil particle sizes from the ambient emissions data set could better explain observed differences in the applied aerodynamic shear rates needed to initiate particle mobilization. This information might help to improve the evaluation of the applicability of classical wind erosion theory to the effects of pavement texture and aerodynamic roughness height on paved road  $PM_{10}$  emissions that result from aerodynamic shear.

APPENDIX A

Table 1. Mini PI-SWERL™ Emitted Mass at 3000 RPM and Sand Patch MTD

Site Name	Location	DSRM (MTD)	Sand patch(MTD)	3000 RPM Mass(mg)	(Clean) 3000 RPM Mass(mg)
Evergold & Coral Sea	P2S1	0.417	0.412	0.225	0.001
Evergold & Coral Sea	P3S1	0.533	0.539	0.072	0.015
Goldhill & Richmar	P3S1	0.553	0.544	0.277	0
Goldhill & Richmar	P2S1	0.569	0.562	0.233	0.001
Goldhill & Richmar	P1S1	0.603	0.581	0.172	0.002
Crestdale	P2S2	0.628	0.646	0.121	0.002
Crestdale	P1S1	0.634	0.623	0.181	0
Crestdale	P2S1	0.651	0.64	0.213	0.002
Crestdale	P1S2	0.655	0.652	0.168	0.001
Crestdale	P3S1	0.675	0.664	0.063	0.001
Crestdale	P3S2	0.711	0.695	0.088	0
Armacost & Calmar Burkholder&	P2S1	0.72	0.754	0.096	0.013
Cabrillo	P2S1	0.743	0.722	0.065	0.002
Armacost & Calmar	P3S1	0.761	0.73	0.021	0.006
Silverspring & Spring Hill	P1S2	0.775	0.765	0.04	0
Armacost & Calmar	P1S1	0.786	0.83	0.116	0
Silverspring & Spring Hill	P2S2	0.79	0.78	0.055	0.002
Duneville & Oakey Burkholder %	P1S2	0.801	0.804	0.081	0.002
Cabrillo	P3S1	0.866	0.873	0.029	0.002
Duneville & Oakey	P2S2	0.963	0.961	0.039	0.007
Maryland & Westminster	P2S1	1.062	1.155	0.035	0.004
Silverspring & Spring Hill	P2S1	1.076	1.028	0.04	0.001
Duneville & Oakey	P3S2	1.127	1.114	0.062	0

Site Name	Location	DSRM (MTD)	Sand patch(MTD)	3000 RPM Mass(mg)	(Clean) 3000 RPM Mass(mg)
Ann Rd & San Mateo	P2S1	1.175	1.228	0.001	0.001
Maryland & Westminster	P3S1	1.202	1.198	0.019	0.002
Ann Rd & San Mateo	P3S1	1.296	1.514	0.001	0
Ann Rd & San Mateo	P1S1	1.314	1.601	0.001	0.001
Maryland & Westminster	P1S1	1.471	1.473	0.05	0.005
Sapphire Light	P1S1	0.831	0.855	0.077	0.001
Sapphire Light	P2S2	0.63	0.64	0.135	0.002
Sapphire Light	P3S1	0.654	0.629	0.172	0.005
Pabco & Tabony	P1S1	0.681	0.689	0.115	0.001
Pabco & Tabony	P2S1	0.667	0.676	0.125	0

Table2. Mini PI-SWERL™ Emitted Mass at 2000 RPM and Sand Patch MTD  
(Controlled Experiment)

Site Name	Location	DSRM (MTD)	Sand patch(MTD)	2000 RPM Mass(mg)	(Clean) 2000 RPM Mass(mg)
Evergold & Coral sea	P2S1	0.417	0.412	0.007	0.001
Evergold & Coral sea	P3S1	0.533	0.539	0.051	0.002
Goldhill & Richmar	P3S1	0.553	0.544	0.009	0.003
Goldhill & Richmar	P2S1	0.569	0.562	0.017	0.001
Goldhill & Richmar	P1S1	0.603	0.581	0.007	0.000
Crestdale	P1S1	0.634	0.623	0.012	0.000
Sapphire Light	P3S1	0.654	0.629	0.030	0.002
Sapphire Light	P2S2	0.63	0.64	0.020	0.001
Crestdale	P2S1	0.651	0.640	0.011	0.000
Crestdale	P2S2	0.628	0.646	0.000	0.001
Crestdale	P1S2	0.655	0.652	0.002	0.000
Crestdale	P3S1	0.675	0.664	0.000	0.000
Pabco & Tabony	P2S1	0.667	0.676	0.003	0.000
Pabco & Tabony	P1S1	0.681	0.689	0.011	0.001
Crestdale	P3S2	0.711	0.695	0.000	0.000



Site Name	Location	DSRM (MTD)	Sand patch(MTD)	2000 RPM Mass(mg)	(Clean) 2000 RPM Mass(mg)
Burkholder	P2S1	0.743	0.722	0.005	0.001
Armacost & Calmar	P3S1	0.761	0.730	0.001	0.004
Armacost & Calmar	P2S1	0.720	0.754	0.001	0.012
Silverspring & Spring Hill	P1S2	0.775	0.765	0.003	0.000
Silverspring & Spring Hill	P2S2	0.790	0.780	0.008	0.001
Duneville & Oakey	P1S2	0.801	0.804	0.013	0.001
Armacost & Calmar	P1S1	0.786	0.830	0.000	0.000
Sapphire Light	P1S1	0.831	0.855	0.039	0.000
Burkholder	P3S1	0.866	0.873	0.002	0.001
Duneville & Oakey	P2S2	0.963	0.961	0.000	0.005
Silverspring & Spring Hill	P2S1	1.076	1.028	0.003	0.001
Duneville & Oakey	P3S2	1.127	1.114	0.002	0.003
Maryland & Westminster	P2S1	1.062	1.155	0.001	0.001
Maryland & Westminster	P3S1	1.202	1.198	0.000	0.000
Ann Rd & San Mateo	P2S1	1.175	1.228	0.000	0.001
Maryland & Westminster	P1S1	1.471	1.473	0.005	0.003
Ann Rd & San Mateo	P3S1	1.296	1.514	0.000	0.000
Ann Rd & San Mateo	P1S1	1.314	1.601	0.000	0.001

## APPENDIX B

### C++ Code for Width and Peak or Valley Determination

```
#include<stdio.h>

#include<math.h>
#include<conio.h>

//Defining the structure

void main()
{
    FILE *fp1, *fp2, *fp3, *fp4;
    int i, n, m, flag[1000], flag1[1000], counter, maxflag, k, no[55], j;
    int count=0;
    float x[1000], z5[1000], sx[100][400],sz5[100][400], sum, width1,
peak1;
    float average[55], width[55], peak[55];

    fp1=fopen("inputfile.txt","r+");
    if(fp1==NULL)
    {
        puts("cannot open the data file");
        exit();
    }
    fp2=fopen("outputfile.txt","w");
    fp3=fopen("out2putfile.txt","w");
    fp4=fopen("in2putfile.txt","r+");

    //General comments on program
    printf("\tIF DATA POINTS EXCEED 1000 INCREASE
MEMORY SPACE\n");
    printf("\tBefore store input data, write number of data points\n");
    printf("\tIf above all are true press any key to continue\n");
    getch();

    //Scanning number of data points from input file.
```

```

fscanf(fp1,"%d",&n);

for(i=0;i<n;i++)    {
    x[i]=0.0;
    z5[i]=0.0;
    flag1[i]=0;
    flag[i]=0;
}

//Input data scanning for finding out number of bands and number
of points in each band
for(i=0;i<n;i++)
{
    fscanf(fp1,"%f%f",&x[i],&z5[i]);
}
for(i=0;i<n;i++)
{
    fprintf(fp3,"%5.2ft%5.2fn",x[i],z5[i]);
}

flag1[0]=count;
if(z5[0]>0&&z5[1]>0||z5[0]==0&&z5[1]==0||z5[0]<0&&z5[1]<0)
m=1;
else flag[0]=1;

//Break point tracking
for(i=1;i<n;i++)
{
    if(z5[i-1]>0&&z5[i]>0||z5[i-1]==0&&z5[i]==0||z5[i-1]<0&&z5[i]<0)
    {
        flag1[i]=count;
        m+=1;
        flag[i]=m;
    }
    else
    {
        count+=1;
        flag1[i]=count;

        m=1;
    }
}

```

```

        flag[i]=m;
    }
}
maxflag=count;
printf("Max Flag=%d",maxflag);

//We can track break points using flag1.

//for(i=0;i<n;i++) fprintf(fp2,"%d\t%d\n",flag1[i],flag[i]);

//Counting number of points in each band
for(i=0;i<maxflag;i++) no[i]=0;
k=0;
for(i=0;i<n-1;i++)
{
    if(flag[i]>=flag[i+1])
    {
        no[k]=flag[i];
        k+=1;
    }
}
no[maxflag]=flag[n-1];
//for(i=0;i<=maxflag;i++) fprintf(fp2,"%d\n",no[i]);
printf("\nK=%d\n",k);

//Now we are going to analyze data

//Scanning Data point again from input file 2 for analysis
for(i=0;i<=maxflag;i++)
{
    k=no[i];
    for(j=0;j<k;j++)
    {
        fscanf(fp4,"%f%f",&sx[i][j],&sz5[i][j]);
    }
}

//Average and width calculation

for(i=0;i<=maxflag;i++)
{
    k=no[i];
    sum=0;
    for(j=0;j<k;j++)

```

```

        {
            if(k==1)
            {
                sum=sz5[i][j];
                //peak=sz5[i][j];
                //width1=0.0;
            }
            else
            {
                sum+=sz5[i][j];
                //width1=sx[i][k-1]-sx[i][0];
            }
        }
        if(k==1) width1=0.0;
        width1=sx[i][k-1]-sx[i][0];
        average[i]=sum/k;
        width[i]=width1;

//printf("Average=%5.2ftWidth=%5.2fn",average[i],width[i]);
}
//Finding Peak//presently we are working here
for(i=0; i<=maxflag;i++) peak[i]=0.0;
for(i=0; i<=maxflag;i++)
{
    k=no[i];
    for(j=0;j<k;j++)
        sz5[i][j]=sz5[i][j]*100;
}

for(i=0;i<=maxflag;i++)
{
    k=no[i];
    if(k>1)
    {
        //peak1=sz5[i][0];
        for(j=0;j<k;j++)
        {
            if(sz5[i][j]>0)
            {
                if(sz5[i][j]>peak[i])
                    peak[i]=sz5[i][j];
            }
            else if(sz5[i][j]<peak[i]) peak[i]=sz5[i][j];
        }
    }
}

```

```

        }
    }
    else peak[i]=sz5[i][0];

    printf("K=%d\tAverage=%5.2f\tPeak=%5.2f\tWidth=%5.2f\n",k,average[i],peak[i]/100,width[i]);
}

fprintf(fp2,"WIDTH\tPEAK\tAVERAGE\n");
for(i=0;i<=maxflag;i++)
fprintf(fp2,"%5.2f\t%5.2f\t%5.2f\n",width[i],peak[i]/100,average[i]);

fclose(fp1);
fclose(fp2);
fclose(fp3);
fclose(fp4);
}

```

## REFERENCES

- Abe, H, J. J. Henry, J. Wambold, and A. Tamai, Measurements of Pavement Macrotecture with Circular Texture Meter. In Transportation Research Record 1764. Transportation Research Board, Washington, D.C., pp 201-209, 2002.
- Amemiya, S, Y. Tsurita, T. Masuda, A. Asawa, K. Tanaka, T. Katoh, M. Mohri and T. Yamashina, Investigations of environmental problems caused by studded tyres of automobiles using PIXE, Nucl. Instrum. Methods Phys. Res. B3, 516–521, 1984.
- American Concrete Institute (ACI), Texturing Concrete Pavement, ACI Committee 325, ACI-325.6R-88. American Concrete Institute, Detroit, MI, 1988.
- American Society for Testing and Materials, Standard Test Method for Measuring Pavement Macrotecture Depth Using a Volumetric Technique, ASTM E 965, Book of Standards, Vol. 04.03, Road and paving materials. West Conshohocken, PA, 2001.
- American Society for Testing and Materials, Standard Practice for Calculating Pavement Macrotecture Mean Profile Depth, ASTM E 1845, Book of Standards, Vol. 04.03, Road and paving materials. West Conshohocken, PA, 2001
- American Society for Testing and Materials, Standard Test Method for Measuring Pavement Macrotecture Properties Using the Circular Track Meter, ASTM E 2157, Book of Standards, vol. 04.03, Road and paving materials. West Conshohocken, PA, 2001.
- Atkins, N. H, Highway Materials, Soils, and Concretes, Third Edition, 1997.
- Bagnold, R., A., The physics of Blown Sand and Desert Dunes, Methuen, London, 1941.
- California Department of Transportation (CDT), California Road Dust Scoping Report, Dr Dev Niemeier, 2000.
- Chepil, W.S, Improved Rotary Sieve for Measuring Stte and Stability of Dry Soil Structure, Soil Science Society of America Proceedings, 16, 113-117, 1952.
- Clark County Department of Air Quality and Environmental (DAQEM), PM10 State Implementation Plan for Clark County. Chapter 3: PM10 Emissions Inventory, 2001.

Douglas, H, I. Brian, and D. Prowell, Evaluation of Circular Texture Meter for Measuring Surface Texture of Pavements, National Center for Asphalt Technology (NCAT) report, 2004.

Etyemezian, V, G. Nikolich, S. Ahonen, M. Pitchford, M. Sweeney, J. Gillies and H. Kuhns, The Portable In-Situ Wind Erosion Laboratory (PI-SWERL): A new method to measure windblown dust properties and potential for emissions, *Atmospheric Environment*, 41, 3789–3796, 2007.

Etyemezian, V, H. Kuhns, G. Nikolich, Precision and repeatability of the TRAKER vehicle-based paved road dust emission measurement, *Atmospheric Environment*, 40, 2953–2958, 2006.

Etyemezian, V, H. Kuhns, J. Gillies, J. Chow, K. Hendrickson, M. McGown and M. Pitchford, Vehicle-based road dust emission measurement (III): Effect of speed, traffic volume, location, and season on PM<sub>10</sub> road dust emissions in the Treasure Valley, ID, *Atmospheric Environment*, 37, 4583–4593, 2003b.

Etyemezian, V, H. Kuhns, J. Gillies, M. Gree., M. Pitchford and J. Watson, Vehicle-based road dust emission measurement: I-methods and Calibration, *Atmospheric Environment*, 37, 4559-4571, 2003a.

Federal Highway Administration (FHWA), Final report, Correlation of Surface Texture, Segregation, and Measurement of Air Voids, NJ, 2002.

Federal Highway Administration (FHWA), Pavement Surface Analysis Laboratory, (<http://www.tfhrc.gov/about/pavesurf.htm>), 2005, date accessed, July 12, 2008.

Federal Highway Administration (FHWA), Technical notes, ROSANV (<http://www.tfhrc.gov/hnr20/rosan/rosandoc.htm>), 1997, Date accessed, July 12, 2008.

Fitz, D. R, and C. Bufalino, Measurement of PM<sub>10</sub> emission factors from paved roads using on-board particle sensors. Air and Waste Management Association Symposium on Air Quality Measurement Methods and Technology-2002, San Francisco, CA November 13-15, 2002.

Fitz, D.,J, F. Dominici, S. M. Jonathan, S. L. Zeger, Estimating Particulate Matter-Mortality Dose-Response Curves and Threshold Levels: An Analysis of Daily Time-Series for the 20 Largest US Cities, *American Journal of Epidemiology*, 152(5), 397-406, 2000.

Fitz, D.F. R, K. Bumiller, V. Etyemezian, H. Kuhns and G. Nikolich, Measurement of PM<sub>10</sub> Emission Rates from Roadways in Las Vegas, Nevada Using a SCAMPER Mobile Platform with Real-Time Sensors, In: 14<sup>th</sup> International Emission Inventory Conferences, April 12–14, Las Vegas, Nevada, 2005.



Fitz,D., Measurements of PM10 Emission Factors from Unpaved roads in Arizona to Determine the Efficiency of Dust suppressants, Draft final report submitted to Sierra Research, Inc. CA, 2005.

Flintsch, G. W, E. de León, K. K. McGhee, and I. L. Al-Qadi, Pavement Surface Macrotecture Measurement and Application, Virginia Tech Transportation Institute, TRB Annual Meeting, 2003.

Fukuzaki, N, T. Yanaka and Y. Urushiyama, Effects of studded tires on roadside airborne dust pollution in Niigata, Japan, *Atmospheric Environment*, 20, 377–386, 1986.

Garland, J. A, Some recent studies of the resuspension of deposited material from soil and grass, in *Precipitation Scavenging, Dry Deposition and Resuspension*, vol. 2, edited by H. R. Pruppacher, R. G. Semonin, and W. G. N. Slinn, Elsevier, Amsterdam The Netherlands, 1087–1097, 1983.

Genndy. E and A. A. Shalaby, Mean Profile Depth of Pavement Surface Macrotecture Using Photometric Sterio Techniques, *American Society of Civil Engineering*, 0733-947X, 133:7(433), 2007.

Gillette, D. A, J. Adams, A. Endo, D. Smith and R. Kihl, Threshold Velocities for Input of Soil Particles into the Air by Desert Soils, *Journal of Geophysical Research*, 85(C10), 5621-5630, 1980.

Greeley, R, and J. D. Iversen, *Wind as a geological process on Earth, Mars, Venus and Titan*, Cambridge Univ. Press , New York, 1985.

Henry, J. J, NCHRP Synthesis 291, *Evaluation of Pavement Friction Characteristics*, TRB, National Research Council, Washington, DC, 2000.

Holman, J.P, *Experimental Methods for Engineer*, Seventh edition, 2001.

Irwin, H.P, A simple omnidirectional sensor for wind tunnel studies of pedestrian level winds. *Journal of Wind Engineering and Industrial Aerodynamics*, 7(3), 219–239, 1981.

Kaarle, T. H, J. Kupiainen, M. R"ais"anen, T. M"akel and R. Hillamo, Generation of urban road dust from anti-skid and asphalt concrete aggregates, *Journal of Hazardous Material*, 132, 39-46, 2006.

Kantamaneni. R, G. F. Adams, L. Bamesberger, E. Allwine, H. Westberg, B. Lamb and C. Claiborn, The measurement of roadway PM<sub>10</sub> emissions rates using atmospheric tracer ratio techniques, *Atmospheric Environment*, 30, 4209–4223, 1996.

Kuhns, H, V. Etyemezian, D. Landwehr, C. MacDougall, M. Pitchford and M. Green, Testing Re-entrained Aerosol Kinetic Emissions from Roads (TRAKER): a new approach to infer silt loading on roadways, *Atmospheric Environment*, 35, 2815-2825, 2001.

Kuhns, H, V. Etyemezian, M. Green, K. Hendrickson, M. McGown, K. Barton and M. Pitchford, Vehicle-based road dust emission measurement—Part II: Effect of precipitation, wintertime road sanding, and street sweepers on inferred PM<sub>10</sub> emission potentials from paved and unpaved roads, *Atmospheric Environment*, 37, 4573–4582, 2003.

Langston, R, R. Merle, D. Hart, V. Etyemezian, H. Kuhns, J. Gillies, Fitz. D, K. Bumiller, D. James, The Preferred Alternative Method For Measuring Paved Road Dust Emissions For Emissions Inventories: “Mobile Technologies Vs. The Traditional Ap-42 Methodology”, 2008.

Light, J, Pocatello Road Dust Study. 98-RP92B.05(A448), Presentation at air and Waste Management Association’s 91<sup>st</sup> Annual Meeting and Exhibition, San Diego, California, June 14-18, 1998.

MaGaNa Instruments, Inc Digital Surface Roughness Meter (DSRM): User Manual, Concruf v. 1.2.3, 2008.

McGhee, K, G. W. Flintsch, High-Speed Texture Measurement of Pavements, Virginia Transportation Research Council, Charlottesville, Virginia, 2003.

McGhee, K, K, and G. W. Flintsch, High-speed Texture Measurements of Pavements. VTRC 03-R9. Virginia Transportation Research Council, Charlottesville, 2003.

Mokarem. W. D, Virginia Transportation Research Council, (VTRC), Use of the Digital Surface Roughness Meter in Virginia, Charlottesville, VA, 2006.

Operator’s manual, Hydrotimer Outflow meter  
([http://www.hydrotimer.com/operator\\_manual.pdf](http://www.hydrotimer.com/operator_manual.pdf)), date accessed June 13, 2008.

Rodrigues, G. B, Improved Techniques for Estimation of Paved Road PM<sub>10</sub> Emissions, UNLV thesis, 2006.

Rohde, S, On the Effect of Pavement Microtexture on thin film Traction, *Int. J. Mech. Sci.*, 18, 95-101, 1975.

Salvatore, C and S. Taormina, Texture analysis of aggregate for wearing courses in asphalt pavement, *International Journal of Pavement Engineering*, 8(1), 45-54, 2006.

Schwartz, J and A. Marcus, Mortality and Air Pollution in London: A Time series Analysis, *American Journal of Epidemiology*, 131, 185-194, 1990.

Shao, Y. H., Lu., A Simple Expression for Wind Erosion Threshold Friction Velocity, *Journal of Geophysical Research*, 105(D17), 22,437-22,443, 2006.

Sweeney, M, V. Etyemezian, T. Macpherson, W. Nickling, J. Gillies, G. Nikolich, and E. McDonald, Comparison of PI-SWERL with dust emission measurements from a straight-line field wind tunnel, *Journal of Geophysical Research*, 113, 2008.

Tervahattu, H. Kaarle J. Kupiainen b, Mika R"ais"anen, Timo M"akel" a d, Risto Hillamo, Generation of urban road dust from anti-skid and asphalt concrete aggregates, *Journal of Hazardous Material* 132 , page 39-46, 2006.

U. S. Environmental Protection Agency (EPA) Manual "Control of Open Fugitive Dust Sources", EPA Manual, 1988.

U. S. Environmental Protection Agency (EPA), Emission Factor Documentation for AP-42, section 13.2.1, Paved roads, MRI project No 9712-44, 1993.

U. S. Environmental Protection Agency (EPA), AP-42, Compilation of Air Pollutant Emissions factor, Stationary Point and Area Sources. Chapter 13.2.1-V.1, 5<sup>th</sup> Edition, January, 1995.

U. S. Environmental Protection Agency (EPA), Addendum to Emission Factor Documentation for AP-42, section 13.2.1, Paved roads, MRI project No 4604-02, 1997.

U.S Environmental Protection Agency<sup>a</sup>(EPA) Particulate Matter, PM10 standards (<http://www.epa.gov/particles/standards.html>), 2006 ,(Date accessed June, 2008)

U.S Environmental Protection Agency<sup>b</sup>(EPA) PM<sub>10</sub> NAAQS Implementation ([http://www.epa.gov/ttn/naaqs/pm/pm10\\_index.html](http://www.epa.gov/ttn/naaqs/pm/pm10_index.html)), 2006,(Date accessed June 2008).

U.S Environmental Protection Agency<sup>c</sup>(EPA) AP-42 Chapter 13.2.1, Paved Roads (<http://www.google.com/search?hl=en&q=EPA%2Bpaved+road+emission+factor%2C+13.2.1>), , 2006,(Date accessed June 2007).

World Road Association (PIARC), Report of the committee on Surface Characteristics, XVIII World Road Congress, Brussels, Belgium, 1987.

VITA

Graduate College  
University of Nevada, Las Vegas

Swarup China

Home Address:

1555 E Rochelle Ave Apt # 245  
Las Vegas, Nevada, 89119

Degrees:

Bachelor of Technology, Civil Engineering, 2006  
Visvesvaraya National Institute of Technology, Nagpur, India

Thesis Title: Effects of Pavement Macrotecture on PM<sub>10</sub> Emissions from Paved Roads

Thesis Examination Committee:

Committee Chair, Dr. David E. James, Ph.D., Associate Vice Provost for Academic Programs, Associate Professor of Civil and Environmental Engineering  
Committee Member, Dr. Jamica Batista Ph.D., Associate Professor of Civil Engineering  
Committee Member, Dr. Thomas Piechota, Ph.D., Associate Professor of Civil Engineering  
Additional Committee Member, Dr. Vic Etyemezian, Ph.D., Associate Research Professor, Atmospheric Sciences, Desert Research Institute  
Graduate Faculty Representative, Dr. Ashok Singh, Ph.D., Professor of Hotel Management